Quantum cluster theories

Thomas Maier*

Computational Science and Mathematics Division, Oak Ridge National Laboratory, Oak Ridge, Tennessee 37831-6164, USA

Mark Jarrell

Department of Physics, University of Cincinnati, Cincinnati, Ohio 45221-0011, USA

Thomas Pruschke

Theoretical Physics, University of Göttingen, Tammannstrasse 1, D-37077 Göttingen, Germany

Matthias H. Hettler

Forschungszentrum Karlsruhe, Institut für Nanotechnologie, Postfach 3640, D-76021 Karlsruhe, Germany

(Published 6 October 2005)

This article reviews quantum cluster theories, a set of approximations for infinite lattice models which treat correlations within the cluster explicitly, and correlations at longer length scales either perturbatively or within a mean-field approximation. These methods become exact when the cluster size diverges, and most recover the corresponding mean-field approximation when the cluster size becomes 1. Although quantum cluster theories were originally developed to treat disordered systems, they have more recently been applied to the study of ordered and disordered correlated systems, which will be the focus of this review. After a brief historical review, the authors provide detailed derivations of three cluster formalisms: the cluster perturbation theory, the dynamical cluster approximation, and the cellular dynamical mean-field theory. They compare their advantages and review their applications to common models of correlated electron systems.

CONTENTS

*Electronic address: maierta@ornl.gov

I. INTRODUCTION

A. Brief history

The theoretical description of interacting many-particle systems remains one of the grand challenges in condensed-matter physics. The field of strongly correlated electron systems has gained theoretical and experimental interest through the discovery of heavy-fermion compounds and high-temperature superconductors. In this class of systems the strength of the interactions between particles is comparable to or larger than their kinetic energy, i.e., any theory based on a perturbative expansion around the noninteracting limit is at the least questionable. Theoretical tools to describe these systems are therefore faced with extreme difficulties, due to the nonperturbative nature of the problem. A large body of work has been devoted to a direct (numerically) exact solution of finite-size systems using exact diagonalization or quantum Monte Carlo methods. Exact diagonalization, however, is severely limited by the exponential growth of computational effort with system size, while quantum Monte Carlo methods suffer from the sign problem at low temperatures. Another difficulty of these methods arises from their strong finite-size effects, often ruling out the reliable extraction of low energy scales that are important in capturing the competition between different ground states often present in strongly correlated systems.

Mean-field theories are defined in the thermodynamic limit and therefore have different truncation errors than finite-size simulations. With applications to a wide variety of extended systems from spin models to models of correlated electrons and/or bosons, mean-field theories are extremely popular and ubiquitous throughout science.

Generally, mean-field theories divide the infinite number of degrees of freedom into two sets. A small set of degrees of freedom is treated either exactly or with an approximation that goes beyond the mean-field level, while the effects of the remaining degrees of freedom are summarized as a mean field acting on the first set. Throughout this review, by mean-field theory, we refer to the class of approximations which account for the correlations between spatially localized degrees of freedom explicitly, while treating those at longer length scales with an effective medium. The small set of local degrees of freedom can, in principle, be treated exactly. Such local approximations become exact in the limit of infinite coordination number or equivalently infinite dimensions D (Itzykson and Drouffe, 1989); however, nonlocal corrections become important in finite dimensions. The purpose of this review is to discuss methods for correlated electron systems that incorporate nonlocal corrections to local approximations.

Many different local approximations have been developed for systems with itinerant degrees of freedom. Early attempts focused on disordered systems, and included the virtual-crystal approximation (Nordheim, 1931a, 1931b; Parmenter, 1955; Schoen, 1969) and the average-T matrix approximation (Beeby and Edwards, 1962; Schwartz *et al.*, 1971). However, the most successful local approximation for disordered systems is the coherent-potential approximation (CPA) developed by Soven (1967) and others (Taylor, 1967; Shiba, 1971). This method is distinguished from the others in that it becomes exact in both the limit of dilute and concentrated disordered impurity systems, as well as the limit of infinite dimensions.

There have been many attempts to extend the CPA formalism to correlated systems, starting with the dynamical CPA of Sumi (1974) [see also Kakehashi (2002)], the extended noncrossing approximation of Kim *et al.* (1990; Kuramoto, 1985), and the lattice noncrossing approximation of Grewe (1987; Grewe *et al.*, 1988). A great breakthrough was achieved with the development of the dynamical mean-field theory (DMFT) in a series of works, starting with the seminal papers of Metzner and Vollhardt (1989) and of Müller-Hartmann (1989b) (for a review see Pruschke *et al.*, 1995; Georges *et al.*, 1996). The dynamical CPA and the DMFT employ the same mapping between the cluster and the lattice problems. They differ mostly in their starting philosophy. The dynamical CPA employs the CPA equations to relate the impurity solution to the lattice, whereas in the DMFT the irreducible quantities calculated on the impurity are used to construct the lattice quantities.

Despite the success of these mean-field approaches, they share the critical flaw of neglecting the effects of nonlocal fluctuations. Thus they are unable to capture the physics of, e.g., spin waves in spin systems, localization in disordered systems, or spin-liquid physics in correlated electronic systems. Nonlocal corrections are required to treat even the initial effects of these phenomena and to describe phase transitions to states described by a nonlocal order parameter.

The first attempt to add nonlocal corrections to mean-field theories was made by Bethe (1935) by adding cor-

rections to the Weiss mean-field theory (Weiss, 1907). Here, the lattice problem is mapped onto a self-consistently embedded finite-size spin cluster composed of a central site and z nearest neighbors embedded in a mean field. For small z, the resulting theory provides a remarkably large and accurate correction to the transition temperature (Kikuchi, 1951; Suzuki, 1986).

Many attempts have been made to apply similar ideas to disordered electronic systems (Gonis, 1992). Most approaches were hampered by the difficulty of constructing a fully causal theory, with positive spectral functions. Several causal theories were developed including the embedded-cluster method (Gonis, 1992) and the molecular CPA (MCPA) by Tsukada (1969) (for a review see Ducastelle, 1974). These methods generally are obtained from the local approximation by replacing the impurity by a finite-size cluster in real space. As a result these approaches suffer from the lack of translational invariance, since the cluster has open boundary conditions and only the surface sites couple to the mean field.

Similar effort has been expended to find cluster extensions to the DMFT. Early attempts were not fully self-consistent (Kampf, 1991) or suffered from causality violations (van Dongen, 1994; Schiller and Ingersent, 1995). However, fully causal self-consistent methods have been developed, most notably the dynamical cluster approximation (DCA; Hettler *et al.*, 1998, 2000) and the cellular dynamical mean-field theory (CDMFT; Kotliar *et al.*, 2001). They reduce the complexity of the lattice problem by mapping it to a finite-size cluster self-consistently embedded in a mean field. The main difference with their classical counterparts arises from the presence of quantum fluctuations. Mean-field theories for quantum systems with itinerant degrees of freedom cut off spatial fluctuations but take full account of temporal fluctuations. As a result the mean field is a time- or frequency-dependent quantity. Even an effective cluster problem consisting of only a single site (DMFT) is a highly nontrivial many-body problem. cellular DMFT and the dynamical cluster approximation mainly differ in the nature of the effective cluster problem. The cellular DMFT shares an identical mapping of the lattice to the cluster problem with the molecular CPA and hence also violates translational symmetries on the cluster. The dynamical cluster approximation maps the lattice to a periodic and therefore translationally invariant cluster.

A numerically more tractable cluster approximation to the thermodynamic limit was developed by Gros and Valenti (1993). In this formalism the self-consistent coupling to a mean field is neglected. This leads to a theory in which the self-energy of an isolated finite-size cluster is used to approximate the lattice propagator. As shown by Sénéchal *et al.* (2000), this cluster extension of the Hubbard-I approximation is obtained as the leading-order approximation in a strong-coupling expansion in the hopping amplitude and hence this method was named the cluster perturbation theory.

Generally, cluster formalisms share the basic idea of approximating the effects of correlations in the infinite lattice problem with those on a finite-size quantum cluster. We refer to this class of techniques as quantum cluster theories. In contrast to finite-system simulations, these techniques are built for the thermodynamic limit. In this review we focus on the three most established quantum cluster approaches, the dynamical cluster approximation, the cellular DMFT, and the cluster perturbation theory formalisms. The cellular DMFT approach was originally formulated for general, possibly nonorthogonal basis sets. In this review we restrict the discussion to the usual, completely localized orthogonal basis set and refer the reader to Kotliar *et al.* (2001) for the generalization to arbitrary basis sets.

The organization of this article is as follows: To familiarize the reader with the concept of cluster approaches, we develop in Sec. I.B a cluster generalization of the Weiss mean-field theory for spin systems. Section II sets up the theoretical framework of the cellular DMFT, dynamical cluster approximation, and cluster perturbation theory formalisms by presenting two derivations based on different starting philosophies. The derivation based on the locator expansion in Sec. II.A is analogous to the cluster generalization of the Weiss mean-field method and thus is physically very intuitive. The derivation based on the cluster approximation to diagrams defining the grand potential in Sec. II.B is closely related to the reciprocal space derivation of the DMFT by Müller-Hartmann (1989b). The nature of the different quantum cluster approaches together with their advantages and weaknesses are assessed in Sec. II.D. Discussions of the effective cluster problem, generalizations to broken-symmetry states, and the calculation of response functions are presented in Secs. II.E, II.F, and II.G. The remainder of Sec. II is devoted to describing the application of the dynamical cluster approximation formalism to disordered systems in Sec. II.H and to a brief discussion of alternative methods proposed to introduce nonlocal corrections to the DMFT method in Sec. II.I. In Sec. III we review the various perturbative and nonperturbative techniques available to solve the effective cluster problem of quantum cluster approaches. We include a detailed assessment of their advantages and limitations. Although numerous applications of quantum cluster approaches to models of many-particle systems are found in the literature, this field is still in its early stages and currently very active. A large body of work has been concentrated on the Hubbard model. We review the progress made on this model in Sec. IV together with applications to several other strongly correlated models. Section V concludes the review, stressing the limitations of quantum cluster approaches and proposing possible directions for future research in this field.

B. Corrections to Weiss theory

As an intuitive example of the formalism developed in the next sections we consider a systematic cluster extension of the Weiss mean-field theory for a lattice of interacting Ising spins. This discussion is especially helpful in illustrating many new aspects of cluster approaches as

compared to finite-size simulations. Whereas this methodology was developed for correlated electronic systems, and has significant limitations when applied to spin systems, this simple example will illustrate the qualitative features of the method in an exactly solvable model, the one-dimensional Ising model,

$$H = -J\sum_i \sigma_i\sigma_{i+1} - h\sum_i \sigma_i, \tag{1}$$

where $\sigma_i = \pm 1$ are Ising spins, h is an external magnetic field, and the exchange integral $J>0$ acts between nearest neighbors only, favoring ferromagnetism. The generalization of this approach to higher dimensions and quantum spin systems is straightforward.

We start by dividing the infinite lattice into N/N_c clusters of size N_c (see Fig. 3 in Sec. II.A) with origin $\tilde{x}$ and the exchange integral J_{ij} into intracluster ($\mathbf{J}_c$) and intercluster ($\delta\mathbf{J}$) parts,

$$\mathbf{J}(\tilde{x}_i - \tilde{x}_j) = \mathbf{J}_c\delta_{\tilde{x}_i,\tilde{x}_j} + \delta\mathbf{J}(\tilde{x}_i - \tilde{x}_j), \tag{2}$$

where each of the terms is a matrix in the N_c cluster sites. The central approximation of cluster theories is to retain correlation effects within the cluster and neglect them between the clusters. A natural formalism to implement this approximation is the locator expansion. The spin susceptibility $\chi_{ij} = \beta(\langle\sigma_i\sigma_j\rangle - \langle\sigma_i\rangle\langle\sigma_j\rangle)$, where $\beta = 1/T$ is the inverse temperature, can be approximated in a locator expansion in the intercluster part $\delta\mathbf{J}$ of the exchange interaction

$$\boldsymbol{\chi}(\tilde{x}_i - \tilde{x}_j) = \boldsymbol{\chi}^o\delta_{\tilde{x}_i,\tilde{x}_j} + \boldsymbol{\chi}^o\sum_l \delta\mathbf{J}(\tilde{x}_i - \tilde{x}_l)\boldsymbol{\chi}(\tilde{x}_l - \tilde{x}_j), \tag{3}$$

where we used again a matrix notation in the N_c cluster sites. In general $\boldsymbol{\chi}^o$ is the susceptibility of an embedded cluster. Here, for illustration purposes, we use the simpler approximation to take $\boldsymbol{\chi}^o$ to be the susceptibility of an isolated cluster, i.e., $\boldsymbol{\chi}^o = \boldsymbol{\chi}(\delta\mathbf{J}=0)$. By using the translational invariance of quantities in the superlattice $\tilde{x}$, this expression can be simplified in the reciprocal space $\tilde{q}$ of $\tilde{x}$ to

$$\boldsymbol{\chi}(\tilde{q}) = \boldsymbol{\chi}^o + \boldsymbol{\chi}^o\delta\mathbf{J}(\tilde{q})\boldsymbol{\chi}(\tilde{q}). \tag{4}$$

This locator expansion has two well-defined limits. For an infinite-size cluster it recovers the exact result, since the surface to volume ratio vanishes, making $\delta\mathbf{J}$ irrelevant, and thus $\boldsymbol{\chi} = \boldsymbol{\chi}^o$. For a single site cluster, $N_c = 1$, it recovers the Weiss mean-field theory. This is intuitively clear since for $N_c = 1$, fluctuations between all sites are neglected. With the susceptibility of a single isolated site $\chi^o = 1/T$ and $\delta J(\tilde{q}=0) = J(q=0) = J$, we obtain for the uniform susceptibility

$$\chi(q=0) = \frac{1}{1/\chi^o - J(q=0)} = \frac{1}{T - T_c} \tag{5}$$

the mean-field result with critical temperature $T_c = J$.

For cluster sizes larger than one, translational symmetry within the cluster is violated since the clusters have open boundary conditions and $\delta\mathbf{J}$ only couples sites on the surface of the clusters. As detailed in the next section, this shortcoming can be formally overcome and translational invariance restored by considering an analogous expression to the locator expansion (4) in the Fourier space Q of the cluster,

$$\chi(Q,\tilde{q}) = \chi^o(Q) + \chi^o(Q)\delta J(Q,\tilde{q})\chi(Q,\tilde{q}) = \frac{1}{1/\chi^o(Q) - \delta J(Q,\tilde{q})}, \tag{6}$$

with analogous relations for the intracluster and intercluster parts of J,

$$\delta J(Q,\tilde{q}) = J(Q+\tilde{q}) - \bar{J}(Q), \tag{7}$$

$$\bar{J}(Q) = \frac{N_c}{N}\sum_{\tilde{q}} J(Q+\tilde{q}). \tag{8}$$

Here, $\tilde{q}$ is a vector in the reciprocal space of $\tilde{x}$, and Q is a vector in the reciprocal space of the cluster sites. The Fourier transform of the exchange integral is given by $J(Q+\tilde{q}) = J\cos(Q+\tilde{q})$, the intracluster exchange is $\bar{J}(Q)$, while the intercluster exchange is $\delta J(Q,\tilde{q})$. As we shall see in the next section, the resulting formalism is analogous to the dynamical cluster approximation for itinerant fermion systems.

In analogy to the Weiss theory, the lattice system can now be mapped onto an effective cluster model embedded in a mean field, since correlations between the clusters are neglected. The susceptibility restricted to cluster sites is obtained by averaging or coarse graining over the superlattice wave vectors $\tilde{q}$,

$$\bar{\chi}(Q) = \frac{N_c}{N}\sum_{\tilde{q}} \chi(Q,\tilde{q}) = \frac{1}{1/\chi^o(Q) - \Gamma(Q)}, \tag{9}$$

with the hybridization function

$$\Gamma(Q) = \frac{\frac{N_c}{N}\sum_{\tilde{q}} \delta J^2(Q,\tilde{q})\chi(Q,\tilde{q})}{1 + \frac{N_c}{N}\sum_{\tilde{q}} \delta J(Q,\tilde{q})\chi(Q,\tilde{q})}. \tag{10}$$

This follows from the fact that the isolated cluster susceptibility $\chi^o(Q)$ does not depend on the integration variable $\tilde{q}$ in Eq. (9).

This expression defines the effective cluster model

$$\mathcal{H}_c = -\sum_Q \bar{J}(Q)\sigma(Q)\sigma(-Q) - h\sigma(Q=0) - \sum_{Q,\tilde{q}} \delta J(Q,\tilde{q})\sigma(Q)\langle\sigma(-Q-\tilde{q})\rangle, \tag{11}$$

where $\sigma(Q)$ [$\sigma(q)$] denotes the cluster (lattice) Fourier transform of σ_i and $\langle\cdots\rangle$ the expectation value calculated with respect to the cluster Hamiltonian $\mathcal{H}_c$. As in the Weiss theory, the cluster model is used to self-consistently determine the order parameter $\langle\sigma(Q+\tilde{q})\rangle = \langle\sigma(Q)\rangle\delta(\tilde{q})$ in the ferromagnetic state.

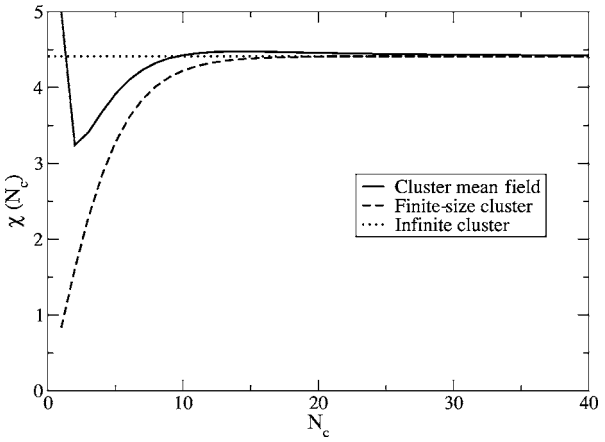

FIG. 1. The cluster and finite-size estimates of the uniform lattice susceptibility in the 1D Ising model vs cluster size when $J=1$ and $T=1.2$.

The uniform susceptibility $\chi(Q=0,\tilde{q}=0)$ contains information about the nature of this cluster approach, its critical properties, and its convergence with cluster size. The sum in Eq. (8) may be solved analytically,

$$\bar{J}(Q=0)=J(N_c/\pi)\sin(\pi/N_c). \tag{12}$$

The isolated cluster susceptibility $\chi^o(Q)$ can also be calculated analytically by using the transfer-matrix method to give (Goldenfeld, 1992)

$$\chi^o(Q=0)=\beta\exp(2K)\frac{1-[\tanh(K)]^{N_c}}{1+[\tanh(K)]^{N_c}}, \tag{13}$$

where $K=\beta\bar{J}(Q=0)=\beta J(N_c/\pi)\sin(\pi/N_c)$. With these expressions the uniform lattice susceptibility Eq. (6) becomes

$$\chi(T)=\frac{1}{1/\chi^o(Q=0)-\delta J(Q=0,\tilde{q}=0)}$$
$$=\frac{1}{1/\chi^o(Q=0)-J[1-(N_c/\pi)\sin(\pi/N_c)]}. \tag{14}$$

The cluster estimate of the lattice susceptibility interpolates between the Weiss result and the exact lattice result as N_c increases. It may be used to reveal some of the properties of cluster approximations and to compare the cluster results to both the finite-size calculation and the exact result in the thermodynamic limit.

First, both the cluster mean-field result Eq. (14) and the finite-size result Eq. (13) with $K=\beta J$ may be regarded as approximations to the thermodynamic result. However, as illustrated in Fig. 1, the cluster mean-field result is closer to the exact result for small N_c than the finite-size result. This reflects the superior starting point of the cluster approximation compared to the finite-size calculation. The cluster approximation is an expansion about the mean-field result, whereas the finite-size calculation is an expansion about the atomic limit.

It is instructive to explore the convergence of the cluster result analytically. For large N_c, the character of the susceptibility Eq. (14) can be split into three regimes. At very high temperatures

$$\chi(T)\approx\frac{1}{T-\Theta}\ \text{for}\ T\gg J, \tag{15}$$

where $\Theta\approx 2J+(J/6)(\pi/N_c)^2$. At intermediate temperatures,

$$\chi(T)\approx\beta e^{2\beta J}\left[1-\frac{\beta J}{3}\left(\frac{\pi}{N_c}\right)^2\right]\quad\text{for}\ J\gg T\gg T_c. \tag{16}$$

The true critical behavior of the system can be resolved by studying the properties of this intermediate temperature regime. At both high and intermediate temperatures, the susceptibility differs from the exact result by corrections of order $\mathcal{O}(1/N_c^2)$. At low temperatures, very close to the transition to the ferromagnetic state, deviations from the exact result are far larger. Here, for large clusters

$$\chi(T)\sim\frac{N_c}{T-T_c}, \tag{17}$$

with the critical temperature $T_c>0$, whereas the exact susceptibility in this regime $\chi(T)\approx\beta\exp(2\beta J)$ does not diverge until zero temperature. This discrepancy is expected for cluster mean-field approximations, since they treat long length scales in a mean-field way. Hence cluster mean-field approximations generally predict finite transition temperatures for any finite cluster size due to their residual mean-field character, independent of dimensionality. With increasing cluster size, however, the transition temperature will be suppressed by the explicit inclusion of longer wavelength fluctuations.

For cluster sizes larger than 1, all three regions are evident in the plot of the cluster mean-field estimate of the inverse susceptibility, shown in Fig. 2. For $N_c=8$ and $N_c=16$, the high- and low-temperature parts are linear in temperature, with the crossover region in between. In numerical simulations, with significant sources of numerical noise especially close to the ordering transition, it can be difficult to resolve the true low-temperature mean-field behavior. Exponents extracted from fits to the susceptibility in such simulations will likely be dominated by the intermediate-temperature regime. Note that for larger clusters, the intermediate regime actually reflects the temperature dependence of the infinite lattice.

Despite the large deviations of the cluster result from the exact result close to the transition, we may still extract correct physics through finite-size extrapolation. In general, for a system where the correlations build like $\xi\sim|(T-T_c)/T_c|^{-\nu}$, we expect $T_c\sim T_c^*+aL_c^{-1/\nu}$, where T_c^* is the exact transition temperature, L_c is the linear cluster size, and a is a positive real constant (Suzuki, 1986). However, for the one-dimensional (1D) Ising system, $\xi\sim(1/2)\exp(\beta J)$, so more care must be taken. Fortunately, an analytic expression for the transition tempera-

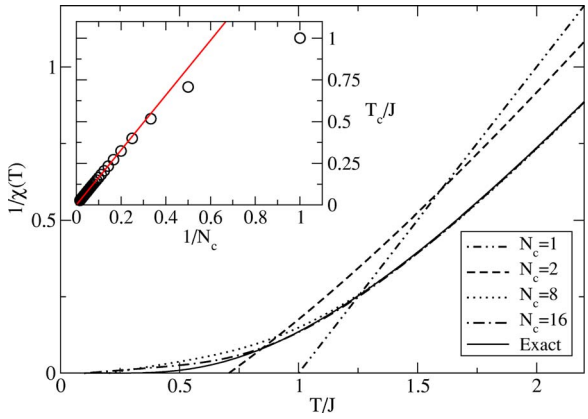

FIG. 2. (Color in online edition) The inverse susceptibility vs temperature. The Weiss behavior at low T, where $1/\chi(T)$ is linear in T, illustrates that the transition is always mean-field-like. The true critical behavior of the transition is reflected in the crossover region for $T \lesssim J$ and larger N_c. Inset: transition temperature for the 1D Ising model vs inverse cluster size when $J=1$, obtained with the cluster mean-field approach. For large clusters, $T_c \sim J\pi^2/6N_c$, shown as a solid line.

ture may be extracted from Eq. (14). For large clusters, $T_c \approx JN_c[(1/6)(\pi/N_c)^2 - (1/120)(\pi/N_c)^4]$. This behavior is shown in the inset of Fig. 2 with the circles depicting the numerical values for T_c and the solid line the asymptotic $\sim 1/N_c$ behavior.

In this section, some of the properties of quantum cluster approaches have been illustrated with an analytically solvable model. However, an accurate treatment of spin systems requires a fully self-consistent numerical calculation of the susceptibility employing some of the techniques discussed below.

II. QUANTUM CLUSTER THEORIES

In this section we provide two derivations of quantum cluster approaches for systems with itinerant quantum degrees of freedom. The locator expansion in Sec. II.A is analogous to the cluster extension of the Weiss mean-field theory developed in the preceding section. Section II.B provides a microscopic derivation based on cluster approximations to the thermodynamic grand potential. A detailed discussion of the nature of quantum cluster approaches and the effective cluster model is presented in Secs. II.D and II.E. Generalizations for broken-symmetry phases, the calculation of susceptibilities, and the application to disordered systems is explained in Secs. II.F, II.G, and II.H and a brief discussion of alternative cluster methods is presented in Sec. II.I.

A. Locator approach to quantum cluster theories

In this section, we derive a number of cluster formalisms for itinerant many-body systems using an analogous approach to that discussed in Sec. I.B for classical spin systems. For simplicity we assume in this section that no symmetry breaking occurs; the treatment of broken-symmetry phases is discussed in Sec. II.F. The basic idea is to write down a locator expansion, i.e., an expansion in space around a finite-size cluster. As with their classical counterparts, quantum cluster theories approximate the lattice problem with many degrees of freedom by an effective cluster problem with few degrees of freedom embedded in an external bath or mean field created from the remaining degrees of freedom. By neglecting correlations that extend beyond the cluster size, one can then formulate a theory in which the lattice system is replaced by an effective cluster embedded in a mean-field host. While the formalism derived here is analogous to the formalism discussed in Sec. I.B for spin systems, there are significant differences. Since we are dealing with itinerant fermions, the theory is built upon the single-particle Green's function instead of the two-particle spin-correlation function, and the mean field is dynamical due to the itinerant nature of the particles.

This derivation is illustrated in the example of the extended single-band Hubbard model,

$$H = \sum_{ij,\sigma} t_{ij} c_{i\sigma}^\dagger c_{j\sigma} + \frac{1}{2} \sum_{ij,\sigma\sigma'} U_{ij}^{\sigma\sigma'} n_{i\sigma} n_{j\sigma'}. \tag{18}$$

Here i and j are lattice site indices, the operators $c_{i\sigma}^\dagger$ ($c_{i\sigma}$) create (destroy) an electron with spin σ on site i, $n_{i\sigma} = c_{i\sigma}^\dagger c_{i\sigma}$ is their corresponding number density, and $U_{ij}^{\sigma\sigma'}$ denotes the Coulomb repulsion between electrons with spins σ and σ' on sites i and j. The hopping amplitude between sites i and j is denoted by t_{ij}, its local contribution $t_{ii} = \epsilon_o$, and its Fourier transform to reciprocal space is the dispersion $\epsilon_{\mathbf{k}}$. In this section we limit the discussion to the regular Hubbard model with a purely local interaction $U_{ij}^{\sigma\sigma'} = U(1 - \delta_{\sigma\sigma'})\delta_{ij}$. The more general case of finite nonlocal interactions $U_{ij}^{\sigma\sigma'}$ for $i \neq j$ is discussed in Sec. II.B.

The central quantity upon which we build the locator expansion is the single-particle thermodynamic Green's function (τ is the imaginary time, T_τ is the corresponding time-ordering operator, $\beta = 1/T$ is the inverse temperature, and $i\omega_n$ are the fermionic Matsubara frequencies),

$$G_{ij,\sigma}(\tau) = -\langle T_\tau c_{i\sigma}(\tau) c_{j\sigma}^\dagger \rangle, \tag{19}$$

$$G_{ij,\sigma}(i\omega_n) = \int_0^\beta d\tau e^{i\omega_n \tau} G_{ij,\sigma}(\tau), \quad \omega_n = \frac{(2n+1)\pi}{\beta}, \tag{20}$$

or, respectively, its analytical continuation $G_{ij,\sigma}(z) = \langle\langle c_{i\sigma}, c_{j\sigma}^\dagger \rangle\rangle_z$ to complex frequencies z.

To set up a suitable notation for cluster schemes, we take the distance between sites as our unit of length and divide the D-dimensional lattice of N sites into a set of finite-size clusters, each with N_c sites of linear size L_c such that $N_c = L_c^D$. We resolve the first Brillouin zone into a corresponding set of reduced zones which we call cells. This notation is illustrated in Fig. 3 for $D=2$ and $N_c=4$ site clusters. We use the coordinate $\tilde{\mathbf{x}}$ to label the origin of the clusters and $\mathbf{X}$ to label the N_c sites within a cluster, so that the site indices of the original lattice are

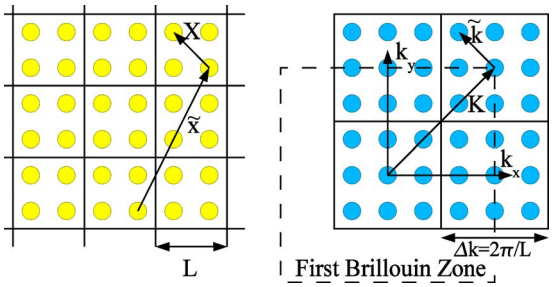

FIG. 3. (Color in online edition) Definition of the coordinates in real (left) and reciprocal (right) space illustrated for $N_c=4$ site clusters. The origin of a cluster is labeled by $\tilde{\mathbf{x}}$, the sites within a cluster by $\mathbf{X}$. The reciprocal space to $\mathbf{X}$ is labeled by $\mathbf{K}$, the wave vectors of the superlattice, i.e., within a cell, by $\tilde{\mathbf{k}}$.

$\mathbf{x}=\mathbf{X}+\tilde{\mathbf{x}}$. The points $\tilde{\mathbf{x}}$ form a superlattice with a reciprocal space labeled by $\tilde{\mathbf{k}}$. The reciprocal space corresponding to the sites $\mathbf{X}$ within a cluster shall be labeled $\mathbf{K}$, with $K_\alpha=n_\alpha(2\pi/L_c)$ and integer n_α. Then the wave vectors in the full Brillouin zone are given by $\mathbf{k}=\mathbf{K}+\tilde{\mathbf{k}}$.

With these conventions, the Fourier transforms of a given function $f(\mathbf{X},\tilde{\mathbf{x}})$ for intracluster and intercluster coordinates are defined as

$$f(\mathbf{X},\tilde{\mathbf{x}})=\frac{N_c}{N}\sum_{\tilde{\mathbf{k}}} e^{i\tilde{\mathbf{k}}\cdot\tilde{\mathbf{x}}}f(\mathbf{X},\tilde{\mathbf{k}}), \tag{21}$$

$$f(\mathbf{X},\tilde{\mathbf{k}})=\sum_{\tilde{\mathbf{x}}} e^{-i\tilde{\mathbf{k}}\cdot\tilde{\mathbf{x}}}f(\mathbf{X},\tilde{\mathbf{x}}), \tag{22}$$

$$f(\mathbf{X},\tilde{\mathbf{k}})=\frac{1}{N_c}\sum_{\mathbf{K}} e^{i(\mathbf{K}+\tilde{\mathbf{k}})\cdot\mathbf{X}}f(\mathbf{K},\tilde{\mathbf{k}}), \tag{23}$$

$$f(\mathbf{K},\tilde{\mathbf{k}})=\sum_{\mathbf{X}} e^{-i(\mathbf{K}+\tilde{\mathbf{k}})\cdot\mathbf{X}}f(\mathbf{X},\tilde{\mathbf{k}}). \tag{24}$$

To separate out the cluster degrees of freedom, the hopping amplitude t and the self-energy Σ (defined from the Green's function via the Dyson equation $G^{-1}=G_0^{-1}-\Sigma$ with the noninteracting Green's function G_0) are split into intracluster and intercluster parts,

$$\mathbf{t}(\tilde{\mathbf{x}}_i-\tilde{\mathbf{x}}_j)=\mathbf{t}_c\delta_{\tilde{\mathbf{x}}_i,\tilde{\mathbf{x}}_j}+\delta\mathbf{t}(\tilde{\mathbf{x}}_i-\tilde{\mathbf{x}}_j), \tag{25}$$

$$\mathbf{\Sigma}(\tilde{\mathbf{x}}_i-\tilde{\mathbf{x}}_j,z)=\mathbf{\Sigma}_c(z)\delta_{\tilde{\mathbf{x}}_i,\tilde{\mathbf{x}}_j}+\delta\mathbf{\Sigma}(\tilde{\mathbf{x}}_i-\tilde{\mathbf{x}}_j,z). \tag{26}$$

All the quantities are $N_c\times N_c$ matrices in the cluster sites, $\mathbf{t}_c=\mathbf{t}(\tilde{\mathbf{x}}=0)$ and $\mathbf{\Sigma}_c(z)=\mathbf{\Sigma}(\tilde{\mathbf{x}}=0,z)$ are the intracluster hopping and self-energy, while $\delta\mathbf{t}(\tilde{\mathbf{x}})$ and $\delta\mathbf{\Sigma}(\tilde{\mathbf{x}},z)$ are the corresponding intercluster quantities which are only finite for $\tilde{\mathbf{x}}\neq 0$.

1. Cluster perturbation theory and cellular dynamical mean-field theory

With these definitions we write the Green's function using a locator expansion, an expansion in $\delta\mathbf{t}$ and $\delta\mathbf{\Sigma}$ around the cluster limit. In matrix notation in the N_c cluster sites it reads

$$\mathbf{G}(\tilde{\mathbf{x}}_i-\tilde{\mathbf{x}}_j,z)=\mathbf{g}(z)\delta_{\tilde{\mathbf{x}}_i\tilde{\mathbf{x}}_j}+\mathbf{g}(z)\sum_l[\delta\mathbf{t}(\tilde{\mathbf{x}}_i-\tilde{\mathbf{x}}_l)+\delta\mathbf{\Sigma}(\tilde{\mathbf{x}}_i-\tilde{\mathbf{x}}_l,z)]\mathbf{G}(\tilde{\mathbf{x}}_l-\tilde{\mathbf{x}}_j,z), \tag{27}$$

where the $N_c\times N_c$ matrix

$$\mathbf{g}(z)=[(z+\mu)\mathbb{1}-\mathbf{t}_c-\mathbf{\Sigma}_c(z)]^{-1} \tag{28}$$

is the Green's function of the cluster decoupled from the remainder of the system (μ is the chemical potential). Since translational invariance in the superlattice $\tilde{\mathbf{x}}$ is preserved, this expression may be simplified by Fourier transforming the intercluster coordinates to give

$$\mathbf{G}(\tilde{\mathbf{k}},z)=\mathbf{g}(z)+\mathbf{g}(z)[\delta\mathbf{t}(\tilde{\mathbf{k}})+\delta\mathbf{\Sigma}(\tilde{\mathbf{k}},z)]\mathbf{G}(\tilde{\mathbf{k}},z). \tag{29}$$

The central approximation that unites all cluster formalisms is to truncate the self-energy to the cluster by neglecting $\delta\mathbf{\Sigma}$ to arrive at

$$\mathbf{G}(\tilde{\mathbf{k}},z)=\mathbf{g}(z)+\mathbf{g}(z)\delta\mathbf{t}(\tilde{\mathbf{k}})\mathbf{G}(\tilde{\mathbf{k}},z)=[\mathbf{g}^{-1}(z)-\delta\mathbf{t}(\tilde{\mathbf{k}})]^{-1}. \tag{30}$$

As we discuss in Sec. II.D.1, this approximation corresponds to truncating the potential energy to the cluster.

The remaining self-energy term $\mathbf{\Sigma}_c(z)$ implicitly contained in the propagator $\mathbf{g}(z)$ in Eq. (30) is restricted to the cluster degrees of freedom. Hence it can be calculated nonperturbatively in an effective cluster model as a functional $\mathbf{\Sigma}_c(z)=\mathcal{F}[\bar{\mathbf{G}}(z)]$, where

$$\bar{\mathbf{G}}(z)=\frac{N_c}{N}\sum_{\tilde{\mathbf{k}}}\mathbf{G}(\tilde{\mathbf{k}},z) \tag{31}$$

is the $\tilde{\mathbf{k}}$-averaged or coarse-grained $\mathbf{G}(\tilde{\mathbf{k}},z)$, i.e., the Green's function restricted to the cluster. As discussed in the next section this approximation is consistent with neglecting intercluster momentum conservation, i.e., neglecting the phase factors $e^{i\tilde{\mathbf{k}}\cdot\tilde{\mathbf{x}}}$ on the vertices of the self-energy diagrams.

Using the expression (30) for the lattice Green's function and the fact that $\mathbf{g}(z)$ does not depend on $\tilde{\mathbf{k}}$, the coarse-grained Green's function $\bar{\mathbf{G}}$ can be written as

$$\bar{\mathbf{G}}(z)=[\mathbf{g}^{-1}(z)-\mathbf{\Gamma}(z)]^{-1}, \tag{32}$$

with a hybridization function $\mathbf{\Gamma}$ defined by

$$\mathbf{\Gamma}(z)=\left[\mathbb{1}+\frac{N_c}{N}\sum_{\tilde{\mathbf{k}}}\delta\mathbf{t}(\tilde{\mathbf{k}})\mathbf{G}(\tilde{\mathbf{k}},z)\right]^{-1}\times\left[\frac{N_c}{N}\sum_{\tilde{\mathbf{k}}}\delta\mathbf{t}(\tilde{\mathbf{k}})\mathbf{G}(\tilde{\mathbf{k}},z)\delta\mathbf{t}(\tilde{\mathbf{k}})\right]. \tag{33}$$

Its physical content is that of an effective amplitude for fermionic hopping processes from the cluster into the host and back again into the cluster. The denominator in Eq. (33) is a correction that excludes the cluster from the effective medium. $\mathbf{\Gamma}(z)$ thus plays an analogous role to

that of the internal magnetic field in mean-field approximations of spin systems. However, due to the itinerant character of the fermionic degrees of freedom, it is a dynamical quantity.

Both the cluster perturbation theory and the cellular DMFT formalisms may be defined at this point. A self-consistent set of equations is formed from $\mathbf{G}$ as a functional of $\mathbf{\Sigma}_c$ using Eq. (30) together with Eq. (28), and with an appropriate choice of a cluster solver (see Sec. III), $\mathbf{\Sigma}_c$ as a functional of $\bar{\mathbf{G}}$. In the cellular DMFT approximation the hybridization $\mathbf{\Gamma}$ is determined self-consistently with Eq. (33), i.e., from the translational invariance of the superlattice. The resulting self-consistency cycle is discussed in Sec. II.C.2. The cluster perturbation theory formalism is obtained when $\mathbf{\Gamma}$ is neglected. The Green's function $\mathbf{g}(z)$ then becomes the Green's function of an isolated cluster and the cluster perturbation theory result for the lattice Green's function is obtained immediately via Eq. (30) without self-consistency. Thus the renormalization of the cluster degrees of freedom due to the coupling to the host described by $\mathbf{\Gamma}$ is neglected in the cluster perturbation theory but included in the cellular DMFT formalism.

2. Dynamical cluster approximation

The dynamical cluster approximation (DCA) formalism is motivated by the need to restore translational invariance within the cluster. Since the intercluster hopping $\delta\mathbf{t}(\tilde{\mathbf{k}})$ is finite for sites on the surface of the cluster and zero for bulk sites, only surface sites hybridize with the host. Hence translational invariance with respect to the cluster sites $\mathbf{X}$ is violated. The cause of this violation can be seen by representing the hopping integral $\mathbf{t}(\tilde{\mathbf{k}})$ as the intracluster Fourier transform of the dispersion $\epsilon_{\mathbf{K}+\tilde{\mathbf{k}}}$ using Eq. (23),

$$[\mathbf{t}(\tilde{\mathbf{k}})]_{\mathbf{X}_i\mathbf{X}_j} = \frac{1}{N_c}\sum_{\mathbf{K}} e^{i(\mathbf{K}+\tilde{\mathbf{k}})\cdot(\mathbf{X}_i-\mathbf{X}_j)}\epsilon_{\mathbf{K}+\tilde{\mathbf{k}}}. \tag{34}$$

The violation of translational symmetry is caused by the phase factors $e^{i\tilde{\mathbf{k}}\cdot(\mathbf{X}_i-\mathbf{X}_j)}$ associated with the superlattice wave vectors $\tilde{\mathbf{k}}$. Thus translational symmetry can be restored by using the Fourier transform

$$[\mathbf{t}_{\mathrm{DCA}}(\tilde{\mathbf{k}})]_{\mathbf{X}_i\mathbf{X}_j} = [\mathbf{t}(\tilde{\mathbf{k}})]_{\mathbf{X}_i\mathbf{X}_j} e^{-i\tilde{\mathbf{k}}\cdot(\mathbf{X}_i-\mathbf{X}_j)} = \frac{1}{N_c}\sum_{\mathbf{K}} e^{i\mathbf{K}\cdot(\mathbf{X}_i-\mathbf{X}_j)}\epsilon_{\mathbf{K}+\tilde{\mathbf{k}}}. \tag{35}$$

Since $\mathbf{t}_{\mathrm{DCA}}$ is fully cyclic in the cluster sites, the DCA intracluster and intercluster hopping integrals can be written as cluster Fourier transforms

$$[\mathbf{t}_{c,\mathrm{DCA}}]_{\mathbf{X}_i\mathbf{X}_j} = \frac{1}{N_c}\sum_{\mathbf{K}} e^{i\mathbf{K}\cdot(\mathbf{X}_i-\mathbf{X}_j)}\bar{\epsilon}_{\mathbf{K}}, \tag{36}$$

$$[\delta\mathbf{t}_{\mathrm{DCA}}(\tilde{\mathbf{k}})]_{\mathbf{X}_i\mathbf{X}_j} = \frac{1}{N_c}\sum_{\mathbf{K}} e^{i\mathbf{K}\cdot(\mathbf{X}_i-\mathbf{X}_j)}\delta t(\mathbf{K}+\tilde{\mathbf{k}}) \tag{37}$$

with

$$\bar{\epsilon}_{\mathbf{K}} = \frac{N_c}{N}\sum_{\tilde{\mathbf{k}}} \epsilon_{\mathbf{K}+\tilde{\mathbf{k}}}, \tag{38}$$

$$\delta t(\mathbf{K}+\tilde{\mathbf{k}}) = \epsilon_{\mathbf{K}+\tilde{\mathbf{k}}} - \bar{\epsilon}_{\mathbf{K}}. \tag{39}$$

Since these hopping integrals retain translational invariance within the cluster, the cluster self-energy $\mathbf{\Sigma}_c$ and hybridization function $\mathbf{\Gamma}$ are translationally invariant. The lattice Green's function, Eq. (30), hence becomes diagonal in cluster Fourier space,

$$G(\mathbf{K}+\tilde{\mathbf{k}},z) = g(\mathbf{K},z) + g(\mathbf{K},z)\,\delta t(\mathbf{K}+\tilde{\mathbf{k}})G(\mathbf{K}+\tilde{\mathbf{k}},z) = \frac{1}{g^{-1}(\mathbf{K},z) - \delta t(\mathbf{K}+\tilde{\mathbf{k}})}, \tag{40}$$

with the Green's function decoupled from the host,

$$g(\mathbf{K},z) = [z - \bar{\epsilon}_{\mathbf{K}} + \mu - \Sigma_c(\mathbf{K},z)]^{-1}. \tag{41}$$

Along the lines presented above, the DCA cluster self-energy $\Sigma_c(\mathbf{K},z)$ is calculated as a functional of the coarse-grained Green's function,

$$\bar{G}(\mathbf{K},z) = \frac{N_c}{N}\sum_{\tilde{\mathbf{k}}} G(\mathbf{K}+\tilde{\mathbf{k}},z) = \frac{1}{g^{-1}(\mathbf{K},z) - \Gamma(\mathbf{K},z)}, \tag{42}$$

which defines the hybridization function

$$\Gamma(\mathbf{K},z) = \frac{\frac{N_c}{N}\sum_{\tilde{\mathbf{k}}} \delta t^2(\mathbf{K}+\tilde{\mathbf{k}})G(\mathbf{K}+\tilde{\mathbf{k}},z)}{1+\frac{N_c}{N}\sum_{\tilde{\mathbf{k}}} \delta t(\mathbf{K}+\tilde{\mathbf{k}})G(\mathbf{K}+\tilde{\mathbf{k}},z)}. \tag{43}$$

The self-consistent procedure for determining the DCA cluster self-energy $\Sigma_c(\mathbf{K},z)$ is analogous to that for cellular DMFT and is discussed in detail in Sec. II.C.2. It is also possible to formulate an analog to the cluster perturbation formalism based on the dynamical cluster approximation. The Green's function $g(\mathbf{K},z)$ then becomes the Green's function of an isolated periodic cluster with coarse-grained dispersion [Eq. (38)] and interactions. The result of this combined approach for the lattice Green's function is obtained immediately via Eq. (40) without self-consistency.

B. Diagrammatic approach to quantum cluster theories

In this section we provide a microscopic derivation of the cluster perturbation theory, cellular DMFT, and DCA formalisms based on different cluster approximations to the diagrammatic expression for the grand potential. The advantage of this approach is that it allows us to apply almost all of the diagrammatic technology that has been developed over the past several decades to a new set of cluster formalisms. Furthermore we are

able to assess the quality of these approximations with respect to their thermodynamic properties. The most significant disadvantage is that the approach developed here applies only to systems that are amenable to a diagrammatic expansion.

The following ideas will be illustrated on the extended Hubbard model, Eq. (18). We use the notation introduced in Sec. II.A, Fig. 3, i.e., the cluster centers are denoted by $\tilde{\mathbf{x}}$ and sites within the cluster by $\mathbf{X}$. The wave vectors $\tilde{\mathbf{k}}$ and $\mathbf{K}$ are their respective conjugates.

Baym and Kadanoff (1961; see also Baym, 1962) showed that thermodynamically consistent approximations may be constructed by requiring that the single-particle self-energy $\mathbf{\Sigma}$ fulfill

$$\mathbf{G}_0^{-1} - \mathbf{G}^{-1} = \Sigma = \frac{\delta\Phi[\mathbf{G}]}{\delta\mathbf{G}}. \tag{44}$$

That is, we require that the self-energy be expressible as a functional derivative of the Baym-Kadanoff Φ functional with respect to the Green's function $\mathbf{G}$ and that the approximation be self-consistent. The Baym-Kadanoff generating functional $\Phi[\mathbf{G},\mathbf{U}]$ is diagrammatically defined as a skeletal graph sum over all distinct, compact, closed, connected diagrams constructed from the Green's function $\mathbf{G}$ and the interaction $\mathbf{U}$. Thus the diagrammatic form of the approximate generating functional together with an appropriate set of Dyson and Bethe-Salpeter equations completely defines the diagrammatic formalism.

As described in standard textbooks (Abrikosov *et al.*, 1963) the relation between the grand potential functional Ω and the Φ functional is expressed in terms of the linked cluster expansion as

$$\Omega[\mathbf{G},\mathbf{U}] = -k_B T\{\Phi[\mathbf{G},\mathbf{U}] - \mathrm{Tr}\ln(-\mathbf{G}) - \mathrm{Tr}(\mathbf{\Sigma}\mathbf{G})\}, \tag{45}$$

where the trace indicates summation over cluster sites $\mathbf{X}$, superlattice wave vectors $\tilde{\mathbf{k}}$, frequency, and spin. With the condition (44), the grand potential is stationary with respect to $\mathbf{G}$, i.e., $\delta\Omega/\delta\mathbf{G}=0$. Such approximations are thermodynamically consistent, i.e., observables calculated from the Green's function $\mathbf{G}$ agree with those calculated as derivatives of the grand potential Ω. As shown by Baym (1962), the requirement (44) together with momentum and energy conservation at the vertices also assures that the approximation preserves Ward identities, i.e., satisfies conservation laws.

While prominent examples of conserving approximations such as the Hartree-Fock theory and the fluctuation-exchange approximation (Bickers *et al.*, 1989) typically restrict the diagrams in Φ to a certain subclass, usually the lowest-order diagrams in U, quantum cluster approaches go a different route: They reduce the infinite number of degrees of freedom over which Φ is evaluated to those of a finite-size cluster. In contrast to perturbative approaches, however, all classes of diagrams are kept.

1. Cluster perturbation theory

The simplest way to reduce the degrees of freedom in $\Phi[\mathbf{G}]$ is to replace the full-lattice Green's function $\mathbf{G}(\tilde{\mathbf{k}},z)$ by the Green's function $\mathbf{g}(z)=[(z+\mu)\mathbb{1}-\mathbf{t}_c-\mathbf{\Sigma}_c(z)]^{-1}$ of an isolated cluster of size N_c. Consequently the self-energy $\mathbf{\Sigma}_c=\delta\Phi[\mathbf{g}]/\delta\mathbf{g}$ obtained from Φ is the self-energy of an isolated finite-size cluster. This, however, leads to a theory that lacks self-consistency. Moreover, one has to make the *ad hoc* assumption that the lattice self-energy is identical to that obtained from the cluster, $\mathbf{\Sigma}_c$. The left-hand side of Eq. (44) then yields the form for the lattice Green's function

$$\mathbf{G}(\tilde{\mathbf{k}},z) = [\mathbf{G}_0^{-1}(\tilde{\mathbf{k}},z) - \mathbf{\Sigma}_c(z)]^{-1}, \tag{46}$$

where all the quantities are $N_c\times N_c$ matrices in the cluster sites. Since the bare-lattice Green's function is given by $\mathbf{G}_0(\tilde{\mathbf{k}},z)=[(z+\mu)\mathbb{1}-\mathbf{t}(\tilde{\mathbf{k}})]^{-1}$ and the hopping can be split into intracluster and intercluster parts [see Eq. (25)], $\mathbf{t}(\tilde{\mathbf{k}})=\mathbf{t}_c+\delta\mathbf{t}(\tilde{\mathbf{k}})$, we obtain

$$\mathbf{G}(\tilde{\mathbf{k}},z) = [\mathbf{g}^{-1}(z) - \delta\mathbf{t}(\tilde{\mathbf{k}})]^{-1}. \tag{47}$$

This form was derived in Sec. II.A from the locator expansion Eq. (30) by ignoring the hybridization $\mathbf{\Gamma}$ between cluster and host. According to Eq. (46), the cluster perturbation theory can be viewed as the approximation obtained by replacing the self-energy in the Dyson equation of the lattice Green's function $\mathbf{G}$ by the self-energy of an isolated cluster $\mathbf{\Sigma}_c$. This idea was first developed by Gros and Valenti (1994) and applied to the three-band Hubbard model. A different approach to deriving the cluster perturbation theory was taken by Pairault *et al.* (1998; see also Pairault *et al.*, 2000; Sénéchal *et al.*, 2002). They showed that Eq. (47) is obtained as the leading-order term in a strong-coupling expansion in the hopping $\delta\mathbf{t}$ between sites on different clusters.

According to the above derivation, the cluster Green's function $\mathbf{g}$ is to be calculated on a cluster with open boundary conditions. Since the intercluster hopping $\delta\mathbf{t}$ is treated perturbatively, i.e., differently from the intracluster hopping $\mathbf{t}_c$, translational invariance for sites $\mathbf{X}$ in the cluster is violated. Consequently, we have as a generalization of the Fourier transform Eq. (24), omitting the frequency dependence for convenience,

$$G(\mathbf{k},\mathbf{k}') = \frac{1}{N_c}\sum_{\mathbf{Q}}\sum_{\mathbf{X}_i,\mathbf{X}_j} e^{-i\mathbf{k}\cdot\mathbf{X}_i}G(\mathbf{X}_i,\mathbf{X}_j,\mathbf{k})e^{i\mathbf{k}'\cdot\mathbf{X}_j} \times\delta(\mathbf{k}-\mathbf{k}'-\mathbf{Q}), \tag{48}$$

where $\mathbf{k}$ and $\mathbf{k}'$ are wave vectors in the full Brillouin zone and $\mathbf{Q}$ is a wave vector in the cluster reciprocal space.[1] To restore translational invariance in the full-lattice Green's function, the cluster perturbation theory

[1]Here we used the relation $\mathbf{G}(\tilde{\mathbf{k}})=\mathbf{G}(\mathbf{k})$, which follows from Eq. (22) when $\mathbf{k}$ is replaced by $\mathbf{k}=\tilde{\mathbf{k}}+\mathbf{K}$.

approximates $G(\mathbf{k},\mathbf{k}')$ by the $\mathbf{Q}=0$ contribution to obtain

$$G_{\mathrm{CPT}}(\mathbf{k}) = \frac{1}{N_c}\sum_{\mathbf{X}_i,\mathbf{X}_j} e^{-i\mathbf{k}\cdot(\mathbf{X}_i-\mathbf{X}_j)} G(\mathbf{X}_i,\mathbf{X}_j,\mathbf{k}) \tag{49}$$

as the translationally invariant propagator used to calculate spectra. With this approximation, the cluster perturbation theory provides a very economical method for calculating the lattice Green's function of an infinite-size ($N\to\infty$) Hubbard-like model from the Green's function (or equivalently self-energy) of an isolated cluster of finite size $N_c \ll N$. From $G_{\mathrm{CPT}}(\mathbf{k})$ one can calculate single-particle quantities such as photoemission spectra, kinetic and potential energies, double occupancy, etc.

To reduce the numerical cost, it was suggested to use periodic boundary conditions on the cluster by adding the appropriate hopping terms to the intracluster hopping $\mathbf{t}_c$ and subtracting them from the intercluster hopping $\delta\mathbf{t}$ (Dahnken *et al.*, 2002). However, as discussed by Sénéchal *et al.* (2002), periodic boundary conditions lead to less accurate spectra for the 1D Hubbard model than open boundary conditions. This *a posteriori* argument for open boundary conditions is substantiated by calculations within Potthoff's self-energy functional approach (see Sec. II.I) which show that the grand potential of the system is only stationary in the limit of open boundary conditions (Potthoff *et al.*, 2003).

2. Cellular DMFT

A superior approximation may be obtained if, instead of the isolated-cluster Green's function $\mathbf{g}$, the full-lattice Green's function $\mathbf{G}$ restricted to cluster sites is used to evaluate the functional Φ. This approximation can be motivated microscopically by approximating the momentum conservation on internal vertices in the diagrams defining Φ, which is described by the Laue function

$$\Delta = \sum_{\mathbf{x}} e^{i\mathbf{x}\cdot(\mathbf{k}_1+\mathbf{k}_2+\cdots,-\mathbf{k}_1'-\mathbf{k}_2'-\cdots)} = N\delta_{\mathbf{k}_1+\mathbf{k}_2+\cdots,\mathbf{k}_1'+\mathbf{k}_2'+\cdots}. \tag{50}$$

Here $\mathbf{k}_1,\mathbf{k}_2$ are the momenta entering the vertex and $(\mathbf{k}_1',\mathbf{k}_2')$ the momenta leaving it. Müller-Hartmann (1989b) showed that the DMFT may be derived by completely ignoring momentum conservation at each internal vertex and setting $\Delta=1$. Then one may freely sum over all of the internal momentum labels, and the Green's functions in the diagrams are replaced by the local Green's function $G_{ii}=1/N\Sigma_{\mathbf{k}}G(\mathbf{k})$.

The cellular DMFT and dynamical cluster approximation techniques may also be defined by their respective approximations to the Laue function. In the cellular DMFT the Laue function is approximated by

$$\Delta_{\mathrm{CDMFT}} = \sum_{\mathbf{X}} e^{i\mathbf{X}\cdot(\mathbf{K}_1+\tilde{\mathbf{k}}_1+\mathbf{K}_2+\tilde{\mathbf{k}}_2+\cdots-\mathbf{K}_1'-\tilde{\mathbf{k}}_1'-\mathbf{K}_2'-\tilde{\mathbf{k}}_2'-\cdots)}. \tag{51}$$

Thus the cellular DMFT omits the phase factors $e^{i\tilde{\mathbf{k}}\cdot\tilde{\mathbf{x}}}$ resulting from the position of the cluster in the original lattice, but keeps the phase factors $e^{i\tilde{\mathbf{k}}\cdot\tilde{\mathbf{X}}}$. The latter are directly responsible for the violation of translational invariance. As in the coherent-potential approximation (CPA), all quantities in the cellular DMFT are functions of two cluster momenta, $\mathbf{K}_1,\mathbf{K}_2$, or two sites, $\mathbf{X}_1$, $\mathbf{X}_2$, respectively.

If the cellular DMFT Laue function Eq. (51) is applied to diagrams in Φ, each Green's-function leg is replaced by the cellular DMFT coarse-grained Green's function (the frequency dependence is dropped for notational convenience)

$$\begin{aligned}\bar{G}(\mathbf{X}_1,\mathbf{X}_2) &= G(\mathbf{X}_1,\mathbf{X}_2;\tilde{\mathbf{x}}=0)\\ &= \frac{1}{N^2}\sum_{\substack{\mathbf{K}_1,\mathbf{K}_2\\ \tilde{\mathbf{k}}_1,\tilde{\mathbf{k}}_2}} e^{i(\mathbf{K}_1+\tilde{\mathbf{k}}_1)\cdot\mathbf{X}_1} G(\mathbf{K}_1,\mathbf{K}_2;\tilde{\mathbf{k}}_1,\tilde{\mathbf{k}}_2) e^{-i(\mathbf{K}_2+\tilde{\mathbf{k}}_2)\cdot\mathbf{X}_2}\\ &= \frac{N_c^2}{N^2}\sum_{\tilde{\mathbf{k}}_1,\tilde{\mathbf{k}}_2} G(\mathbf{X}_1,\mathbf{X}_2,\tilde{\mathbf{k}}_1,\tilde{\mathbf{k}}_2),\end{aligned} \tag{52}$$

or in matrix notation for the cluster sites $\mathbf{X}_1$ and $\mathbf{X}_2$,

$$\bar{\mathbf{G}}(z) = \frac{N_c}{N}\sum_{\tilde{\mathbf{k}}} \mathbf{G}(\tilde{\mathbf{k}},z), \tag{53}$$

since $\mathbf{G}$ is diagonal in $\tilde{\mathbf{k}}_1,\tilde{\mathbf{k}}_2$ due to the translational invariance of the superlattice. Similarly each interaction line is replaced by its coarse-grained result (we suppressed the spin dependence for notational convenience),

$$\bar{\mathbf{U}} = \frac{N_c}{N}\sum_{\tilde{\mathbf{k}}} \mathbf{U}(\tilde{\mathbf{k}}). \tag{54}$$

The summations over the cluster sites $\mathbf{X}$ within each diagram remain to be performed. As a consequence of coarse graining the propagators in Φ, the cellular DMFT self-energy

$$\bar{\mathbf{\Sigma}}_c(z) = \frac{\delta\Phi[\bar{\mathbf{G}}(z),\bar{\mathbf{U}}]}{\delta\bar{\mathbf{G}}(z)} \tag{55}$$

is restricted to cluster sites and consequently independent of $\tilde{\mathbf{k}}$. Note that by definition, $\bar{\mathbf{G}}$ and $\bar{\mathbf{U}}$ are truncated outside the cluster, i.e., if the interaction $\mathbf{U}$ is nonlocal, $\bar{\mathbf{U}}$ includes only interactions within, but not between, clusters.

The cellular DMFT estimate of the lattice grand potential is obtained by substituting the cellular DMFT approximate generating functional $\Phi[\bar{\mathbf{G}},\bar{\mathbf{U}}]$ into Eq. (45). From the condition that the grand potential be stationary with respect to the lattice Green's function, $\delta\Omega/\delta\mathbf{G}=0$, one obtains a relation between the lattice self-energy and the cluster self-energy

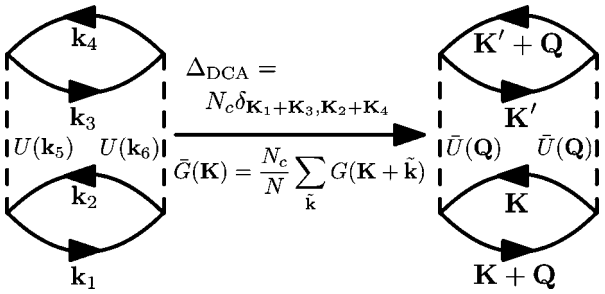

FIG. 4. A second-order term in the generating functional Φ of the Hubbard model. The dashed line represents the interaction U, and the solid line on the left-hand side (right-hand side) the lattice (coarse-grained) single-particle Green's function G ($\bar{G}$). With the dynamical cluster approximation (DCA) Laue function, the wave vectors collapse onto those of the cluster and each lattice Green's function is replaced by its coarse-grained average.

$$\Sigma(\mathbf{K}_1,\mathbf{K}_2;\tilde{\mathbf{k}}_1,\tilde{\mathbf{k}}_2) = \sum_{\mathbf{X}_1,\mathbf{X}_2} e^{-i(\mathbf{K}_1+\tilde{\mathbf{k}}_1)\cdot\mathbf{X}_1}\Sigma_c(\mathbf{X}_1,\mathbf{X}_2)e^{i(\mathbf{K}_2+\tilde{\mathbf{k}}_2)\cdot\mathbf{x}_2}. \tag{56}$$

With Eq. (52) the left-hand side of Eq. (44) then becomes the coarse-graining relation,

$$\bar{\mathbf{G}}(z) = \frac{N_c}{N}\sum_{\tilde{\mathbf{k}}} [\mathbf{G}_0^{-1}(\tilde{\mathbf{k}},z) - \boldsymbol{\Sigma}_c(z)]^{-1} \tag{57}$$

with the bare Green function $\mathbf{G}_0(z)=[(z+\mu)\mathbb{1}-\mathbf{t}(\tilde{\mathbf{k}})]^{-1}$.

3. Dynamical cluster approximation

In the DCA the phase factors $e^{i\tilde{\mathbf{k}}\cdot\mathbf{X}}$ in Eq. (51) are omitted too, so that the approximation to the Laue function becomes

$$\Delta_{\mathrm{DCA}} = N_c\delta_{\mathbf{K}_1+\mathbf{K}_2+\cdots,\mathbf{K}_1'+\mathbf{K}_2'+\cdots} \tag{58}$$

and the Green's-function legs in Φ are replaced by the coarse-grained Green's function

$$\bar{G}(\mathbf{K},z) = \frac{N_c}{N}\sum_{\tilde{\mathbf{k}}} G(\mathbf{K}+\tilde{\mathbf{k}},z), \tag{59}$$

since Green's functions can be freely summed over the N/N_c wave vectors $\tilde{\mathbf{k}}$ of the superlattice. Similarly, the interactions are replaced by the DCA coarse-grained interaction

$$\bar{U}(\mathbf{K}) = \frac{N_c}{N}\sum_{\tilde{\mathbf{k}}} U(\mathbf{K}+\tilde{\mathbf{k}}). \tag{60}$$

As with the cellular DMFT, coarse graining the interaction reduces the effect of nonlocal interactions to within the cluster. This collapse of the diagrams in the Φ functional onto those of an effective cluster problem is illustrated in Fig. 4 for a second-order contribution.

The resulting compact graphs are functionals of the coarse-grained Green's function $\bar{G}(\mathbf{K})$ and interaction $\bar{U}(\mathbf{K})$ and thus depend on the cluster momenta $\mathbf{K}$ only. For example, when $N_c=1$, only the local part of the interaction survives the coarse graining. As with the cellular DMFT, within the DCA it is important that both the interaction and the Green's function be coarse grained (Hettler *et al.*, 2000). As a consequence of the collapse of the Φ diagrams, the DCA self-energy

$$\Sigma_c(\mathbf{K},z) = \frac{\delta\Phi[\bar{G}(\mathbf{K},z),\bar{U}]}{\delta\bar{G}(\mathbf{K},z)} \tag{61}$$

depends only on the cluster momenta $\mathbf{K}$.

To obtain the DCA estimate of the lattice grand potential, we substitute the approximate generating functional $\Phi[\bar{G}(\mathbf{K}),\bar{U}(\mathbf{K})]$ into Eq. (45). The grand potential is stationary with respect to $\mathbf{G}$,

$$\frac{\delta\Omega[\bar{G}(\mathbf{K}),\bar{U}(\mathbf{K})]}{\delta G(\mathbf{k})} = \Sigma_c(\mathbf{K}) - \Sigma(\mathbf{k}) = 0, \tag{62}$$

when $\Sigma(\mathbf{k})=\Sigma_c(\mathbf{K})$ is used as the approximation for the lattice self-energy corresponding to $\Phi[\bar{G}(\mathbf{K}),\bar{U}]$. The self-consistency condition on the left-hand side of Eq. (44) then becomes the coarse-graining relation,

$$\bar{G}(\mathbf{K},z) = \frac{N_c}{N}\sum_{\tilde{\mathbf{k}}} [G_0^{-1}(\mathbf{K}+\tilde{\mathbf{k}}) - \Sigma_c(\mathbf{K},z)]^{-1} \tag{63}$$

with the bare Green's function $G_0(\mathbf{K}+\tilde{\mathbf{k}},z)=[z-\epsilon_{\mathbf{K}+\tilde{\mathbf{k}}}+\mu]^{-1}$.

C. Technical details

1. Cluster selection

In this section, we describe a sensible scheme for selecting the cluster geometries. For cluster perturbation theory and the cellular DMFT, little is presently known about the effect of different cluster geometries. In contrast, for the DCA, much can be learned from the simulations of finite-size systems, where periodic boundary conditions are typically used. Many different periodic cluster geometries may be used to tile the full lattice. Care should be taken to ensure that the lattice point-group symmetry and, more significantly, the configuration and number of neighbors in each near-neighbor shell of the clusters do not differ too greatly from those of the original lattice (Betts *et al.*, 1996; Jarrell, Maier, Huscroft, and Moukouri, 2001). Initially, DCA calculations were performed with clusters that had the same geometry as the lattice; i.e., for a square lattice, square clusters were used; although the high-symmetry direction of the clusters need not point along those of the lattice (Jarrell, Maier, Huscroft, and Moukouri, 2001).

However, Haan *et al.* (1992) showed that certain parallelogram clusters could also produce good results in finite-size exact diagonalization calculations. Parallelogram clusters offer the distinct advantage of many more possible tilings, so that these clusters may be selected for quality. Betts *et al.* greatly expanded upon this idea, and

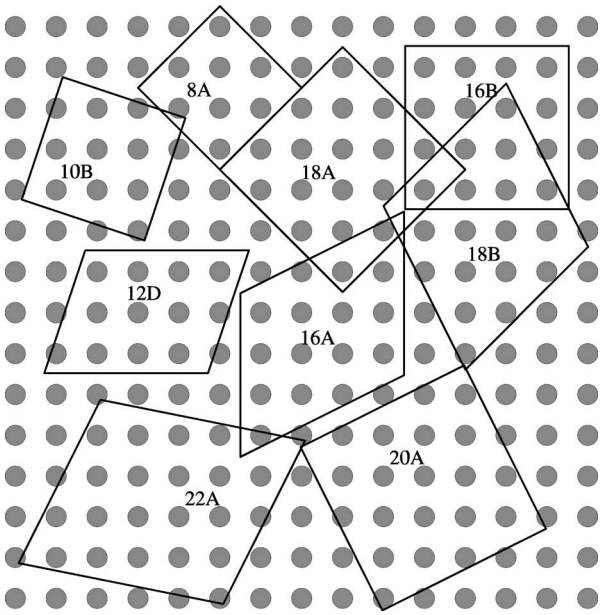

FIG. 5. The best bipartite periodic clusters with $N_c \leqslant 22$ for the square lattice. All are used for scaling, with the exception of 16*B*, which is highly imperfect. From Betts *et al.*, 1999.

developed a grading scheme to determine which clusters should be used (Betts *et al.*, 1996, 1999). Their main qualification is the imperfection of the near-neighbor shells.

For an infinite square lattice, which is by definition perfect, there are $4n$ vertices that are in the nth near-neighbor shell. A topologically perfect cluster would have a complete set of independent neighbors for each of the $j-1$ neighbor shells, fewer than $4j$ neighbors in the jth shell, and none in further shells. When performing finite-size scaling calculations with these clusters, Betts *et al.* (1996, 1999) find that perfect clusters generally produce results that fall on the scaling curve, while imperfect clusters generally produce results that lie off the scaling curve. The squareness of the cluster is also relevant, as are other properties. For example, the calculation of antiferromagnetism requires bipartite clusters. Those with $8 \leqslant N_c \leqslant 22$ are shown in Fig. 5. These clusters are perfect, except for 16*B*, which is highly imperfect. Because of this, and the fact that it is equivalent to a four-dimensional hypercube, it produced poor results in scaling calculations. Clusters with $N_c < 8$ were rejected since they do not have independent neighbors. A cluster with $N_c = 4$ has the additional shortcoming of being equivalent to a one-dimensional chain.

More complex clusters may be generated by the method of Lyness *et al.* (1991), who showed that any finite lattice in dimension D may be tiled by an upper-triangular matrix formulation. Their method may be used to automate the generation of clusters, and has been used to develop improved finite-sized scaling methods for simple cubic (Betts and Stewart, 1997), face-centered-cubic (Stewart *et al.*, 1997), and body-centered-cubic (Betts *et al.*, 1998) lattices.

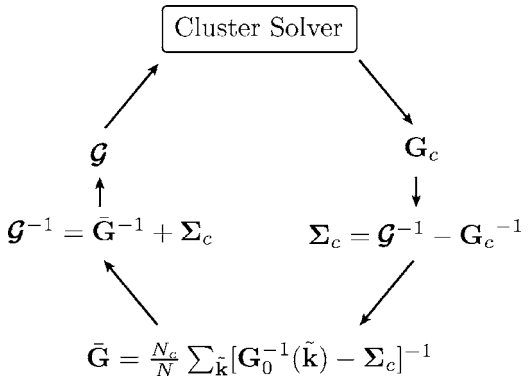

FIG. 6. Sketch of the cellular DMFT and DCA embedded-cluster algorithms. The iteration starts with computing the coarse-grained Green's function $\bar{\mathbf{G}}$ using an initial guess for the cluster self-energy $\mathbf{\Sigma}_c$. The cluster excluded Green's function $\mathcal{G}$ is then used to define the effective cluster problem which yields a new estimate of $\mathbf{\Sigma}_c$.

2. Self-consistency scheme

The coarse-graining equations [Eqs. (63) and (57) for the DCA and cellular DMFT, respectively] together with a suitable cluster solver, form a nonlinear set of equations that have to be solved self-consistently to determine the cluster self-energy. For cluster solvers that sum up all diagrams of $\mathbf{\Sigma}_c$, in contrast to a skeletal expansion of $\mathbf{\Sigma}_c$, an additional step is necessary. In order not to overcount self-energy diagrams, $\mathbf{\Sigma}_c$ is to be calculated as a functional of the corresponding bare propagator to $\bar{\mathbf{G}}$, the excluded-cluster Green's function,

$$\mathcal{G}(z) = [\bar{\mathbf{G}}^{-1}(z) + \mathbf{\Sigma}_c(z)]^{-1}. \tag{64}$$

This equation[2] unambiguously defines the self-consistent iteration procedure illustrated in Fig. 6:

(i) the iteration is started by guessing an initial cluster self-energy $\mathbf{\Sigma}_c(z)$, usually zero or the result from second-order perturbation theory, to

(ii) calculate the coarse-grained quantities

$$\bar{\mathbf{G}}(z) = \frac{N_c}{N} \sum_{\tilde{\mathbf{k}}} [\mathbf{G}_0^{-1}(\tilde{\mathbf{k}}, z) - \mathbf{\Sigma}_c(z)]^{-1},$$

$$\bar{\mathbf{U}} = \frac{N_c}{N} \sum_{\tilde{\mathbf{k}}} \mathbf{U}(\tilde{\mathbf{k}}).$$

[2] A unifying matrix notation is used. In the cellular DMFT, the quantities are matrices in the N_c cluster sites and in particular $[\mathbf{G}_0^{-1}(\tilde{\mathbf{k}}, z)]_{\mathbf{X}_i \mathbf{X}_j} = (z+\mu)\delta_{\mathbf{X}_i \mathbf{X}_j} - [\mathbf{t}(\tilde{\mathbf{k}})]_{\mathbf{X}_i \mathbf{X}_j}$. For the DCA, the matrices are diagonal in the cluster momenta $\mathbf{K}$ and $[\mathbf{G}_0^{-1}(\tilde{\mathbf{k}}, z)]_{\mathbf{K}\mathbf{K}} = z + \mu - \epsilon_{\mathbf{K}+\tilde{\mathbf{k}}}$.

(iii) An effective cluster problem is then set up with the excluded-cluster Green's function $\mathcal{G}(z)$ and $\bar{\mathbf{U}}$.

(iv) The self-energy $\mathbf{\Sigma}_c(z)$ or the cluster Green's function $\mathbf{G}_c(z)$ is calculated in the effective cluster model (see Sec. II.E) by using any of the quantum cluster solvers discussed in Sec. III.

(v) For techniques that produce the cluster Green's function $\mathbf{G}_c$ rather than the self-energy, a new estimate of the cluster self-energy is calculated as $\mathbf{\Sigma}_c(z)=\mathcal{G}^{-1}(z)-\mathbf{G}_c^{-1}(z)$.

The iteration is closed by recalculating the coarse-grained Green's function $\bar{\mathbf{G}}(z)$ in step (ii) with the new estimate of the cluster self-energy. This procedure is repeated until the cluster Green's function $\mathbf{G}_c(z)$ equals the coarse-grained Green function $\bar{\mathbf{G}}(z)$ to within the desired accuracy.

3. Calculation of the lattice self-energy

Another significant difference between the cellular DMFT and the dynamical cluster approximation appears in the calculation of the lattice self-energy. The DCA approach approximates the lattice self-energy by a constant within a DCA cell in momentum space, $\Sigma(\mathbf{K}+\tilde{\mathbf{k}},z)=\Sigma_c(\mathbf{K},z)$. Therefore the self-energy is a step function in $\mathbf{k}$ space. In order to obtain smooth nonlocal quantities such as the Fermi surface or the band structure, an interpolated $\Sigma(\mathbf{k},z)$ may be used. Bilinear interpolation in two dimensions is guaranteed to preserve the sign of the function, but leads to kinks in $\Sigma(\mathbf{k},z)$. Yielding the smoothest possible interpolation of $\Sigma(\mathbf{K},z)$, the use of an Akima spline (Akima, 1970) which does not overshoot is consistent with the DCA assumption that the self-energy is a smoothly varying function in $\mathbf{k}$ space. However, it is important to note that this interpolated self-energy should not be used in the self-consistent loop, because this can lead to violations of causality, as discussed in Sec. II.D.6.

In the cellular DMFT, the lattice self-energy is given by the Fourier transform of the cluster self-energy [see Eq. (56)],

$$\Sigma(\mathbf{k},\mathbf{k}',z)=\frac{1}{N_c}\sum_{\mathbf{Q}}\sum_{\mathbf{X}_i,\mathbf{X}_j}e^{i\mathbf{k}\cdot\mathbf{X}_i}\Sigma_c(\mathbf{X}_i,\mathbf{X}_j,z)e^{-i\mathbf{k}'\cdot\mathbf{X}_j}\times\delta(\mathbf{k}-\mathbf{k}'-\mathbf{Q}). \tag{65}$$

Since a cellular DMFT cluster violates translational invariance, the lattice self-energy depends on two momenta, $\mathbf{k}$ and $\mathbf{k}'$, which can differ by a wave vector $\mathbf{Q}$ of the cluster reciprocal space. To restore translational invariance, the cellular DMFT approximates the lattice self-energy by the $\mathbf{Q}=0$ contribution, to give (Gros and Valenti, 1994; Sénéchal *et al.*, 2000; Kotliar *et al.*, 2001)

$$\Sigma(\mathbf{k},z)=\frac{1}{N_c}\sum_{\mathbf{X}_i,\mathbf{X}_j}e^{-i\mathbf{k}\cdot(\mathbf{X}_i-\mathbf{X}_j)}\Sigma_c(\mathbf{X}_i,\mathbf{X}_j,z). \tag{66}$$

In real space, the lattice self-energy

$$\Sigma(\mathbf{x}_i,\mathbf{x}_j,z)=\frac{1}{N_c}\sum_{\mathbf{X}_i,\mathbf{X}_j}\Sigma_c(\mathbf{X}_i,\mathbf{X}_j)\delta_{\mathbf{X}_i-\mathbf{X}_j,\mathbf{x}_i-\mathbf{x}_j} \tag{67}$$

is thus obtained by averaging over those cluster self-energy elements $\Sigma(\mathbf{X}_i,\mathbf{X}_j)$ where the distance $\mathbf{X}_i-\mathbf{X}_j$ equals the distance $\mathbf{x}_i-\mathbf{x}_j$. As explained by Biroli and Kotliar (2002), the factor $1/N_c$ leads to an underestimate of nonlocal self-energy contributions at small cluster sizes, since the number of contributions for fixed $\mathbf{x}_i-\mathbf{x}_j>0$ in the sum Eq. (67) is always smaller than N_c. As a possible solution to this problem, Biroli and Kotliar (2002) suggested replacing Eq. (67) for the lattice self-energy by a weighted sum that preserves causality. One could, for example, weight the terms in the sum by their number instead of N_c to achieve better results.

It is important to note that, as in the DCA, the lattice self-energy, Eq. (66) or Eq. (67), does not enter the self-consistent loop. Biroli *et al.* (2004), however, realized that a translationally invariant formulation of the cellular DMFT algorithm could be obtained by replacing the cluster self-energy $\mathbf{\Sigma}_c(z)$ by the translationally invariant lattice self-energy $\mathbf{\Sigma}(\tilde{\mathbf{k}})$, Eq. (66), in the coarse-graining step Eq. (53). Despite the dependence on $\tilde{\mathbf{k}}$, this form of $\mathbf{\Sigma}(\tilde{\mathbf{k}})$ can be shown to preserve causality (Biroli *et al.*, 2004).

D. Discussion

In this section we discuss many of the fundamental properties of these techniques. The essential approximation (Sec. II.D.1) common to all techniques has many consequences. As discussed in Sec. II.D.2, quantum cluster approximations have significant capabilities but also limitations. The approximations also affect conservation laws and the nature of the cluster model, as described in Secs. II.D.3 and II.D.4. Of course, the resulting approximations are now functions of the cluster size (Sec. II.D.5). The truncation of correlations to the cluster makes it difficult to form a causal theory (Sec. II.D.6) and makes it essential to take only irreducible quantities from the cluster to form the lattice propagators (Sec. II.D.7).

1. Nature of approximation

The diagrammatic derivation of Sec. II.B shows that a common aspect of all quantum cluster approaches is the approximation of the lattice self-energy $\mathbf{\Sigma}$ by the self-energy of a finite-size cluster. In each case, the single-particle propagator used to calculate $\mathbf{\Sigma}$ is that of the cluster. In cluster perturbation theory, the propagator of an isolated cluster is used, while in the cellular DMFT and DCA, the self-energy is calculated from the lattice propagator restricted to the sites inside the cluster. In the latter cases, this leads to a self-consistent theory, with a single-particle coupling between the cluster and a mean-field host. Quantum cluster approaches hence extend conventional mean-field approximations and introduce nonlocal correlations by replacing the insoluble lat-

tice Hamiltonian by some manageable finite portion—possibly with effective model parameters—and reintroducing the thermodynamic limit by a mean-field-type treatment of the remaining system. Thus the fundamental approximation common to all these approaches is that correlations within the cluster are treated explicitly, while those at longer length scales are described at the single-particle mean-field level. In the DCA, for example, the $\mathbf{k}$ dependence of the self-energy is approximated on a coarse grid of cluster $\mathbf{K}$ points [see Eq. (61)] at intervals $\Delta K = 2\pi/L_c$. This approximation assumes a weakly k-dependent self-energy which, according to Nyquist's sampling theorem (Elliot and Rao, 1982), reproduces correlations up to a spatial range $\xi \lesssim L_c/2$. Therefore quantum cluster approaches are good approximations to systems with significant screening, where correlations are expected to be short ranged.

The locator approach in Sec. II.A reveals a complementary interpretation of cluster approximations. We note that the potential energy may be written as $\frac{1}{2}\mathrm{Tr}(\mathbf{\Sigma G})$ (Fetter and Walecka, 1971), where the trace runs over cluster sites, superlattice wave vectors, frequency, and spin. As detailed above, the central feature of cluster expansions is their neglect of the intercluster contributions, $\delta\mathbf{\Sigma}(\tilde{\mathbf{k}}, z)\mathbf{G}(\tilde{\mathbf{k}}, z)$ in Eq. (29). Thus the approximation $\delta\mathbf{\Sigma}(z) = 0$ essentially neglects intercluster corrections to the potential energy in all calculated lattice quantities. On the other hand, the kinetic energy is identified as $\mathrm{Tr}(\mathbf{tG})$. Since its intercluster contribution is *not* neglected, the kinetic and potential-energy contributions are not treated on an equal footing. Indeed this is an essential difference between cluster mean-field approximations and finite-size calculations. In the former the potential energy of the lattice is truncated to that of the cluster, whereas the kinetic energy is not. This leads to a self-consistent theory, generally (but not always) with a single-particle coupling between the cluster and the host. In the potential-energy contribution, both the kinetic and potential energies of the lattice are truncated to their cluster counterparts. Therefore we might expect cluster methods to converge more quickly as a function of cluster size, compared to finite-size techniques, especially for metallic systems with extended states and significant screening (see Sec. IV).

2. Capabilities and limitations

Quantum cluster theories offer unique capabilities for the theoretical description of correlated lattice systems. Since the small parameter in these techniques is a low power of the inverse cluster size (see Sec. II.D.5), it is often possible to solve the cluster problem using an approach that is nonperturbative in the interaction and hence applicable to a whole range of interactions. Such theories allow for the calculation of static and dynamic single-particle and two-particle correlation functions and thus for the determination of various experimentally accessible quantities, such as those related to photoemission, transport, magnetism, and superconductivity. As the fundamental approximation, quantum cluster theories cut off correlations beyond the length scale set by the cluster size while remaining in the thermodynamic limit. As we show in Sec. II.D.5 they allow for systematic improvement by increasing the cluster size and recover the mean-field–exact result in the single-site–infinite-size cluster limit.

One must bear in mind, however, the limitations of quantum cluster approaches originating in the spatial cutoff of correlations. Due to the neglect of long-wavelength fluctuations, quantum cluster approximations may yield transitions to ordered phases which are otherwise prohibited by the Mermin-Wagner theorem. In addition, quantum cluster methods fail as a classical or quantum critical point is approached. In fact, since the critical behavior close to the transition is determined by the long-wavelength limit, quantum cluster approaches always yield mean-field exponents. However, a finite-size scaling analysis of the cluster size dependence of thermodynamic quantities may give valuable information about the critical behavior of the system. The critical exponent ν, for example, may be determined from the cluster size scaling of the critical temperature [see Sec. I.B, Suzuki (1986), and Hettler *et al.* (2000)]. Although the mean-field quantum cluster approaches are too close to mean-field theory to permit a proof of phase transitions, they allow one to investigate a system's tendency to certain types of orders and to identify the possible existence of long-ranged correlations.

Studies with larger cluster sizes can help to alleviate this problem and suppress the spurious transitions found for small clusters by including longer-wavelength fluctuations and thus driving transition temperatures down. Finite-size simulations of small systems, in contrast, experience difficulty in finding long-range order. Here, larger systems have to be simulated in order to see a tendency towards ordering. Thus, while finite-size techniques have difficulty finding true transitions, quantum cluster approaches make it challenging to suppress spurious transitions. Properties that are suppressed by fluctuations may disappear in the large-cluster limit, whereas those that are driven by fluctuations should persist as the cluster size is increased. Fluctuation-induced properties such as the Mott-Hubbard gap in the Hubbard model should become more pronounced in larger clusters, since longer-ranged fluctuations are included. By contrast, finite-size simulations usually overestimate gaps in small systems. This complementarity of quantum cluster approaches and finite-size techniques is discussed in more detail in Sec. IV.A.

From a purely technical point of view, the solution of the effective cluster model (see Sec. II.E) remains a formidable task (see Sec. III for techniques), as potentially exact cluster solvers become numerically quite expensive as the number of local and spatial degrees of freedom on the cluster increases. The underlying many-particle problem usually inhibits the consideration of the full electronic structure, and the restriction to low-energy scales becomes necessary. Hence the models that can be treated numerically exactly within quantum clus-

ter methods are usually limited to a few correlated orbitals.

3. Conservation and thermodynamic consistency

The DCA and cellular DMFT approximations are both self-consistent and Φ derivable since they satisfy Eq. (44). Thus they are thermodynamically consistent in the Baym-Kadanoff sense. Observables calculated from the lattice Green's function $\mathbf{G}$ agree with those calculated as derivatives of the lattice grand potential Ω. Since the cluster perturbation theory is not self-consistent, it is not thermodynamically consistent. However, none of these approaches is conserving in the Baym-Kadanoff sense, since they all violate local momentum conservation by approximating the Laue momentum conservation function. Thus each of these approaches is likely to violate some set of Ward identities (Hettler *et al.*, 2000).

4. Nature of effective cluster problem

In contrast to the DMFT, a unique setup for the embedded-cluster theory does not exist. Depending on the treatment of boundary conditions (see Sec. II.A and Biroli and Kotliar, 2002), differences in the coupling of the cluster to its environment arise (see comparison in Sec. II.D.4 below). In fact, there exist infinitely many realizations of embedded-cluster theories for any given model Hamiltonian (Biroli and Kotliar, 2002; Okamoto *et al.*, 2003; Potthoff, 2003b; Potthoff *et al.*, 2003), two of which we focus on in this review.

Detailed comparisons of the DCA and cellular DMFT algorithms were presented by Biroli and Kotliar (2002), Maier, Gonzalez, *et al.* (2002), Maier and Jarrell (2002), Biroli *et al.* (2004), and Aryanpour, Maier, and Jarrell (2005). Both approximations share the underlying idea and general algorithm, and differ only in the form used for the hopping matrix $\mathbf{t}$ [see Eq. (35)]. The purpose of this and the following section is to examine the effects of this, at first sight, small difference on the effective cluster problem and the convergence properties.

We illustrate the nature of the effective cluster problems using a 1D model with nearest-neighbor hopping t, on-site energy $\epsilon_0=0$, and cluster size L_c. The generalization to higher dimension or longer-ranged hopping terms is straightforward. The cellular DMFT uses the original form for the hopping matrix $\mathbf{t}(\tilde{k})$ which is obtained, for example, as an intercluster Fourier transform [see Eq. (22)] of $\mathbf{t}(\tilde{x})$. Only entries between neighboring sites inside the cluster $[\mathbf{t}(\tilde{k})]_{X_i,X_i\pm1}=-t$ and between neighboring sites on the surface of the cluster $[\mathbf{t}(\tilde{k})]_{X_i,X_i\pm(L_c-1)}=-te^{\mp i\tilde{k}L_c}$ are finite. The former entries form the intracluster hopping matrix $\mathbf{t}_c=N_c/N\Sigma_{\tilde{k}}\mathbf{t}(\tilde{k})$ while the latter entries form the intercluster hopping matrix $\delta\mathbf{t}(\tilde{k})=\mathbf{t}(\tilde{k})-\mathbf{t}_c$. Both amplitudes are given by the original hopping t. For the effective cluster problem this translates to the fact that only sites on the surface of the cluster couple to the effective medium, while sites inside the cluster couple only to their neighboring sites in the cluster. Hence the cluster problem has open boundary conditions, and translational invariance is violated within the cluster. The lattice Green's function $\mathbf{G}(\tilde{k})$ [see Eq. (30)] is a matrix in the cluster sites and cannot be diagonalized by going over to cluster K space. Therefore the coarse-graining step, Eq. (31), is performed in real space.

The DCA restores translational invariance by setting $[\mathbf{t}_{\mathrm{DCA}}(\tilde{k})]_{X_iX_j}=[\mathbf{t}(\tilde{k})]_{X_iX_j}e^{-i\tilde{k}\cdot(X_i-X_j)}$ [see Eq. (35)]. As a consequence, its matrix elements become identical and are given by $-te^{\mp i\tilde{k}}$ between sites $X_j=X_i\mp1$ and $X_j=X_i\pm(L_c-1)$. Hence the DCA hopping matrix $\mathbf{t}_{\mathrm{DCA}}(\tilde{k})$ is fully cyclic with respect to the cluster sites, and the lattice Green's function $\mathbf{G}(\tilde{k})$ is diagonalized by going over to cluster K space. The DCA intracluster hopping matrix $\mathbf{t}_{c,\mathrm{DCA}}=N_c/N\Sigma_{\tilde{k}}\mathbf{t}_{\mathrm{DCA}}(\tilde{k})$ is also cyclic with finite matrix elements

$$[\mathbf{t}_{c,\mathrm{DCA}}]_{X_i,X_j}=-t\frac{L_c}{\pi}\sin\frac{\pi}{L_c}, \tag{68}$$

between sites $X_j=X_i\pm1$ and $X_j=X_i\pm(L_c-1)$, and the problem of the DCA cluster therefore has periodic boundary conditions. At finite cluster size L_c, the intracluster hopping is reduced by the factor $1/6(\pi/L_c)^2+\mathcal{O}[(\pi/L_c)^4]$ compared to its lattice counterpart t. In the limit of infinite cluster size it becomes t. This reduction in the intracluster coupling is compensated for by the intercluster hopping, which is long ranged in nature,

$$[\delta\mathbf{t}_{\mathrm{DCA}}(\tilde{x})]_{X_iX_j}=-t\left(\frac{\sin[(\tilde{x}\mp1)\pi/L_c]}{(\tilde{x}\mp1)\pi/L_c}-\frac{\sin(\pi/L_c)}{\pi/L_c}\delta_{\tilde{x},0}\right), \tag{69}$$

between sites $X_j=X_i\mp1$ and $X_j=X_i\pm(L_c-1)$. It is important to note that $\delta\mathbf{t}_{\mathrm{DCA}}$ couples all the sites in the cluster to sites in the effective medium. It vanishes for $\tilde{x}=0$ and decreases as $1/\tilde{x}$ with increasing $\tilde{x}$. We also note that

$$\delta\mathbf{t}_{\mathrm{DCA}}\sim1/L_c \tag{70}$$

for large linear cluster sizes L_c and emphasize that this result holds generally in any dimension D.

These results show that the restoration of translational invariance in the DCA is achieved by mapping the lattice onto a cluster with periodic boundary conditions, reduced hopping integrals $t_{c,\mathrm{DCA}}$, and coupling of every site in the cluster to a neighboring site in the effective medium through long-ranged hopping integrals $\delta t_{\mathrm{DCA}}(\tilde{x})$. Similar conclusions about the nature of the effective cellular DMFT and DCA cluster problems were reached in a study of the large-U limit of the Falicov-Kimball model [see Eq. (182)], i.e., the classical Ising model (Biroli *et al.*, 2004).

We stress that clusters with linear size $L_c=2$ are special in the DCA. Here both terms in the intracluster hopping Eq. (68) give a contribution to the same matrix element. Hence the nearest-neighbor hopping is given

by $-2t(L_c/\pi)\sin(\pi/L_c)$, i.e., with the prefactor $-2t$ instead of $-t$ for larger clusters. This reflects the fact that every site sees its nearest neighbor twice due to the periodic boundary conditions. Nonlocal fluctuations are thus enhanced in clusters with linear size $L_c=2$ as seen, for example, in a stronger suppression of transition temperatures (see Sec. IV.D.2).

5. Systematics

The quantum cluster approaches discussed here have well-defined limits. Cluster perturbation theory, cellular DMFT, and the DCA become exact in the weak-coupling limit, the strong-coupling limit, and the limit of infinite cluster size, $N_c\to\infty$. In the weak-coupling limit, the cluster self-energy vanishes and the exact solution is given by the noninteracting Green's function, which is reproduced in all three approaches. In the strong-coupling limit, all the sites in the lattice are decoupled. The effective cluster problem reduces to a single-site problem without coupling to a mean field, since the hybridization function Γ vanishes in this limit. The cluster Green's function then becomes the Green's function of an isolated site and solves the problem exactly. In the limit $N_c\to\infty$, the effective cluster problem becomes identical to the original problem and the cluster Green's function becomes the exact Green's function of the full system.

At intermediate couplings and cluster size $N_c=1$, the cellular DMFT and the DCA both reduce to the DMFT for a finite-dimensional system. In this limit, both the cellular DMFT and DCA Laue functions [Eqs. (51) and (58)] reduce to $\Delta=1$, Φ is evaluated with the local Green's function and local contribution of the interactions, and the DMFT is recovered. In contrast, the cluster perturbation theory reduces to the Hubbard-I approximation (Hubbard, 1963) when $N_c=1$ where the self-energy is approximated by that of an isolated atom (Gros and Valenti, 1994; Sénéchal *et al.*, 2000, 2002).

Quantum cluster approaches can thus be viewed as interpolation schemes between the DMFT or Hubbard-I result at $N_c=1$ and the exact result at $N_c\to\infty$. That quantum cluster methods are systematic in the cluster size may be rigorously shown within the analysis presented in the preceding section. The approximation performed by the DCA and the cellular DMFT is to replace the exact lattice Green's function G by its coarse-grained quantity $\bar{G}$ in diagrams for the generating functional Φ (see Sec. II.B). For example, in the DCA, where, with the nomenclature introduced in Sec. II.A, the lattice self-energy is written as $\Sigma(\mathbf{k})=\Sigma_c(\mathbf{K})+\delta\Sigma(\mathbf{K}+\tilde{\mathbf{k}})$ and $\Sigma_c(\mathbf{K})$ is the DCA cluster self-energy, the relationship between $G(\mathbf{k})$ and $\bar{G}(\mathbf{K})$ is given by

$$G(\mathbf{k})=\frac{1}{1/\bar{G}(\mathbf{K})-\delta t(\mathbf{K},\tilde{\mathbf{k}})-\delta\Sigma(\mathbf{K},\tilde{\mathbf{k}})+\Gamma(\mathbf{K})}. \tag{71}$$

We note that a similar expression holds for the cellular DMFT. $G(\mathbf{k})$ thus differs from $\bar{G}(\mathbf{K})$ in the intercluster hopping δt, the self-energy corrections $\delta\Sigma$, and the hybridization function Γ. Since the diagrams in Φ are summed over $\tilde{\mathbf{k}}$ and $N_c/N\Sigma_{\tilde{\mathbf{k}}}\delta t(\tilde{\mathbf{k}})=0$ the terms having the same order as $\delta t(\tilde{\mathbf{k}})\sim 1/L_c$ vanish [see Eq. (70)]. If we assume that the self-energy has corrections of the same or higher order in $1/L_c$ as Γ, the convergence of Φ with cluster size is entirely determined by Γ.

To leading order, the hybridization with the mean-field Γ vanishes like δt^2 as the cluster size increases [see Eqs. (33) and (43)]. In the cellular DMFT the magnitude of $\delta\mathbf{t}$ is of order 1 for the sites on the surface of the cluster and 0 otherwise. The average hybridization per cluster site in the cellular DMFT thus scales as

$$\bar{\Gamma}_{\mathrm{CDMFT}}=\frac{1}{N_c}\mathrm{Tr}[\mathbf{\Gamma}_{\mathrm{CDMFT}}]\sim\mathcal{O}\left(\frac{1}{L_c}\right), \tag{72}$$

where the trace runs over cluster sites and frequency. This behavior is evident because only the $2D(L_c^{D-1})$ sites on the surface contribute to the sum and $N_c=L_c^D$. In the DCA, $\delta t=\mathcal{O}(1/L_c)$ [see Eq. (70)]. The average hybridization of the DCA cluster to the effective medium scales faster to zero as

$$\bar{\Gamma}_{\mathrm{DCA}}=\frac{1}{N_c}\mathrm{Tr}[\mathbf{\Gamma}_{\mathrm{DCA}}]\sim\mathcal{O}\left(\frac{1}{L_c^2}\right) \tag{73}$$

since each of the N_c terms contributes a term of the order $\mathcal{O}(1/L_c^2)$. Thus the differences in boundary conditions between cellular DMFT and the DCA translate directly to different asymptotic behaviors for large cluster sizes N_c.

With the scaling relations (72) and (73) we find for the cellular DMFT that $\Phi_{\mathrm{CDMFT}}\approx\Phi+\mathcal{O}(1/L_c)$ while the DCA converges as $\Phi_{\mathrm{DCA}}\approx\Phi+\mathcal{O}(1/L_c^2)$. Since $\Sigma=\delta\Phi/\delta G$, it converges with L_c as the corresponding Φ. The exact lattice self-energy Σ is therefore approximated by the cluster self-energy Σ_c according to

$$\Sigma=\Sigma_c^{\mathrm{DCA}}+\mathcal{O}(1/L_c^2), \tag{74}$$

$$\Sigma=\Sigma_c^{\mathrm{CDMFT}}+\mathcal{O}(1/L_c). \tag{75}$$

Hence both quantum cluster approaches, the DCA and cellular DMFT, have systematic expansions in the cluster size. With increasing cluster size, the generating functional Φ and hence the self-energy and the grand potential converge to the exact result, with corrections $\mathcal{O}(1/L_c^2)$ in the DCA and with corrections $\mathcal{O}(1/L_c)$ in cellular DMFT.

The scaling behavior Eqs. (72) and (73) of the CDMFT and DCA average hybridization strengths for both approaches was verified numerically for the 1D Falicov-Kimball model by Maier and Jarrell (2002; see also Maier, Gonzalez, *et al.*, 2002). Here we review the effects of the different scaling behaviors of the average hybridization on the phase transition in this model. The Hamiltonian of the Falicov-Kimball model is discussed in Sec. IV.B, Eq. (182). It can be considered as a simplified Hubbard model with only one spin species being

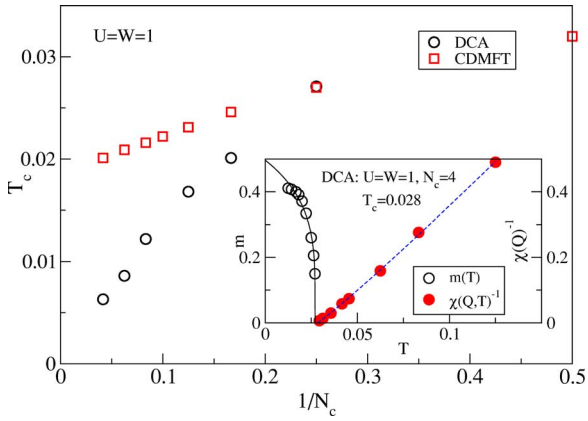

FIG. 7. (Color in online edition) Transition temperature vs inverse cluster size: circles, calculated with the DCA Monte Carlo technique; squares, cellular DMFT Monte Carlo when $U=W=4t=1$. Inset: DCA order parameter $m(T)$ and inverse charge susceptibility $\chi(Q)^{-1}$ vs temperature. Taken from Maier, Gonzalez, *et al.*, 2002.

itinerant. However, it still shows a complex phase diagram, including a Mott gap for large U at half-filling, an Ising-like charge ordering with the corresponding transition temperature T_c being zero in one dimension, and phase separation in all dimensions (Freericks and Zlatić, 2003). Since the 1D Falicov-Kimball model is in the 1D Ising universality class, we expect similar scaling behavior to that observed in the results for the 1D Ising model in Sec. I.B. In particular, we expect finite transition temperatures within both cluster approximations due to their residual mean-field character. Their effective cluster models were solved with a Monte Carlo approach described by Hettler *et al.* (2000).

The DCA transition temperature T_c was determined from the divergence of the lattice charge susceptibility $\chi(Q)$ calculated from the particle-hole correlation function as detailed in Sec. II.G. In the cellular DMFT formalism the calculation of lattice susceptibilities is difficult if not impossible due to the lack of translational invariance. Here T_c is determined from the calculation of the charge order parameter m as detailed in Sec. II.F. For the DCA both techniques are illustrated in the inset to Fig. 7.

As for the 1D Ising model (see Fig. 2 in Sec. I.B), the DCA result for T_c scales to zero almost linearly in $1/N_c$ for large N_c. Moreover, the T_c obtained from the DCA is smaller and thus closer to the exact result than the T_c obtained from cellular DMFT. The cellular DMFT does not show any scaling behavior and in fact seems to tend to a finite value for T_c as $N_c \to \infty$. As explained above, this striking difference can be attributed to the different boundary conditions. The open boundary conditions of a cellular DMFT cluster result in a large surface contribution so that $\bar{\Gamma}_{\mathrm{CDMFT}} > \bar{\Gamma}_{\mathrm{DCA}}$. This engenders pronounced mean-field behavior that stabilizes the finite-temperature transition for the cluster sizes treated in Fig. 7. For larger cluster sizes, the bulk contribution to the cellular DMFT grand potential should dominate, so that T_c is expected to fall to zero.

Complementary results are found in simulations of finite-size systems. In general, systems with open boundary conditions are expected to have a surface contribution in the grand potential of order $\mathcal{O}(1/L_c)$ (Fisher and Barber, 1972). This term is absent in systems with periodic boundary conditions. As a result, simulations of finite-size systems with periodic boundary conditions converge much more quickly than those with open boundary conditions (Landau, 1976).

The DCA converges faster than the cellular DMFT for critical properties as well as extended cluster quantities due to the different boundary conditions and the coupling to the mean field. As detailed above, each site in the DCA cluster experiences the same coupling to the effective medium, while in the cellular DMFT only sites on the boundary of the cluster couple to the mean-field host. Provided that the system is far from a transition, the sites in the center of the cellular DMFT cluster couple to the mean field only through propagators which fall exponentially with distance. Local results such as the single-particle density of states thus converge more quickly in the cellular DMFT than in the DCA when measured on a central site (see Maier, Gonzalez, *et al.*, 2002).

6. Causality

To formulate a systematic embedded-cluster theory that is causal, i.e., one in which the retarded Green's functions have poles only in the lower half of the complex plane [or a self-energy with $\mathrm{Im}\,\Sigma(\mathbf{k},\omega+i0^+)<0$] turned out to be a difficult task. Early attempts to formulate cluster extensions to DMFT (van Dongen, 1994; Schiller and Ingersent, 1995) encountered negative portions in the single-particle spectral functions, a clear violation of causality. The origin of the problem is easily illustrated with an example: Consider a single-band Hubbard model, with near-neighbor hopping t and dispersion $\epsilon_{\mathbf{k}}$, for which we know the local and near-neighbor contributions to the self-energy $\Sigma_0(\omega)$ and $\Sigma_1(\omega)$. A straightforward lattice estimate from just these two components is $\Sigma(\mathbf{k},\omega) \approx \Sigma_0(\omega) + (\epsilon_{\mathbf{k}}/t)\Sigma_1(\omega)$. However, $\mathrm{Im}\,\Sigma_1(\omega)$, being nonlocal, has no definite sign and $\epsilon_{\mathbf{k}}/t$ can become large near the band edges. Therefore causality violations in the form of $\mathrm{Im}\,\Sigma(\mathbf{k},\omega+i0^+)>0$ can occur for regions of wave vectors close to the band edges.

Explicit proofs for causality have been given for the DCA (Hettler *et al.*, 2000), the molecular CPA (Ducastelle, 1974), and the cellular DMFT[3] (Kotliar *et al.*, 2001; see also Biroli *et al.*, 2004). Instead of summarizing the proofs for the different methods, we here give a unified argument for causality, based on projection techniques.

[3]Since the mappings between the cluster and the lattice in the cellular DMFT and the molecular CPA are identical, the same proof should apply for both formalisms.

We start with Eqs. (28), (30), and (31). Note that all quantities appearing in these equations are in general matrices in the cluster indices. We now define a set of vectors $|f_0^\mu\rangle$ ($\mu=1,\ldots,N_c$), such that for any cluster quantity $\mathbf{A}(\tilde{\mathbf{k}})$ the coarse-graining step Eq. (31) can be expressed as

$$\frac{N_c}{N}\sum_{\tilde{\mathbf{k}}}\mathbf{A}(\tilde{\mathbf{k}}) = \frac{1}{\mathbf{O}_0}(\vec{f}_0|\mathcal{A}|\vec{f}_0) \tag{76}$$

with a suitably chosen linear operator $\mathcal{A}$. Here $\mathbf{O}_0 = (\vec{f}_0|\vec{f}_0)$ is the overlap matrix for the vectors $|f_0^\mu\rangle$, which we may choose to be the identity matrix without loss of generality. In particular, the coarse-grained Green's function may be written as

$$\bar{\mathbf{G}}(z) = (\vec{f}_0|\frac{1}{z-\mathcal{H}}|\vec{f}_0). \tag{77}$$

We now introduce idempotent projection operators

$$\mathcal{P}_0 = |\vec{f}_0)(\vec{f}_0|, \quad \mathcal{Q}_0 = 1 - \mathcal{P}_0 \tag{78}$$

and then rewrite Eq. (77) as (Maier *et al.*, 2000b)

$$\bar{\mathbf{G}}(z) = \Bigg[z\mathbb{1} - (\vec{f}_0|\mathcal{H}|\vec{f}_0) - (\vec{f}_0|\mathcal{H}\mathcal{Q}_0\frac{1}{z-\mathcal{Q}_0\mathcal{H}\mathcal{Q}_0}\mathcal{Q}_0\mathcal{H}|\vec{f}_0)\Bigg]^{-1}. \tag{79}$$

Since

$$\frac{N_c}{N}\sum_{\tilde{\mathbf{k}}}\delta\mathbf{t}(\tilde{\mathbf{k}}) = \delta\mathbf{t}(\tilde{\mathbf{x}}=0) = 0 \tag{80}$$

it follows that $z\mathbb{1}-(\vec{f}_0|\mathcal{H}|\vec{f}_0)=\mathbf{g}(z)^{-1}$. If we further define

$$\mathbf{\Gamma}(z) = (\vec{f}_0|\mathcal{H}\mathcal{Q}_0\frac{1}{z-\mathcal{Q}_0\mathcal{H}\mathcal{Q}_0}\mathcal{Q}_0\mathcal{H}|\vec{f}_0) \tag{81}$$

we recover the form (32) obtained from the locator expansion for $\bar{\mathbf{G}}(z)$.

Causality violations for embedded-cluster theories like the cellular DMFT and DCA can arise only in the "cluster exclusion" step, Eq. (64), in which the host Green's function $\mathcal{G}$ is computed. Combining Eqs. (28) and (64), we see that for causality to hold, the hybridization function $\mathbf{\Gamma}$ has to be causal itself. To prove causality of $\mathbf{\Gamma}$, let us iterate the above procedure. We define $|\vec{f}_1) = \mathcal{Q}_0\mathcal{H}|\vec{f}_0)$ with $\mathbf{O}_1=(\vec{f}_1|\vec{f}_1)$, an operator $\mathcal{H}_1=\mathcal{Q}_0\mathcal{H}\mathcal{Q}_0$, and corresponding projection operators $\mathcal{P}_1$ and $\mathcal{Q}_1$. It is straightforward to show that

$$\mathbf{O}_1 = \left(\frac{N_c}{N}\sum_{\tilde{\mathbf{k}}}\delta\mathbf{t}(\tilde{\mathbf{k}})^2\right) \coloneqq \boldsymbol{\gamma}^2. \tag{82}$$

With this convention we may rewrite Eq. (81) as

$$\mathbf{\Gamma}(z) = \boldsymbol{\gamma}^2\Bigg[z\mathbb{1} - \frac{1}{\mathbf{O}_1}(\vec{f}_1|\mathcal{H}_1|\vec{f}_1) - \frac{1}{\mathbf{O}_1}(\vec{f}_1|\mathcal{H}_1\mathcal{Q}_1\frac{1}{z-\mathcal{Q}_1\mathcal{H}_1\mathcal{Q}_1}\mathcal{Q}_1\mathcal{H}_1|\vec{f}_1)\Bigg]^{-1}. \tag{83}$$

With some tedious but straightforward algebra one finds

$$z\mathbb{1} - \frac{1}{\mathbf{O}_1}(\vec{f}_1|\mathcal{H}_1|\vec{f}_1) = \frac{1}{\boldsymbol{\gamma}^2}\frac{N_c}{N}\sum_{\tilde{\mathbf{k}}}\delta\mathbf{t}(\tilde{\mathbf{k}})\mathbf{G}(\tilde{\mathbf{k}},z)^{-1}\delta\mathbf{t}(\tilde{\mathbf{k}})$$

with $\mathbf{G}(\tilde{\mathbf{k}},z)$ given by Eq. (30). Finally, one can move the prefactors $\boldsymbol{\gamma}$ in (83) from the numerator into the denominator and vice versa to obtain

$$\mathbf{\Gamma}(z) = \boldsymbol{\gamma}\frac{1}{\frac{N_c}{N}\sum_{\tilde{\mathbf{k}}}\mathbf{U}(\tilde{\mathbf{k}})\mathbf{G}(\tilde{\mathbf{k}},z)^{-1}\mathbf{U}(\tilde{\mathbf{k}})^\dagger - \mathbf{\Gamma}_1(z)}\boldsymbol{\gamma}, \tag{84}$$

where $\mathbf{U}(\tilde{\mathbf{k}})=\boldsymbol{\gamma}^{-1}\delta\mathbf{t}(\tilde{\mathbf{k}})$ and

$$\mathbf{\Gamma}_1(z) = \frac{1}{\boldsymbol{\gamma}}(\vec{f}_1|\mathcal{H}_1\mathcal{Q}_1\frac{1}{z-\mathcal{Q}_1\mathcal{H}_1\mathcal{Q}_1}\mathcal{Q}_1\mathcal{H}_1|\vec{f}_1). \tag{85}$$

The above scheme can be continued to yield an expression for $\bar{\mathbf{G}}(z)$ as a continued fraction

$$\bar{\mathbf{G}}(z)^{-1} = \mathbf{g}(z)^{-1} - \boldsymbol{\gamma}\frac{1}{\frac{N_c}{N}\sum_{\tilde{\mathbf{k}}}\mathbf{U}(\tilde{\mathbf{k}})\mathbf{G}(\tilde{\mathbf{k}},z)^{-1}\mathbf{U}(\tilde{\mathbf{k}})^\dagger - \cdots}\boldsymbol{\gamma}. \tag{86}$$

The only dependence on z in the last term representing $\mathbf{\Gamma}(z)$ comes from $\mathbf{G}(\tilde{\mathbf{k}},z)$, which fulfills causality requirements. Thus $\mathbf{\Gamma}(z)$ is also causal by construction, which is what is needed for causality of the algorithm.

The above derivation puts certain limits on various approximations of the cluster algorithms, and may be motivated by numerical reasons. It is, for example, tempting to replace the well-defined cluster quantity $\mathbf{\Sigma}_c(z)$ in Eq. (28) by some approximation to $\mathbf{\Sigma}(z)$, i.e., the full self-energy. As has been discussed in some detail by Okamoto *et al.* (2003; see also Sec. II.I), such a procedure will generally lead to causality violations. The ultimate effect of such violations on the interesting low-energy results is difficult to ascertain, but at least there should be doubt about the quantitative accuracy.

The result in Eq. (86) also has an appealing interpretation in terms of quantum impurity problems: From the general structure of the propagator of a quantum impurity model one can identify the quantity $\boldsymbol{\gamma}^2=\Sigma_{\tilde{\mathbf{k}}}\delta\mathbf{t}(\tilde{\mathbf{k}})^2$ with the squared (effective) hybridization matrix between impurity and host degrees of freedom and

$$\mathbf{G}_h(z) \coloneqq \left[\frac{N_c}{N}\sum_{\tilde{\mathbf{k}}}\mathbf{U}(\tilde{\mathbf{k}})\mathbf{G}(\tilde{\mathbf{k}},z)^{-1}\mathbf{U}(\tilde{\mathbf{k}})^\dagger - \cdots\right]^{-1} \tag{87}$$

with the (effective) propagator for the host degrees of freedom.

7. Reducible versus irreducible quantities

The one-particle self-energy $\mathbf{\Sigma}$ and its many-particle counterparts carry the information about the many-body physics of a model. It is built from irreducible diagrams, i.e., graphs that cannot be separated into parts by cutting a Green's-function line. In contrast, the single-particle Green's function or a susceptibility is a reducible quantity. The cluster theories discussed use only the irreducible cluster quantities such as the single-particle self-energy to build the reducible lattice quantities such as the single-particle Green's function.

This may be motivated physically for systems with significant screening. The irreducible lattice self-energy accurately reflects short-ranged correlations within the screening cloud. It is well approximated with its cluster counterpart, in which long-range correlations are cut off by the finite size of the cluster. On the other hand, the phase accumulated by the propagation of a particle through the lattice is described by the single-particle Green's function. Since this accumulated phase is crucial in the description of the quantum dynamics, it is important that the single-particle Green's function remain accurate at long length scales. Therefore it must not be approximated by its cluster counterpart.

More formally, consider the grand potential functional Eq. (45). It is expressed as a sum over all closed connected distinct graphs constructed from the bare Green's function $\mathbf{G}_0$ and interaction $\mathbf{U}$. The subset of compact graphs constructed from the dressed Green's function $\mathbf{G}$ and interaction $\mathbf{U}$ comprise the Baym-Kadanoff generating functional $\Phi[\mathbf{G},\mathbf{U}]$, which is expressed as a skeletal graph sum over all distinct, compact, closed, connected graphs. Compact diagrams have no internal parts representing corrections to the Green's function $\mathbf{G}$. In quantum cluster theories the graphs for the irreducible Φ are approximated by their cluster counterparts. As an example, consider the limit of infinite dimensions, used by Metzner and Vollhardt (1989) to derive the DMFT. In this limit most closed connected graphs are local, since both the bare and dressed Green's functions fall off quickly with distance r, $G(r)\sim D^{-r/2}$. Only the set of graphs corresponding to noncompact corrections remains nonlocal. To see this, consider the simplest nonlocal corrections to noncompact and compact parts of the grand potential of a Hubbard-like model, illustrated in Fig. 8. Here the upper circle is a set of graphs composed of intrasite propagators restricted to site n, and the lower circle is a set of intrasite propagators restricted to the origin. Consider all such nonlocal corrections on the shell of sites which are n mutually orthogonal unit translations from the origin. In the limit of high dimensions, there are $2^n D!/[(D-n)!n!]\sim\mathcal{O}(D^n)$ such sites. Since as $D\to\infty$, $G(r)\sim D^{-r/2}$ (Metzner and Vollhardt, 1989), the legs on the compact correction contribute a factor $\mathcal{O}(D^{-2n})$, whereas those on the noncompact correction contribute $\mathcal{O}(D^{-n})$. Therefore the compact nonlocal correction falls as D^{-n} and vanishes as $D\to\infty$; whereas the noncompact correction remains of order 1, regardless of how far site n is from the origin. As a result, the generating functional, which is composed of only compact graphs, is a functional of the local Green's function and interaction in this limit,

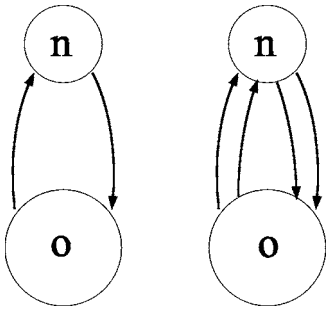

FIG. 8. Noncompact (left) and compact (right) nonlocal corrections to the grand potential. Here the upper and lower circles are meant to represent a set of graphs that are closed except for the external lines shown, and restricted to site n (the origin).

$$\Phi[\mathbf{G},\mathbf{U}]=\Phi[G_{ii},U_{ii}]+\mathcal{O}(1/D). \tag{88}$$

A similar analysis was done for the DCA cluster problem by Aryanpour *et al.* (2002). They found that the corrections from sites outside the cluster associated with compact diagrams were quite small (i.e., high order in the linear cluster size $1/L_c$), justifying the approximation

$$\Phi[\mathbf{G},\mathbf{U}]\approx\Phi[\bar{G}(\mathbf{K}),\bar{U}(\mathbf{K})], \tag{89}$$

while those associated with noncompact diagrams were large and could not be neglected. The same analysis may be done for the cellular DMFT, simply by replacing the DCA graphs by those for the cellular DMFT.

Thus the essential feature of the DMFT, the DCA, and the cellular DMFT is to approximate the lattice generating functional Φ by its cluster counterpart in the estimate of the lattice grand potential, Eq. (45). Concomitantly the derivatives of Φ, i.e., the lattice self-energy and vertex functions, are approximated by their respective cluster counterparts. This once more underlines why in embedded-cluster theories it is necessary always to work with the irreducible quantities of the cluster; they are the only quantities that correspond directly to their lattice counterparts.

E. Effective cluster model

Quantum cluster approaches reduce the complexity of the lattice problem with an infinite number of spatial degrees of freedom to a (numerically) solvable system with N_c spatial degrees of freedom. As detailed in Sec. II.B, this is achieved through the approximation of $\Phi[\mathbf{G},\mathbf{U}]$, the exact Baym-Kadanoff functional of the exact Green's function $\mathbf{G}$ and interaction $\mathbf{U}$, by a spatially localized quantity $\Phi[\bar{\mathbf{G}},\bar{\mathbf{U}}]$ which is a functional of the corresponding (coarse-grained) quantities restricted to the cluster sites, $\bar{\mathbf{G}}=N_c/N\Sigma_{\tilde{\mathbf{k}}}\mathbf{G}(\tilde{\mathbf{k}})$ and $\bar{\mathbf{U}}=N_c/N\Sigma_{\tilde{\mathbf{k}}}\mathbf{U}(\tilde{\mathbf{k}})$.

$\Phi[\bar{\mathbf{G}},\bar{\mathbf{U}}]$ may be calculated nonperturbatively as the solution of a quantum cluster model,

$$\mathcal{H}_c = H_{c,0} + H_{c,I}. \tag{90}$$

$\mathcal{H}_c$ consists of a noninteracting term $H_{c,0}$ describing the bare cluster degrees of freedom and their coupling to a host. The interacting term $H_{c,I}$ is related to the corresponding term in the original lattice model through the coarse-grained interaction $\bar{\mathbf{U}}$. This ensures that the functional dependencies of the cluster functional Φ_c and its lattice counterpart Φ are identical.

The noninteracting term $H_{c,0}$ is fixed by the requirement that the Green's function $\mathbf{G}_c$ of the cluster model equal the coarse-grained Green's function $\bar{\mathbf{G}}$ of the original model,

$$\mathbf{G}_c \equiv \bar{\mathbf{G}} = [\boldsymbol{\mathcal{G}}^{-1} - \boldsymbol{\Sigma}_c]^{-1}, \tag{91}$$

and hence is specified by the excluded-cluster Green's function $\boldsymbol{\mathcal{G}}$ [see Eq. (64)].

For Green's functions or action-based cluster solvers like perturbation theory or quantum Monte Carlo, $H_{c,0}$ can be encoded in the excluded-cluster Green's function $\boldsymbol{\mathcal{G}}$. The corresponding cluster action S_c for the fermionic cluster degrees of freedom represented by the Grassmann variables γ,γ^* reads in imaginary time and cluster real space

$$S_c[\gamma,\gamma^*] = -\int_0^\beta d\tau \int_0^\beta d\tau' \sum_{ij,\sigma} \gamma^*_{i\sigma}(\tau)\mathcal{G}_{ij,\sigma}(\tau-\tau')\gamma_{j\sigma}(\tau') + \int_0^\beta d\tau \sum_{ij,\sigma\sigma'} \frac{\bar{U}^{\sigma\sigma'}_{ij}}{2}\gamma^*_{i\sigma}(\tau)\gamma^*_{j\sigma'}(\tau)\gamma_{j\sigma'}(\tau)\gamma_{i\sigma}(\tau), \tag{92}$$

where we used the shorthand notation i, j for the cluster sites $\mathbf{X}_i,\mathbf{X}_j$. Note that for the cellular DMFT the quantities $\mathcal{G}_{ij}$ and $\bar{U}^{\sigma\sigma'}_{ij}$ are given by Eqs. (54) and (64), respectively, while for the DCA they are given by the cluster Fourier transforms of $\mathcal{G}(\mathbf{K})=[\bar{G}^{-1}(\mathbf{K},z)+\Sigma_c(\mathbf{K},z)]^{-1}$ and $\bar{U}^{\sigma\sigma'}(\mathbf{K})$ [see Eq. (60)].

For Hamiltonian-based techniques, like the noncrossing approximation, exact diagonalization, or numerical renormalization group, one needs an explicit formulation of $H_{c,0}$. To set up the bare part $H_{c,0}$, it is convenient to use Eq. (32) for the cellular DMFT or (42) for the DCA, together with Eq. (91) to represent the excluded-cluster Green's function $\boldsymbol{\mathcal{G}}$. In cellular DMFT, we have with Eq. (28)

$$\boldsymbol{\mathcal{G}}(z) = [(z+\mu)\mathbb{1} - \mathbf{t}_c - \boldsymbol{\Gamma}(z)]^{-1}, \tag{93}$$

and the matrix elements of the intracluster hopping $\mathbf{t}_c$ are given by the hopping amplitudes of the original lattice, t_{ij} as detailed in Sec. II.D.4. The noninteracting problem is thus split into two parts, cluster degrees of freedom with hopping integrals t_{ij} and their coupling to a dynamic host described by the hybridization function $\boldsymbol{\Gamma}(z)$. The cellular DMFT cluster model can hence be written as (see also Bolech *et al.*, 2003)

$$\mathcal{H}_c = \sum_{ij,\sigma}(t_{ij}-\mu\delta_{ij})c^\dagger_{i\sigma}c_{j\sigma} + \sum_{ij,\tilde{\mathbf{k}},\sigma}\lambda_{ij\tilde{\mathbf{k}}}[a^\dagger_{i\tilde{\mathbf{k}}\sigma}a_{j\tilde{\mathbf{k}}\sigma} + \text{H.c.}] + \sum_{ij,\tilde{\mathbf{k}},\sigma}[V_{ij}(\tilde{\mathbf{k}})c^\dagger_{i\sigma}a_{j\tilde{\mathbf{k}}\sigma} + \text{H.c.}] + \sum_{ij,\sigma\sigma'}\frac{\bar{U}^{\sigma\sigma'}_{ij}}{2}c^\dagger_{i\sigma}c^\dagger_{j\sigma'}c_{j\sigma'}c_{i\sigma}. \tag{94}$$

The first part describes the cluster degrees of freedom with fermionic creation (destruction) operators $c^\dagger_{i\sigma}$ ($c_{i\sigma}$). The second term simulates the host degrees of freedom as a noninteracting conduction band with the help of auxiliary operators $a^\dagger_{i\tilde{\mathbf{k}}\sigma}$ ($a_{i\tilde{\mathbf{k}}\sigma}$) and energy levels $\lambda_{ij\tilde{\mathbf{k}}}$. The coupling between the cluster states and the bath with an amplitude $V_{ij}(\tilde{\mathbf{k}})$ is described by the third term, and the interaction term is given by the last term. The sums over $\tilde{\mathbf{k}}$ run over the N/N_c wave vectors of the superlattice. Integrating out the auxiliary degrees of freedom yields an action of the form (92) with

$$\mathcal{G}_{ij}(z) = [(z+\mu)\mathbb{1} - \mathbf{t}_c - \boldsymbol{\Gamma}_c(z)]^{-1}_{ij}, \tag{95}$$

$$\Gamma_{c,ij}(z) = \sum_{lm,\tilde{\mathbf{k}}} V^*_{il}(\tilde{\mathbf{k}})[z\mathbb{1} - \lambda(\tilde{\mathbf{k}})]^{-1}_{lm}V_{mj}(\tilde{\mathbf{k}}). \tag{96}$$

Self-consistency then requires that the auxiliary parameters $\lambda_{ij\mathbf{k}}$ and $V_{ij}(\tilde{\mathbf{k}})$ be chosen in such a way that the cluster hybridization function $\boldsymbol{\Gamma}_c(z)$ is identical to its lattice counterpart $\boldsymbol{\Gamma}(z)$ defined in Eq. (93). Since Γ_{ij} is only finite on the surface of the cluster (see Sec. II.D.4), $V_{ij}(\tilde{\mathbf{k}})$ only couples sites i on the surface of the cluster to the host. This was numerically verified in cellular DMFT exact diagonalization studies by Bolech *et al.* (2003).

For the DCA we have with Eqs. (41) and (42)

$$\mathcal{G}(\mathbf{K},z) = [z - \bar{\epsilon}_{\mathbf{K}} + \mu - \Gamma(\mathbf{K},z)]^{-1}, \tag{97}$$

and hence the DCA effective cluster model is best represented in cluster $\mathbf{K}$ space as

$$\mathcal{H}_c = \sum_{\mathbf{K},\sigma}(\bar{\epsilon}_{\mathbf{K}}-\mu)c^\dagger_{\mathbf{K}\sigma}c_{\mathbf{K}\sigma} + \sum_{\mathbf{k},\sigma}\lambda_{\mathbf{k}}a^\dagger_{\mathbf{k}\sigma}a_{\mathbf{k}\sigma} + \sum_{\mathbf{K},\tilde{\mathbf{k}},\sigma}[V_{\mathbf{K}}(\tilde{\mathbf{k}})c^\dagger_{\mathbf{K}\sigma}a_{\mathbf{K}+\tilde{\mathbf{k}}\sigma} + \text{H.c.}] + \sum_{\mathbf{K},\mathbf{K}',\mathbf{Q}}\sum_{\sigma\sigma'}\frac{\bar{U}^{\sigma\sigma'}(\mathbf{Q})}{2N_c}c^\dagger_{\mathbf{K}+\mathbf{Q}\sigma}c^\dagger_{\mathbf{K}'-\mathbf{Q}\sigma'}c_{\mathbf{K}'\sigma'}c_{\mathbf{K}\sigma}. \tag{98}$$

The operators $c^\dagger_{\mathbf{K}\sigma}$ ($c_{\mathbf{K}\sigma}$) create (destroy) an electron with momentum $\mathbf{K}$ and spin σ on the cluster. $\bar{U}^{\sigma\sigma'}(\mathbf{Q})$ is the Coulomb repulsion between electrons on the cluster defined in Eq. (60) and the sum over $\tilde{\mathbf{k}}$ in the coupling term again is restricted to the N/N_c wave vectors of the superlattice. Analogously to the cellular DMFT case, the

DCA cluster model yields an action of the form (92) (in cluster Fourier space) with a $\mathcal{G}$ of the form (97) and the cluster hybridization function

$$\Gamma_c(\mathbf{K},z)=\frac{N_c}{N}\sum_{\tilde{\mathbf{k}}}\frac{|V_{\mathbf{K}}(\tilde{\mathbf{k}})|^2}{z-\lambda_{\mathbf{K}+\tilde{\mathbf{k}}}}. \tag{99}$$

The auxiliary parameters of the DCA cluster model are then determined by the condition $\Gamma_c(\mathbf{K})=\Gamma(\mathbf{K})$.

For $N_c=1$ both the cellular DMFT and the DCA cluster models reduce to the single-impurity Anderson model. As detailed in Sec. II.A, the cluster perturbation theory formalism sets the hybridization function $\mathbf{\Gamma}$ to zero, i.e., considers an isolated cluster without coupling to a host. Thus the cluster perturbation theory model is identical to the original lattice model restricted to cluster sites, i.e., given by the first and last terms of the cellular DMFT cluster model Eq. (94).

F. Phases with broken symmetry

For simplicity, in the preceding sections the self-consistent equations of quantum cluster theories were derived assuming the absence of symmetry breaking. In Sec. II.G we review how instabilities to ordered phases can be identified by the computation of response functions. However, to explore the nature as well as possible coexistence of broken-symmetry states, generalizations that explicitly account for the possibility of symmetry breaking on the single-particle level are necessary.

The applicability and modifications required to treat broken-symmetry phases depend on the cluster approach. The cluster perturbation theory formalism is not amenable to the description of ordered phases because its self-energy is that of a finite isolated cluster in which spontaneous symmetry breaking cannot occur. However, Dahnken *et al.* developed a variational extension of this theory (Dahnken *et al.*, 2004) based on the self-energy functional approach by Potthoff (2003b), which yields a self-consistent scheme for studying ordered phases (see Sec. II.I). The cellular DMFT formalism can describe ordered phases which are identifiable by a broken translational symmetry (such as antiferromagnetism) by construction, since the translational symmetry of the cellular DMFT cluster is already broken (see Maier, Gonzalez, *et al.*, 2002; Maier and Jarrell, 2002; Biroli *et al.*, 2004). Hence translationally invariant solutions are often found to be unstable against the ordered one (Biroli *et al.*, 2004). The DCA formalism is translationally invariant by construction, and therefore generalizations of the algorithm are necessary to treat ordered phases. To keep this section concise, we give examples of generalizations of the DCA formalism to a selection of types of broken-symmetry phases along with the mapping onto the corresponding cluster models. The adaption of the presented concepts to the cellular DMFT approach is straightforward.

Once the equations are generalized to account for symmetry breaking, the requisite algorithmic changes are relatively simple. A finite conjugate external field is used to initialize the calculation and break the symmetry. The field is then switched off after a few iterations and the system relaxes to its equilibrium state in the absence of external fields. On the other hand, if the field remains small and finite, the dependence of the order parameter on the field can be determined and used as an alternate way to calculate the susceptibility (by extrapolation to zero field). This approach is especially useful for cluster solvers such as the noncrossing approximation or the fluctuation-exchange approximation, in which the computation of two-particle correlation functions is numerically too expensive.

1. Ferromagnetism

We first consider the formalism necessary to treat ferromagnetism. A finite homogeneous external magnetic field h is introduced which acts on the spin σ of the fermions according to the Zeeman term

$$-h\sum_{i,\sigma}\sigma c_{i\sigma}^{\dagger}c_{i\sigma}. \tag{100}$$

The effect of h on the motion of the electronic degree of freedom, i.e., the diamagnetic term, is neglected for simplicity.[4]

In the presence of a finite h or uniform magnetization, the single-particle Green's functions for up- and down-spin electrons are not equivalent. To account for this SU(2) symmetry breaking, the spin index of the Green's function G_σ, self-energy Σ_σ, and effective medium $\mathcal{G}_\sigma$ (and hence Γ_σ) in the derivation of the DCA equations has to be retained. For a finite uniform magnetic field h the DCA lattice Green's function reads

$$G_\sigma(\mathbf{k},z)=\frac{1}{z-\epsilon_{\mathbf{K}+\tilde{\mathbf{k}}}+\mu+h\sigma-\Sigma_{c,\sigma}(\mathbf{K},z)} \tag{101}$$

and the coarse-grained and corresponding cluster-excluded Green's function,

$$\tilde{G}_\sigma(\mathbf{K},z)=\frac{N_c}{N}\sum_{\tilde{\mathbf{k}}}G_\sigma(\mathbf{K}+\tilde{\mathbf{k}},z), \tag{102}$$

$$\mathcal{G}_\sigma^{-1}(\mathbf{K},z)=G_\sigma^{-1}(\mathbf{K},z)+\Sigma_{c,\sigma}(\mathbf{K},z), \tag{103}$$

become spin dependent.

The action of the effective cluster model is identical to the action in the paramagnetic state, Eq. (92), but the spin indices have to be explicitly retained. It then describes electrons in an external magnetic field h coupled to a spin-dependent host, and self-consistency is established by equating the Green's function of the cluster model with the coarse-grained Green's function (102).

By analogy, for Hamiltonian-based cluster solvers, an additional term

[4]In 2D systems the magnetic field can be applied parallel to the plane to avoid orbital effects.

$$-h\sum_{\mathbf{K},\sigma}\sigma c^{\dagger}_{\mathbf{K}\sigma}c_{\mathbf{K}\sigma} \tag{104}$$

is added to the cluster Hamiltonian, Eq. (98), in the presence of a finite external magnetic field h. The coarse-grained Green's function $\bar{G}$, Eq. (101), is then used to calculate the magnetization $m := 1/N\Sigma_{i\sigma}\sigma\langle n_{i\sigma}\rangle$ according to

$$m = \frac{1}{N_c}\sum_{\mathbf{K},\sigma}\sigma\bar{G}_{\sigma}(\mathbf{K},\tau=0^{-}) \tag{105}$$

or after analytical continuation

$$m = -\frac{1}{\pi}\frac{1}{N_c}\sum_{\mathbf{K}\sigma}\sigma\int_{-\infty}^{+\infty}d\omega f(\omega)\mathrm{Im}\,\bar{G}_{\sigma}(\mathbf{K},\omega+i\delta). \tag{106}$$

2. Superconductivity

In this and the next section we generalize the DCA formalism to treat phases with superconducting and antiferromagnetic order, respectively. For simplicity, we refrain from discussing phases with coexisting superconducting and antiferromagnetic order. The extension to an integrated formalism is straightforward and has been described by Lichtenstein and Katsnelson (2000).

We consider superconducting phases in which the electrons are paired in spin-singlet or triplet states with a vanishing z component of the spin, $S_z=0$, which is indicated by finite values of the order parameter $\Delta_{\mathbf{k}} := \langle c_{\mathbf{k}\uparrow}c_{-\mathbf{k}\downarrow}\rangle$ for some $\mathbf{k}$. In addition to the normal Green's function $G(\mathbf{k},\tau)$ it is therefore necessary to introduce the anomalous Green's function $F(\mathbf{k},\tau)=-\langle T_\tau c_{\mathbf{k}\uparrow}(\tau)c_{-\mathbf{k}\downarrow}\rangle$. The spatial and temporal symmetry of the pairing state can then be inferred from the symmetries of F. Since F describes the pairing of fermions, it necessarily is antisymmetric under the exchange of two particles. The spatial symmetry of the pairing state is determined by the $\mathbf{k}$ dependence of the anomalous Green's function $F(\mathbf{k},\tau)$. If we assume conventional even-frequency pairing $F(\mathbf{k},-\tau)=F(\mathbf{k},\tau)$; in the case of spin-singlet pairing, F has to be symmetric in $\mathbf{k}$, i.e., $F(-\mathbf{k},\tau)=F(\mathbf{k},\tau)$ as is the case for even-parity order parameters such as s-wave and d-wave orders. In the case of spin-triplet pairing, F is antisymmetric in $\mathbf{k}$, i.e., $F(-\mathbf{k},\tau)=-F(\mathbf{k},\tau)$ as in a p-wave state.

The allowed symmetry of the pairing state is restricted by the cluster geometry. It depends upon the $\mathbf{k}$ dependence of the dispersion $\epsilon_{\mathbf{k}}$ and the $\mathbf{K}$ dependence of the cluster self-energy $\boldsymbol{\Sigma}(\mathbf{K},\tau)$. When $N_c=1$, $\boldsymbol{\Sigma}$ is local and the $\mathbf{k}$ dependence of $F(\mathbf{k},\tau)$ is entirely through $\epsilon_{\mathbf{k}}$. Hence only pairing states whose lattice symmetry is described by an order parameter with a local contribution such as s-wave and extended s-wave order can be described[5] by this formalism (Jarrell, 1992; Jarrell and Pruschke, 1993). Larger cluster sizes are necessary to describe order parameters with a symmetry less than the lattice symmetry. For example, simulations with $N_c=4$ are needed to describe phases with a $d_{x^2-y^2}$-wave order parameter which transforms according to $\cos k_x-\cos k_y$.

By utilizing the concept of Nambu spinors,

$$\Psi^{\dagger}_{\mathbf{k}} := (c^{\dagger}_{\mathbf{k}\uparrow}, c_{-\mathbf{k}\downarrow}); \Psi_{\mathbf{k}} = (\Psi^{\dagger}_{\mathbf{k}})^{\dagger}, \tag{107}$$

one can write the self-consistent equations in a more compact form, since the corresponding Green's function matrix in Nambu space,

$$\mathbf{G}(\mathbf{k},z) := \langle\langle\Psi_{\mathbf{k}};\Psi^{\dagger}_{\mathbf{k}}\rangle\rangle_z = \begin{pmatrix} G(\mathbf{k},z) & F(\mathbf{k},z) \\ F^*(\mathbf{k},z^*) & -G^*(-\mathbf{k},-z^*)\end{pmatrix}, \tag{108}$$

contains information about both the normal and anomalous Green's functions. In the presence of an external pairing field $\eta(\mathbf{k})=\eta'(\mathbf{k})+i\eta''(\mathbf{k})$ which couples to $c_{-\mathbf{k}\downarrow}c_{\mathbf{k}\uparrow}$, the noninteracting part of the Hubbard Hamiltonian can be written as $H_0=\Sigma_{\mathbf{k}}\Psi^{\dagger}_{\mathbf{k}}[\epsilon_{\mathbf{k}}\sigma_3-\eta'(\mathbf{k})\sigma_1+\eta''(\mathbf{k})\sigma_2]\Psi_{\mathbf{k}}$ so the DCA lattice Green's function in the superconducting state becomes

$$\mathbf{G}(\mathbf{k},z) = [z\sigma_o-(\epsilon_{\mathbf{k}}-\mu)\sigma_3-\eta'(\mathbf{k})\sigma_1-\eta''(\mathbf{k})\sigma_2 - \boldsymbol{\Sigma}_c(\mathbf{K},z)]^{-1}, \tag{109}$$

where $\mathbf{k}=\mathbf{K}+\tilde{\mathbf{k}}$ and σ_i are the Pauli spin matrices. The diagonal parts of the Nambu matrix $\boldsymbol{\Sigma}_c(\mathbf{K},z)$ describe quasiparticle renormalizations, and the off-diagonal parts contain information about the $\mathbf{K}$ dependence and frequency dependence of the pairing state. Again, the coarse-grained Green's function,

$$\bar{\mathbf{G}}(\mathbf{K},z) = \frac{N_c}{N}\sum_{\tilde{\mathbf{k}}}\mathbf{G}(\mathbf{K}+\mathbf{k},z) = \begin{pmatrix} \bar{G}(\mathbf{K},z) & \bar{F}(\mathbf{K},z) \\ \bar{F}^*(\mathbf{K},z^*) & -\bar{G}^*(-\mathbf{K},-z^*)\end{pmatrix}, \tag{110}$$

is used to calculate the excluded-cluster Green's function,

$$\boldsymbol{\mathcal{G}}(\mathbf{K},z) = [\bar{\mathbf{G}}^{-1}(\mathbf{K},z)+\boldsymbol{\Sigma}_c(\mathbf{K},z)]^{-1}, \tag{111}$$

which together with the coarse-grained interaction $\bar{U}^{\sigma\sigma'}(\mathbf{K})$ defines the action of the corresponding effective cluster model,

$$S_c = -\int_0^{\beta}d\tau\int_0^{\beta}d\tau'\sum_{ij}\boldsymbol{\psi}^{\dagger}_i(\tau)\boldsymbol{\mathcal{G}}_{ij}(\tau-\tau')\boldsymbol{\psi}_j(\tau') + \int_0^{\beta}d\tau\sum_{ij}\frac{\bar{U}^{\sigma\sigma'}_{ij}}{2}[\boldsymbol{\psi}^{\dagger}_i(\tau)\sigma_3\boldsymbol{\psi}_i(\tau)][(\boldsymbol{\psi}^{\dagger}_j(\tau)\sigma_3\boldsymbol{\psi}_j(\tau)]. \tag{112}$$

As in the normal-state case [see Eq. (92)], the cluster action is represented in cluster real space, and all the quantities are cluster Fourier transforms of the corresponding quantities in cluster $\mathbf{K}$ space. The spinors of Grassmann variables $\boldsymbol{\psi}^{\dagger}_i=(\gamma^*_{i\uparrow},\gamma_{i\downarrow})$ and $\boldsymbol{\psi}_i=(\boldsymbol{\psi}^{\dagger}_i)^{\dagger}$ gener-

[5]Note, however, that these order parameters cannot be distinguished.

ate coherent states corresponding to the cluster Fourier transform of the Nambu spinors, Eq. (107). Similarly, the corresponding cluster Hamiltonian in the superconducting state is obtained from the normal-state cluster Hamiltonian Eq. (98) by representing it with the Nambu spinors (107) and adding a U(1) symmetry-breaking term,

$$-\sum_{\mathbf{K}} \Psi_{\mathbf{K}}^{\dagger}[\bar{\eta}'(\mathbf{K})\sigma_1 - \bar{\eta}''(\mathbf{K})\sigma_2]\Psi_{\mathbf{K}}, \tag{113}$$

where $\bar{\eta}(\mathbf{K}) = N_c/N\Sigma_{\tilde{\mathbf{k}}}\eta(\mathbf{K}+\tilde{\mathbf{k}})$ is the coarse-grained pair field.

After self-consistency is established by requiring that the Green's function of the effective cluster model, calculated with the action Eq. (112), equal the coarse-grained Green's function Eq. (110), the order parameter $\Delta_{\mathbf{k}}$ can be calculated. Within the DCA the resolution in $\mathbf{k}$ space is restricted to the cluster $\mathbf{K}$ points and the order parameter is coarse grained,

$$\bar{\Delta}_{\mathbf{K}} = \frac{N_c}{N}\sum_{\tilde{\mathbf{k}}} \langle c_{\mathbf{K}+\tilde{\mathbf{k}}\uparrow} c_{-(\mathbf{K}+\tilde{\mathbf{k}})\downarrow}\rangle = \bar{F}(\mathbf{K}, \tau = 0^+), \tag{114}$$

and given by the equal-time coarse-grained anomalous Green's function $\bar{F}$ (after analytical continuation) as

$$\bar{F}(\mathbf{K}, \tau = 0^+) = \frac{1}{\beta}\sum_n \bar{F}(\mathbf{K}, i\omega_n) = \frac{1}{\pi}\int_0^{\infty} d\omega \tanh\left(\frac{\beta\omega}{2}\right) \mathrm{Im}\, \bar{F}(\mathbf{K}, \omega + i\delta). \tag{115}$$

3. Antiferromagnetic order

In this section we derive the DCA cluster formalism for antiferromagnetism on a bipartite lattice. This formalism is appropriate when $N_c > 1$. A formalism suitable for the case when $N_c = 1$ is discussed in detail by Georges *et al.* (1996) in the context of DMFT.

The antiferromagnetically ordered state is characterized by a spatial variation of the magnetization according to

$$\mathbf{m}(\mathbf{x}) = \mathbf{m} e^{i\mathbf{Q}\cdot\mathbf{x}}, \tag{116}$$

where $\mathbf{x}$ denotes the sites in the lattice and $\mathbf{Q}$ is the antiferromagnetic wave vector [$\mathbf{Q} = (\pi, \pi)$ in 2D]. Hence bipartite lattices can be divided into two inequivalent sublattices with $e^{i\mathbf{Q}\cdot\mathbf{x}} = +1$ for sites $\mathbf{x}$ in the A sublattice and $e^{i\mathbf{Q}\cdot\mathbf{x}} = -1$ for sites $\mathbf{x}$ in the B sublattice. The magnetic ordering thus reduces the translational symmetry of the original lattice. The volume of the magnetic unit cell is twice that of the structural unit cell. Accordingly, the volume of the first Brillouin zone in the antiferromagnetic state is reduced to half the original volume and $\mathbf{Q} = (\pi, \pi)$ becomes a reciprocal-lattice vector.

As a consequence, the correlation function

$$G_{\sigma}(\mathbf{k}, \mathbf{k}+\mathbf{Q}; \tau) = -\langle T_{\tau} c_{\mathbf{k}\sigma}(\tau) c_{\mathbf{k}+\mathbf{Q}\sigma}^{\dagger}\rangle \tag{117}$$

becomes finite. Along the lines of the formalism for the superconducting state it is then convenient to introduce spinors,

$$\Psi_{\mathbf{k}\sigma}^{\dagger} = (c_{\mathbf{k}\sigma}^{\dagger}, c_{\mathbf{k}+\mathbf{Q}\sigma}^{\dagger}); \quad \Psi_{\mathbf{k}\sigma} = (\Psi_{\mathbf{k}\sigma}^{\dagger})^{\dagger}, \tag{118}$$

for the antiferromagnetic state. In the presence of a staggered external magnetic field $h(\mathbf{x}) = h\exp(i\mathbf{Q}\cdot\mathbf{x})$ the noninteracting part of the Hamiltonian for bipartite lattices with $\epsilon_{\mathbf{k}+\mathbf{Q}} = -\epsilon_{\mathbf{k}}$ then becomes $H_0 = \Sigma'_{\mathbf{k}\sigma}\Psi_{\mathbf{k}\sigma}^{\dagger}[\epsilon_{\mathbf{k}}\sigma_3 - \sigma(h/2)\sigma_1]\Psi_{\mathbf{k}\sigma}$ where the prime on the sum indicates summation over the reduced Brillouin zone only. The corresponding Green's function,

$$\mathbf{G}_{\sigma}(\mathbf{k}, z) = \langle\langle \Psi_{\mathbf{k}\sigma}; \Psi_{\mathbf{k}\sigma}^{\dagger}\rangle\rangle_z = \left[z\sigma_o - (\epsilon_{\mathbf{k}} - \mu)\sigma_3 - \sigma\frac{h}{2}\sigma_1 - \mathbf{\Sigma}_c(\mathbf{K}, z)\right]^{-1}, \tag{119}$$

with $\mathbf{k} = \mathbf{K} + \tilde{\mathbf{k}}$, is coarse grained over the DCA cells,

$$\bar{\mathbf{G}}_{\sigma}(\mathbf{K}) = \frac{N_c}{N}\sum_{\tilde{\mathbf{k}}} \mathbf{G}_{\sigma}(\mathbf{K}+\tilde{\mathbf{k}}) = \begin{pmatrix} \bar{G}_{\sigma}(\mathbf{K}, \mathbf{K}) & \bar{G}_{\sigma}(\mathbf{K}, \mathbf{K}+\mathbf{Q}) \\ \bar{G}_{\sigma}(\mathbf{K}+\mathbf{Q}, \mathbf{K}) & \bar{G}_{\sigma}(\mathbf{K}+\mathbf{Q}, \mathbf{K}+\mathbf{Q}) \end{pmatrix}, \tag{120}$$

where we have dropped the frequency argument for convenience. The excluded-cluster Green's function,

$$\boldsymbol{\mathcal{G}}_{\sigma}(\mathbf{K}, z) = [\bar{\mathbf{G}}_{\sigma}^{-1}(\mathbf{K}, z) + \mathbf{\Sigma}_{c,\sigma}(\mathbf{K}, z)]^{-1}, \tag{121}$$

then has two elements, $\mathcal{G}_{\sigma}(\mathbf{K}, \mathbf{K})$ and $\mathcal{G}_{\sigma}(\mathbf{K}, \mathbf{K}+\mathbf{Q})$. As a result, its Fourier transform to real space,

$$\mathcal{G}_{ij,\sigma} = \frac{1}{N_c}\sum_{\mathbf{K}} e^{i\mathbf{K}\cdot(\mathbf{X}_i - \mathbf{X}_j)}\mathcal{G}_{\sigma}(\mathbf{K}) + \frac{1}{N_c}\sum_{\mathbf{K}} e^{i\mathbf{K}\cdot(\mathbf{X}_i - \mathbf{X}_j)} e^{-i\mathbf{Q}\cdot\mathbf{X}_j}\mathcal{G}_{\sigma}(\mathbf{K}, \mathbf{K}+\mathbf{Q}), \tag{122}$$

breaks translational symmetry. The action of the corresponding cluster model in the antiferromagnetic state is then formally identical to the action in the paramagnetic state, Eq. (92). As in the superconducting state the corresponding cluster model is obtained from the paramagnetic cluster model Eq. (98) by changing the representation to the Nambu spinors [Eq. (118)] and adding a symmetry-breaking term,

$$-\sum_{\mathbf{K}\sigma} \sigma\frac{h}{2}\Psi_{\mathbf{K}\sigma}^{\dagger}\sigma_1\Psi_{\mathbf{K}\sigma}, \tag{123}$$

to account for the external staggered magnetic field h.

After convergence, the sublattice magnetization $m = 1/N\Sigma_{i\sigma} e^{i\mathbf{Q}\cdot\mathbf{x}_i}\sigma\langle n_{i\sigma}\rangle$ may be calculated from the off-diagonal component of the Green's-function matrix Eq. (120) according to

$$m = \frac{1}{N_c}\sum_{\mathbf{K}\sigma} \sigma \bar{G}_\sigma(\mathbf{K},\mathbf{K}+\mathbf{Q};\tau=0^-)$$
$$= -\frac{1}{N_c \pi}\sum_{\mathbf{K}\sigma}\int_{-\infty}^{+\infty} d\omega f(\omega)\sigma \,\mathrm{Im}\,\bar{G}_\sigma(\mathbf{K},\mathbf{K}+\mathbf{Q};\omega+i\delta). \tag{124}$$

G. Calculation of susceptibilities

A convenient way to identify continuous phase transitions is to search for divergences of susceptibilities. One particular advantage of quantum cluster theories is that they allow us to consistently calculate these susceptibilities from the corresponding cluster susceptibility (Hettler *et al.*, 2000). Unfortunately, the calculation of two-particle correlation functions in the cellular DMFT formalism is strongly hampered by the violation of translational invariance on the cluster. So, in this section, we shall restrict our attention to the calculation of two-particle quantities in the DCA following Hettler *et al.* (2000) and Jarrell, Maier, Huscroft, and Moukari (2001).

As a specific example, we describe here the calculation of the two-particle Green's function,

$$\chi_{\sigma\sigma'}(q,k,k') = \int_0^\beta\int_0^\beta\int_0^\beta\int_0^\beta d\tau_1 d\tau_2 d\tau_3 d\tau_4 \times e^{i[(\omega_n+\nu)\tau_1-\omega_n\tau_2+\omega_{n'}\tau_3-(\omega_{n'}+\nu)\tau_4]} \times \langle T_\tau c^\dagger_{\mathbf{k}+\mathbf{q}\sigma}(\tau_1)c_{\mathbf{k}\sigma}(\tau_2)c^\dagger_{\mathbf{k}'\sigma'}(\tau_3)c_{\mathbf{k}'+\mathbf{q}\sigma'}(\tau_4)\rangle,$$

where we adopt the conventional notation (Abrikosov *et al.*, 1963) $k=(\mathbf{k},i\omega_n)$, $k'=(\mathbf{k}',i\omega_{n'})$, $q=(\mathbf{q},i\nu_n)$, and T_τ is the time-ordering operator.

$\chi_{\sigma\sigma'}(q,k,k')$ and the irreducible two-particle vertex function $\Gamma_{\sigma\sigma'}(q,k,k')$ (not to be confused with the single-particle hybridization function) are related to each other through the Bethe-Salpeter equation,

$$\chi_{\sigma\sigma'}(q,k,k') = \chi^0_{\sigma\sigma'}(q,k,k') + \chi^0_{\sigma\sigma''}(q,k,k'') \times \Gamma_{\sigma''\sigma'''}(q,k'',k''')\chi_{\sigma'''\sigma'}(q,k''',k'), \tag{125}$$

where $\chi^0_{\sigma\sigma'}(q,k,k'')$ is the noninteracting susceptibility constructed from a pair of fully dressed single-particle Green's functions. As usual, a summation is to be made for repeated indices.

We now make the DCA substitution $\Gamma_{\sigma\sigma'}(\mathbf{q},\mathbf{K}+\tilde{\mathbf{k}},\mathbf{K}'+\tilde{\mathbf{k}}')\to\Gamma_{c\sigma\sigma'}(\mathbf{q},\mathbf{K},\mathbf{K}')$ in Eq. (125) where Γ_c is the irreducible two-particle vertex calculated on the cluster (frequency labels have been suppressed). Note that only the bare and dressed two-particle Green's functions χ depend upon the superlattice wave vectors $\tilde{\mathbf{k}}$. Since χ and χ^0 in the product on the right-hand side of Eq. (125) share no common momentum labels, we may freely sum over the wave vectors $\tilde{\mathbf{k}}$, yielding

$$\bar{\chi}_{\sigma\sigma'}(q,K,K') = \bar{\chi}^0_{\sigma\sigma'}(q,K,K') + \bar{\chi}^0_{\sigma\sigma''}(q,K,K'') \times \Gamma_{c\sigma''\sigma'''}(q,K'',K''')\bar{\chi}_{\sigma'''\sigma'}(q,K''',K'). \tag{126}$$

By coarse graining the Bethe-Salpeter equation, we have greatly reduced its complexity; each of the matrices above is sufficiently small that they may be easily manipulated using standard techniques.

In contrast to the single-particle case, in which the coarse-grained quantities are identical to those of the cluster, the cluster quantity $\chi_{c\sigma\sigma'}(q,K,K')$ is not equal to $\bar{\chi}_{\sigma\sigma'}(q,K,K')$. This is because the self-consistency is established only at the single-particle level. Unlike the single-particle case, in which both $\Sigma_c(K)$ and $\bar{G}(K)$ are directly calculated, neither $\Gamma_{c\sigma\sigma'}(q,K,K')$ nor the coarse-grained susceptibility $\bar{\chi}_{\sigma\sigma'}(q,K,K')$ is calculated during the self-consistency. Instead, the coarse-grained noninteracting susceptibility $\bar{\chi}^0_{\sigma\sigma'}(q,K,K')$ is calculated after the DCA converges, using the relation

$$\bar{\chi}^0_{\sigma\sigma'}[(\mathbf{q},i\nu_n);(\mathbf{K},i\omega_n);(\mathbf{K}',i\omega_{n'})] = \delta_{\sigma\sigma'}\delta_{\mathbf{K}\mathbf{K}'}\delta_{\omega_n\omega_{n'}}\frac{N_c}{N}\sum_{\tilde{\mathbf{k}}} G_\sigma(\mathbf{K}+\tilde{\mathbf{k}},i\omega_n) \times G_\sigma(\mathbf{K}+\tilde{\mathbf{k}}+\mathbf{q},i\omega_n+\nu_n). \tag{127}$$

The corresponding cluster susceptibility is calculated by the cluster solver, e.g., the quantum Monte Carlo process, as discussed in Sec. III.C.1, and the vertex function is extracted by inverting the cluster two-particle Bethe-Salpeter equation,

$$\chi_{c_{\sigma\sigma'}}(q,K,K') = \chi^0_{c_{\sigma\sigma'}}(q,K,K') + \chi^0_{c_{\sigma\sigma''}}(q,K,K'') \times \Gamma_{c_{\sigma''\sigma'''}}(q,K'',K''')\chi_{c_{\sigma'''\sigma'}}(q,K''',K'). \tag{128}$$

If we combine Eqs. (128) and (126), then the coarse-grained susceptibility may be obtained after elimination of $\Gamma_{c_{\sigma\sigma'}}(q,K,K')$ between the two equations. It reads

$$\bar{\boldsymbol{\chi}}^{-1} = \boldsymbol{\chi}_c^{-1} - \boldsymbol{\chi}_c^{0^{-1}} + \bar{\boldsymbol{\chi}}^{0^{-1}}, \tag{129}$$

where, for example, $\bar{\boldsymbol{\chi}}$ is the matrix formed from $\bar{\chi}_{\sigma,\sigma'}(q,K,K')$ for fixed q. The charge (ch) and spin (sp) susceptibilities $\chi_{\mathrm{ch,sp}}(q,T)$ are deduced from $\bar{\chi}$ according to

$$\chi_{\mathrm{ch,sp}}(q,T) = \frac{(k_B T)^2}{N_c^2}\sum_{KK'\sigma\sigma'}\lambda_{\sigma\sigma'}\bar{\chi}_{\sigma\sigma'}(q,K,K'), \tag{130}$$

where $\lambda_{\sigma\sigma'}=1$ for the charge channel and $\lambda_{\sigma\sigma'}=\sigma\sigma'$ for the spin channel. The calculation of particle-particle (i.e., pairing) susceptibilities follows from a straightforward generalization of this formalism. The reader is referred to prior articles on cluster quantum Monte Carlo methods for more details on these topics (Jarrell, Maier, Huscroft, and Moukouri, 2001).

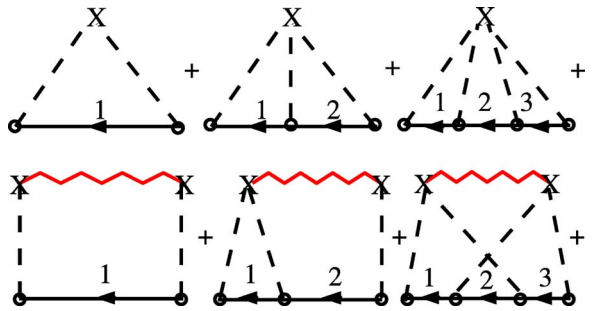

FIG. 9. (Color in online edition) A few low-order diagrams in the irreducible self-energy of a quenched diagonally disordered system. Each circle represents the scattering of a state **k** from sites denoted by **X** and a dotted line. The correlations between the electrostatic potentials on different sites are denoted by the wavy line.

H. Disordered systems

In this section, we describe cluster approximations for disordered systems. The mapping between the lattice and the cluster in the cellular DMFT and the molecular coherent potential approximation is identical, and when the cellular DMFT is applied to disordered systems, it becomes identical to the molecular CPA (Tsukada, 1969; Ducastelle, 1974). The molecular CPA and related techniques for disordered systems are extensively reviewed by Gonis (1992) and will not be discussed here.

In the remainder of this section we describe a version of the DCA for disordered systems that recovers the CPA for $N_c=1$ and becomes exact when $N_c\rightarrow\infty$. This is an extension of the formalism introduced by Jarrell and Krishnamurthy (2001), modified to include the effects of correlated disorder (Jarrell and Johnson, 2004). We consider an Anderson model with diagonal disorder, described by the Hamiltonian

$$H=-t\sum_{\langle ij\rangle,\sigma}(c_{i\sigma}^{\dagger}c_{j\sigma}+c_{j\sigma}^{\dagger}c_{i\sigma})+\sum_{i\sigma}(V_i-\mu)n_{i\sigma}, \tag{131}$$

where $c_{i\sigma}^{\dagger}$ creates a quasiparticle on site i with spin σ and $n_{i\sigma}=c_{i\sigma}^{\dagger}c_{i\sigma}$. The disorder occurs in the local orbital energies V_i which describe the electrostatic potential at site i and thus in the site occupancies labeled by χ. We assume that V_i are quenched random variables distributed according to some specified probability distribution which includes the effects of intersite correlations.

The effect of the disorder potential $\Sigma_{i\sigma}V_in_{i,\sigma}$ may be described using standard diagrammatic perturbation theory (although we eventually sum to all orders). We perturb around the ordered Hamiltonian, described by the first term in Eq. (131).

Translational invariance and momentum conservation are restored by averaging over all allowed values of the site occupancies $\{\xi_i\}$ and the corresponding disorder potentials V_i. We study this effect, for example, on the sixth graph shown in Fig. 9, which makes a contribution to the self-energy

$$\frac{1}{N^4}\sum_{i\neq j,\mathbf{k}_1,\mathbf{k}_2,\mathbf{k}_3}\langle V_i^2V_j^2\rangle G(\mathbf{k}_1)G(\mathbf{k}_2)G(\mathbf{k}_3)\times e^{i\mathbf{x}_i\cdot(\mathbf{k}_1-\mathbf{k}+\mathbf{k}_3-\mathbf{k}_2)}e^{i\mathbf{x}_j\cdot(\mathbf{k}_2-\mathbf{k}_1+\mathbf{k}'-\mathbf{k}_3)}. \tag{132}$$

After averaging over the disorder configurations, $\langle V_i^2V_j^2\rangle$ becomes a function of $\mathbf{x}_i-\mathbf{x}_j$. We identify this average as D_{ij}^{22}. With translational invariance restored, we may complete the Fourier transform and obtain

$$\frac{\delta_{\mathbf{k}\mathbf{k}'}}{N^3}\sum_{\mathbf{k}_1,\mathbf{k}_2,\mathbf{k}_3,\mathbf{q}}D^{22}(\mathbf{q})G(\mathbf{k}_1)G(\mathbf{k}_2)G(\mathbf{k}_3)\times(N\delta_{\mathbf{q}+\mathbf{k}_2+\mathbf{k},\mathbf{k}_1+\mathbf{k}_3}-1). \tag{133}$$

It is easy to extend this argument to all orders in perturbation theory. All graphs are composed of sums of products of Laue functions (e.g., $\Delta=N\delta_{\mathbf{q}+\mathbf{k}_2+\mathbf{k},\mathbf{k}_1+\mathbf{k}_3}$) and Green's functions $G(\mathbf{k})$ and $D^{nm}(\mathbf{q})$, where $D^{nm}(\mathbf{q})$ is the Fourier transform of $D_{ij}^{nm}=\langle V_i^nV_j^m\rangle$.

A hierarchy of approximations may then be constructed by approximating the Laue functions within the graphs. These include the CPA, in which conservation of the internal momentum labels is completely neglected. Here, all of the Laue functions involving the internal momentum labels are set to 1, $\Delta=N\delta_{\mathbf{k}_1+\mathbf{k}_2+\ldots}\rightarrow 1$. In this case we may freely sum over all internal momentum labels, and all terms describing nonlocal correlations, such as those on the bottom of Fig. 9, vanish, whereas the CPA graphs shown on top remain. Different cluster approximations, including the molecular CPA and the DCA, may be constructed by systematically restoring momentum conservation through the appropriate choice of Laue function, as discussed in Sec. II.B

If we choose the DCA Laue function, then we may freely sum over superlattice wave vectors $\tilde{\mathbf{k}}$ within each DCA coarse-graining cell (see Fig. 3). This leads to the replacement of the lattice propagators $G(\mathbf{k})$ and $D^{nm}(\mathbf{k})$ with coarse-grained propagators $\bar{G}(\mathbf{K})$ and $\bar{D}^{nm}(\mathbf{K})$, respectively,

$$\bar{G}(\mathbf{K},z)=\frac{N_c}{N}\sum_{\tilde{\mathbf{k}}}G(\mathbf{K}+\tilde{\mathbf{k}},z), \tag{134}$$

$$\bar{D}^{nm}(\mathbf{K})=\frac{N_c}{N}\sum_{\tilde{\mathbf{k}}}D^{nm}(\mathbf{K}+\tilde{\mathbf{k}}). \tag{135}$$

The first of these sums is straightforward; however, the second requires some investigation due to the powers of the potential.

Here, we calculate $\bar{D}^{nm}(\mathbf{K})$ for a binary A,B alloy where the concentration of A atoms is c and that of B atoms is $1-c$. This calculation can be generalized to multicomponent alloys and may easily be extended for more complex alloys. For the binary alloy, we employ an idempotent formalism where the idempotent $\xi_i=1$, indicating that the site is occupied by an A atom, or $\xi_i=0$, indicating a B-atom site. If we associate $V_i=V_A$ or V_B

for an A or B atom, respectively, then $V_i=\xi_i V_A+(1-\xi_i)V_B$. Then, since $\xi_i^n=\xi_i$ and $(1-\xi_i)^n=1-\xi_i$,

$$\begin{aligned}\langle V_i^n V_j^m\rangle &= \langle[\xi_i V_A+(1-\xi_i)V_B]^n[\xi_j V_A+(1-\xi_j)V_B]^m\rangle \\ &= \langle[\xi_i V_A^n+(1-\xi_i)V_B^n][\xi_j V_A^m+(1-\xi_j)V_B^m]\rangle \\ &= V_\beta^n V_\gamma^m g_{ij}^{\beta\gamma},\end{aligned} \tag{136}$$

where repeated indices in the last line are summed over and

$$g_{ij}^{AA}=\langle\xi_i\xi_j\rangle, \tag{137}$$

$$g_{ij}^{AB}=\langle\xi_i(1-\xi_j)\rangle, \tag{138}$$

$$g_{ij}^{BB}=\langle(1-\xi_i)(1-\xi_j)\rangle \tag{139}$$

are the joint probabilities for occupation of sites i and j by atoms of the designated types.

This formalism may be generalized to a multicomponent alloy $\beta=A,B,C,\ldots$. Since a site may only be occupied by an atom of one type only, in general

$$\langle V_i^n V_j^m\rangle = V_\beta^n V_\gamma^m g_{ij}^{\beta\gamma}. \tag{140}$$

$\langle V_i^n V_j^m\rangle$ is a linear function of the probabilities $g_{ij}^{\beta\gamma}$ for all n and m. Thus the effect of coarse graining $D^{nm}(\mathbf{k})$ is equivalent to coarse graining $g^{\beta\gamma}(\mathbf{k})$ for all n and m.

As an example, consider a binary alloy with only near-neighbor configurational correlations. Here we may write

$$g_{ij}^{\beta\gamma}=g^{0,\beta\gamma}+\alpha(2\delta_{\beta\gamma}-1)\delta_{i+\epsilon,j}, \tag{141}$$

where ϵ indexes the near neighbors to site i, and $g^{0,AA}=c^2$, $g^{0,BB}=(1-c)^2$, and $g^{0,AB}=c(1-c)$ are the joint probabilities for the occupation of different sites for a system without configurational correlations. On a hypercubic lattice of dimension D

$$g^{\beta\gamma}(\mathbf{k})=g^{0,\beta\gamma}\delta_{\mathbf{k},0}+\alpha(2\delta_{\beta\gamma}-1)\sum_{l=1}^{D}\cos(k_l). \tag{142}$$

The corresponding coarse-grained result is

$$\bar{g}^{\beta\gamma}(\mathbf{K})=g^{0,\beta\gamma}\delta_{\mathbf{K},0}+\alpha(2\delta_{\beta\gamma}-1)R\sum_{l=1}^{D}\cos(K_l), \tag{143}$$

where $R=(L_c/\pi)\sin(\pi/L_c)$ is a coarse-graining factor ($L_c=N_c^{1/D}$ is the linear cluster size). If we transform back to the cluster coordinates, then

$$\bar{g}_{ij}^{\beta\gamma}=g^{0,\beta\gamma}+R\alpha(2\delta_{\beta\gamma}-1)\delta_{i+\epsilon,j} \tag{144}$$

are the configurational probabilities for the cluster, where ϵ labels the sites adjacent to i. In the CPA limit, $L_c=1$ and thus R vanishes, indicating the lack of any configurational correlations. In the limit as $N_c=L_c^D\to\infty$, $R=1$, so correlations are systematically restored.

The cluster problem generated by the substitution $\Delta\to\Delta_{\mathrm{DCA}}$ may be solved numerically. Each of the diagrams in Fig. 9 representing N_c independent scatters, or fewer, remains finite; however, scattering diagrams for greater than N_c scatters vanish. The complexity of the problem is further reduced since the nontrivial sums involve only the cluster momenta $\mathbf{K}$ (numbering N_c instead of N). Furthermore, since these diagrams are the same as those from a finite-sized periodic cluster of N_c sites, we can easily sum this series to all orders by numerically solving the corresponding cluster problem. The resulting algorithm is identical to that presented in Sec. II.C.2, except that (i) in the coarse-graining step we must calculate both the coarse-grained correlation function,

$$\bar{g}^{\beta\gamma}(\mathbf{K})=\frac{N_c}{N}\sum_{\tilde{\mathbf{k}}}g^{\beta\gamma}(\mathbf{K}+\tilde{\mathbf{k}}), \tag{145}$$

and the coarse-grained cluster Green's function,

$$\bar{G}(\mathbf{K},z)=\frac{N_c}{N}\sum_{\tilde{\mathbf{k}}}\frac{1}{z+\mu-\epsilon_{\mathbf{K}+\tilde{\mathbf{k}}}-\Sigma_c(\mathbf{K},z)}. \tag{146}$$

(ii) We then solve the cluster problem by performing a weighted average of the cluster Green's function (in matrix notation in the cluster sites),

$$\mathbf{G}=\langle(\boldsymbol{\mathcal{G}}^{-1}-\mathbf{V})^{-1}\rangle, \tag{147}$$

over all disorder configurations. The weighting of each configuration is determined by the Fourier transform of $\bar{g}^{\beta\gamma}(\mathbf{K})$ to obtain the cluster configurational probabilities $\bar{g}_{ij}^{\beta\gamma}$. After convergence is reached, the irreducible cluster quantities may be used to calculate the properties of the lattice.

Quantum cluster theories thus allow for systematic improvement of the CPA by including nonlocal corrections. However, they share with the CPA their limited ability to describe localization effects, since the cluster sites are coupled to a translationally invariant host which effectively acts to delocalize the electrons on the cluster. However, since the crossing graphs, which are known to be responsible for localization, are systematically restored with increasing cluster size, the localization transition might be accessible by a finite-size scaling analysis that remains to be developed.

I. Alternative cluster methods

In this review we decided to focus on the three, in our view, most established cluster methods. This section briefly mentions several other ideas proposed to introduce nonlocal correlations, some of which are complementary to the approaches discussed. For details we refer the reader to the references provided.

1. Self-energy-functional theory

The self-energy-functional theory developed by Potthoff (2003b; see also Potthoff *et al.*, 2003) is a very general unifying concept for existing cluster approaches and in addition provides the power to construct novel cluster algorithms. Similar to the formalism presented in Sec. II.B, this approach views the grand potential Ω as the central quantity. Here, the self-energy $\boldsymbol{\Sigma}$ is considered

the basic dynamic variable and a self-energy functional $\Omega[\mathbf{\Sigma}]=\mathbf{Tr}\ln[-(\mathbf{G}_0^{-1}-\mathbf{\Sigma})^{-1}]+F[\mathbf{\Sigma}]$ is constructed from the Legendre transform $F[\mathbf{\Sigma}]=\Phi[\mathbf{G}[\mathbf{\Sigma}]]-\mathrm{Tr}(\mathbf{\Sigma}\mathbf{G}[\mathbf{\Sigma}])$ of the $\Phi[\mathbf{G}]$ functional. This approach proceeds with setting up a general variational scheme to use dynamical information from a (numerically) solvable reference system $H'=H_0(\mathbf{t}')+H_1(\mathbf{U})$ to approximate the physics of the original system $H=H_0(\mathbf{t})+H_1(\mathbf{U})$. Provided that both systems share the same interaction part H_1, it can be shown that the grand potential of the original system $\Omega_{\mathbf{t}}[\mathbf{\Sigma}]$ may be evaluated exactly from the grand potential Ω', the trial self-energy $\mathbf{\Sigma}(\mathbf{t}')$, and Green's function $\mathbf{G}'$ of the reference system. Variation is then performed with respect to the single-particle parameters $\mathbf{t}'$ of the reference system and the stationary point is determined by $\partial\Omega_{\mathbf{t}}[\mathbf{\Sigma}(\mathbf{t}')]/\partial\mathbf{t}'=0$.

A set of decoupled clusters of size N_c as a reference system H' yields the cluster perturbation theory when the intracluster parameters $\mathbf{t}'$ are fixed to the original values $\mathbf{t}$ (Potthoff *et al.*, 2003). Embedded-cluster theories are constructed by introducing an additional set of n_b bath sites. The DMFT is obtained with a reference system of decoupled sites coupled to $n_b=\infty$ bath sites, while the cellular DMFT is constructed from a set of decoupled clusters with intracluster hopping $\mathbf{t}'=\mathbf{t}$ coupled to $n_b=\infty$ bath sites (Potthoff *et al.*, 2003). Intermediate approximations are constructed by considering a finite number $0<n_b<\infty$ of bath sites. Such an approach for $N_c=1$ was applied to a study of the Mott transition in the Hubbard model by Potthoff (2003a) and Pozgajcić (2004). Furthermore, due to its generality the self-energy-functional approach allows us to improve existing cluster methods. Dahnken *et al.* (2004), for example, constructed a variational cluster perturbation theory within the self-energy-functional theory to extend the applicability of the cluster perturbation theory to broken-symmetry phases.

2. Fictive impurity models

Like the self-energy-functional approach discussed above, this very general approach by Okamoto *et al.* (2003) is centered on the self-energy $\mathbf{\Sigma}$ as the basic dynamic variable. It is based on the idea that the cluster model is merely an algorithm for calculating coefficients in an orthogonal function expansion of the momentum dependence of the electronic self-energy $\Sigma_{\mathrm{approx}}(\mathbf{k},z)=\Sigma_{i=0\cdots n}\Phi_i(\mathbf{k})\Sigma_i(z)$. The coefficients $\Sigma_i(z)$ can then be obtained from the solution of a $n+1$-site fictive impurity model involving $n+1$ mean fields which are fixed by the requirement that the impurity model Green's functions G_i equal the corresponding integrals over the lattice Green's function $G_i(z)=\Sigma_{\mathbf{k}}\Phi_i(\mathbf{k})[G_o^{-1}(\mathbf{k},z)-\Sigma_{\mathrm{approx}}(\mathbf{k},z)]^{-1}$. To include local and nearest-neighbor correlations, the momentum dependence of the self-energy may be expanded up to second order using the orthogonal functions $\Phi_0(\mathbf{k})=1$ and $\Phi_1(\mathbf{k})=e^{ika}$. Since in general the orthogonal functions $\Phi_i(\mathbf{k})$ change sign over the Brillouin zone except for the local term $i=0$, causality is not guaranteed when the expansion is truncated at low order. However, it is shown that simple filtering of the higher-order terms may be used to circumvent these problems (Okamoto *et al.*, 2003).

The DCA may be viewed as a specific example of this approach, in which the indices i correspond to the centers $\mathbf{K}$ of the DCA cells and the functions $\Phi_{\mathbf{K}}(\mathbf{k})$ are set to 1 if $\mathbf{k}$ is contained in the cell represented by $\mathbf{K}$ and 0 otherwise (see Fig. 3). Causality problems are thus avoided by using orthogonal functions which are nonnegative everywhere.

3. Nonlocal effects via spectral density approximation

Laad and van den Bossche (2000) proposed the inclusion of nonlocal $1/D$ corrections by combining DMFT with the spectral density approximation (Roth, 1969) and applied this approach to the Falicov-Kimball model [see Eq. (182)], for which it becomes particularly simple. In the spectral density approximation, the moments of the spectral function are determined (via repeated evaluation of commutators with the Hamiltonian) by complicated but static correlators. For the Falicov-Kimball model, to order $1/D$ the self-energy of the d electrons, $\Sigma_{0,d}(\mathbf{k},z)$, can be expressed in terms of the static susceptibility of the f electrons. This self-energy is purely real, but momentum dependent and is used to approximate the bath self-energy $\Sigma_{0,d}(\mathbf{k},z)$ in the hybridization function $\Gamma(z)=\Sigma_{\mathbf{k}}\{t^2/[z-\epsilon_{\mathbf{k}}+\mu-\Sigma_{0,d}(\mathbf{k},z)]\}$ for the effective impurity problem in $D=\infty$. The impurity self-energy $\Sigma_{\mathrm{imp},d}(z)$ (see Brandt and Mielsch, 1989) is combined with $\Sigma_{0,d}(\mathbf{k},z)$ to create a dynamical, nonlocal self-energy of the form $\Sigma_d(\mathbf{k},z)=\Sigma_{\mathrm{imp},d}(z)+\Sigma_{0,d}(\mathbf{k},z)-\Sigma_{\mathbf{k}}\Sigma_{0,d}(\mathbf{k},z)$. This finally determines the Green's function of the mobile d electrons of the usual form, $G_d(\mathbf{k},z)=[z-\epsilon_{\mathbf{k}}+\mu-\Sigma_d(\mathbf{k},z)]^{-1}$, which is used together with $\Sigma_d(\mathbf{k},z)$ to estimate the susceptibility of the f electrons. $\Sigma_{0,d}(\mathbf{k},z)$ can then be recalculated to close the self-consistency loop.

Results for the density of states (DOS) and spectral function of the Falicov-Kimball model on a square lattice obtained with this method (Laad and van den Bossche, 2000) agree well with known results and with other studies like that of Hettler *et al.* (2000). For a model with true dynamics, however, like the Hubbard model, it is unclear whether the method is even feasible (due to the additional spin-flip and pair-hopping correlators), and the limitation of a purely real bath self-energy is likely to be too restrictive.

4. Nonlocal corrections via projection technique

Using the projection technique Tien has developed a cluster extension of the DMFT by taking into account both local and nonlocal contributions to the dynamics within a relevant subspace of Liouville or operator space (Minh-Tien, 1998, 1999a, 1999b, 2001; Tanh-Hai and Minh-Tien, 2001). The information of a given subspace is stored in static susceptibility and frequency functions while the effects of the remaining subspace are collected

in a dynamic memory function which is approximated by a local quantity. If the relevant subspace is spanned by operators acting on the same or nearest-neighbor sites only, unknown quantities can be calculated in an effective impurity model (Minh-Tien, 1998, 1999a) or, in an improved version, in a two-site cluster model (Minh-Tien, 1999b, 2001; Tanh-Hai and Minh-Tien, 2001).

This approach has not been rigorously proven to be causal, however, its application to the Falicov-Kimball model (Minh-Tien, 1998, 1999b) and the Hubbard model (Minh-Tien, 2001) shows that the spectral function is positive definite and the sum rules of the first few moments of the spectral densities are preserved. The neglect of nonlocal dynamical correlations, however, leads to spurious behavior at low temperatures: A Kondo resonance emerges in the 2D half-filled Hubbard model at low temperatures similar to the behavior observed in DMFT simulations but inconsistent with other cluster calculations which show a pseudogap down to the lowest temperatures (see Sec. IV.D.2).

5. Two-site correlations with composite operators

A dynamical nonperturbative two-site approximation for the Hubbard model based on the composite operator method was developed by Matsumoto and Mancini (1997) and later adopted and improved by Stanescu and Phillips (Stanescu and Phillips, 2001, 2004). By using Hubbard operators as a local basis which exactly diagonalize the interaction part of the Hamiltonian, this approach recovers both the weak-coupling $U \ll t$ and strong-coupling $U \gg t$ limits of the Hubbard model. On-site and nearest-neighbor dynamical correlations are included by expanding the memory function $\delta m(\mathbf{k}, \omega)$, which collects the effects of dynamical correlations, in a two-site approximation. Unknown quantities are expressed in terms of resolvents for the eigenstates of a two-site impurity system and the coupling to the surrounding of the two-site system is treated within the noncrossing approximation.

The application of this technique to the Hubbard model shows qualitative agreement of the single-particle spectra (Matsumoto and Mancini, 1997) in two dimensions with finite-size quantum Monte Carlo results and high accuracy of specific heat results (Stanescu and Phillips, 2001) as compared to the Bethe ansatz solution in one dimension. Although this technique includes only on-site and nearest-neighbor correlations, it already captures important signatures of correlations consistent with DCA-quantum Monte Carlo results for larger clusters (see Sec. IV.D).

III. QUANTUM CLUSTER SOLVERS

Cluster techniques map the lattice system onto a self-consistently embedded quantum cluster model. This section discusses the most promising numerical approaches used to solve this cluster problem. After stressing some general difficulties faced by potential cluster solvers in Sec. III.A, we present several perturbative techniques in Sec. III.B and nonperturbative (numerically) exact techniques in Sec. III.C. While a detailed discussion of the different methods would be highly desirable here, the restricted space allows us only to touch briefly on most methods, referring the interested reader to the references.

A. General remarks

The fundamental difference between a finite-size cluster and the effective cluster problem of quantum cluster theories is the existence of additional quantum-mechanical bath degrees of freedom in the latter. The simplest realization of such a system is of course the well-known Anderson impurity model (Anderson, 1961). In general, its ground and excited states are nontrivial many-body states and typically involve dynamically generated low-energy scales which depend nonanalytically on system parameters. Consequently, any perturbation theory is faced with severe limitations concerning its region of applicability, and the most successful techniques used to solve this fundamental problem of solid-state theory are nonperturbative (Hewson, 1993).

Nevertheless, a variety of tools for solving this model approximately or numerically have been developed over the last 25 years (Hewson, 1993). Since the physics of the Anderson impurity model are very well understood (Hewson, 1993), this knowledge can be employed to judge the quality of results and region of applicability of these various analytical or computational techniques, *a priori* as well as *a posteriori*. This statement does also apply to a large extent to the DMFT, where an effective Anderson impurity model plays the central role (Pruschke *et al.*, 1995; Georges *et al.*, 1996).

The situation becomes much more involved for quantum cluster problems. First, from a purely technical point of view, the complexity of the system can limit the applicability of a method or even rule it out as a potential cluster solver altogether. Similarly important is the complexity of the physics, making it harder to judge the reliability and quality of results obtained with a certain method. In contrast to the single-impurity case, in which the qualitative results to be expected from a calculation can in principle be read off from the input parameters, such a plausibility check for a given method is not possible in quantum cluster models. Experience tells us that even at first sight physically plausible results need to be checked carefully. An example is the occurrence of a quantum phase transition in the two-impurity Kondo model (Jones and Varma, 1987; Jones *et al.*, 1988) driven by the competition between the Ruderman-Kittel-Kasuya-Yosida (RKKY) magnetic interaction favoring a nonlocal singlet and the Kondo effect with its local singlet formation. This quite intuitive result was later reexamined by others and found to be valid only under very special circumstances (Sakai *et al.*, 1990; Sakai and Shimizu, 1992).

Thus, in order to obtain a reliable and consistent understanding of the physics of correlated electron systems in the framework of cluster mean-field theories, it is vital

to employ a variety of complementary and possibly nonperturbative tools to solve the effective quantum cluster model. We therefore discuss in detail the applicability and reliability of different computational and analytical tools.

B. Perturbative techniques

The numerical effort required to solve the cluster problem increases rapidly with the cluster size, in principle exponentially for exact methods. Thus simpler methods, able to reduce the complexity of the problem, are called for, such as the various perturbative methods. One such method, the fluctuation-exchange approximation, is discussed in the following section. A complementary strong-coupling approach handles the interaction exactly, but treats the coupling to the host Γ in a perturbative expansion. An example of this approach is the noncrossing approximation, discussed in Sec. III.B.2.

1. Fluctuation-exchange approximation

The application of the fluctuation-exchange approximation (Bickers *et al.*, 1989; Bickers and White, 1990) as a cluster solver follows immediately from the formulation in Sec. II.B when one considers an infinite subset of diagrams in the cluster $\Phi[\bar{G}]$ functional. It rests on the assumption that the interacting electron system can be viewed as a problem of electrons exchanging self-consistently determined fluctuations of various kinds, i.e., density, spin, and pair fluctuations. In the context of quantum cluster theories, the fluctuation-exchange approximation was applied within the DCA by Aryanpour, Hettler, and Jarrell (2003). Here we briefly review the corresponding formalism.

The generating functional Φ of the fluctuation-exchange approximation is a sum of the three fluctuation contributions (Bickers *et al.*, 1989),

$$\Phi = \Phi_{\mathrm{ph}}^{\mathrm{df}} + \Phi_{\mathrm{ph}}^{\mathrm{sf}} + \Phi_{\mathrm{pp}}, \tag{148}$$

where

$$\Phi_{\mathrm{ph}}^{\mathrm{df}} = -\frac{1}{2}\mathrm{Tr}[\chi_{\mathrm{ph}}]^2 + \frac{1}{2}\mathrm{Tr}\left(\ln(1+\chi_{\mathrm{ph}}) - \chi_{\mathrm{ph}} + \frac{1}{2}\chi_{\mathrm{ph}}^2\right), \tag{149}$$

$$\Phi_{\mathrm{ph}}^{\mathrm{sf}} = \frac{3}{2}\mathrm{Tr}\left(\ln(1-\chi_{\mathrm{ph}}) + \chi_{\mathrm{ph}} + \frac{1}{2}\chi_{\mathrm{ph}}^2\right), \tag{150}$$

$$\Phi_{\mathrm{pp}} = \mathrm{Tr}\left(\ln(1+\chi_{\mathrm{pp}}) - \chi_{\mathrm{pp}} + \frac{1}{2}\chi_{\mathrm{pp}}^2\right), \tag{151}$$

and the trace Tr denotes $(T/N_c)\Sigma_{\mathbf{Q}}\Sigma_n$. With the notation $K=(\mathbf{K},i\omega_m)$, $Q=(\mathbf{Q},i\nu_n)$, where $\mathbf{K},\mathbf{Q}$ are cluster momenta and ω_m (ν_n) is a fermionic (bosonic) Matsubara frequency, we have for the particle-hole susceptibility

$$\chi_{\mathrm{ph}}(Q) = -\frac{UT}{N_c}\sum_K \bar{G}(K+Q)\bar{G}(K), \tag{152}$$

and the particle-particle susceptibility

$$\chi_{\mathrm{pp}}(Q) = \frac{UT}{N_c}\sum_K \bar{G}(Q-K)\bar{G}(K). \tag{153}$$

The self-energy may be calculated from a functional derivative of $\Phi[\bar{G}]$ with the coarse-grained Green's function $\bar{G}$. It is

$$\Sigma_c(K) = \frac{UT}{N_c}\sum_Q [V^{(\mathrm{ph})}(Q)\bar{G}(K-Q) - V^{(\mathrm{pp})}(Q)\bar{G}(Q-K)], \tag{154}$$

where the fluctuation-exchange or so-called FLEX potentials are given by

$$V^{(\mathrm{ph})} = -\chi_{\mathrm{ph}} + \frac{1}{2}\frac{\chi_{\mathrm{ph}}}{1+\chi_{\mathrm{ph}}} + \frac{3}{2}\frac{\chi_{\mathrm{ph}}}{1-\chi_{\mathrm{ph}}}, \tag{155}$$

$$V^{(\mathrm{pp})} = -\chi_{\mathrm{pp}} + \frac{\chi_{\mathrm{pp}}}{1+\chi_{\mathrm{pp}}}. \tag{156}$$

Here we ignored the constant (first-order) Hartree term, which just shifts the chemical potential. The FLEX potentials constitute an infinite sum of fluctuation diagrams similar to the series of density fluctuations also known as the random-phase approximation, which is in fact a subset of the fluctuation-exchange approximation. However, the latter also includes significant spin and pair fluctuations. Note that second-order perturbation theory is reproduced by expanding Eq. (155) to first order in χ_{ph}.

The convolutions in the equations above may be readily computed with the fast Fourier transform (FFT). Straightforward application of the FFT to Green's functions (in particular with fermionic Matsubara frequencies), however, is likely to incur large errors, due to the slow $1/i\omega_n$ decay of the Green's functions and self-energies. Details on how to overcome this technical difficulty can be found in Deisz *et al.* (2003). To obtain real-time (or frequency) data, an analytic continuation of the Green's function or self-energy is necessary. For the fluctuation exchange, this is achieved by means of Padé approximation (Vidberg and Serene, 1977). Real-frequency results and details on the implementation of the Padé approximation are given by Aryanpour, Hettler, and Jarrell (2003).

Naturally, the drawback of weak-coupling methods lies in the fact that some strong-coupling phenomena such as the opening of a Mott gap at half-filling simply cannot be described by the fluctuation-exchange approach. Such an inherent shortcoming cannot be overcome by adding a quantum cluster theory like DCA on top of the fluctuation-exchange approximation. However, other issues like problems with convergence of the self-consistency loop at low temperatures (due to divergences in perturbatively evaluated response functions)

are at least alleviated. Also, since the DCA/FLEX is within the thermodynamic limit, the scaling with cluster size is complementary to that of the plain FLEX on a finite-size system; see Sec. IV.A. In this sense, the combined use of the DCA and fluctuation-exchange approximations provides a means to push the FLEX approach to its limits.

For the cellular DMFT, one can formulate similar expressions, but, as discussed in Sec. II, the self-energy and Green's function are matrices in cluster real space. The matrix inversions needed during the iteration become costly as the cluster size is increased.

2. Noncrossing approximation

The noncrossing approximation (NCA) (Keiter and Kimball, 1971; Grewe, 1983; Keiter and Czycholl, 1983; Kuramoto, 1983) was originally developed for the single-impurity Anderson model and is based on a diagrammatic perturbation theory (Keiter and Kimball, 1970; Kuramoto, 1983) around the atomic limit of this model. A comprehensive and detailed description of the noncrossing approximation and its limitations can be found in the review by Bickers (1987). This approximation has been extensively applied as an approximate solution of the effective impurity model in the context of DMFT (Kuramoto, 1985; Kim *et al.*, 1990; Pruschke *et al.*, 1993a, 1993b; Lombardo *et al.*, 1996; Schmalian *et al.*, 1996; Maier *et al.*, 1999a, 1999b; Zölfl *et al.*, 2000) and the DCA (Maier *et al.*, 2000b).

The perturbation theory used to construct the noncrossing approximation is based on a resolvent technique. It starts from the local part of the cluster Hamiltonian, Eq. (98),

$$H_{c,\mathrm{loc}} = \sum_{\mathbf{K}\sigma} (\bar{\epsilon}_{\mathbf{K}} - \mu) c^{\dagger}_{\mathbf{K}\sigma} c_{\mathbf{K}\sigma} + \sum_{\substack{\mathbf{K},\mathbf{K}'\\ \mathbf{Q}}} \sum_{\sigma\sigma'} \frac{\bar{U}^{\sigma\sigma'}(\mathbf{Q})}{2N_c} c^{\dagger}_{\mathbf{K}+\mathbf{Q}\sigma} c^{\dagger}_{\mathbf{K}'-\mathbf{Q}\sigma'} c_{\mathbf{K}'\sigma'} c_{\mathbf{K}\sigma}. \tag{157}$$

The perturbation expansion is done with respect to the coupling to the continuous auxiliary noninteracting fermions $a_{\mathbf{k}\sigma}$ ($a^{\dagger}_{\mathbf{k}\sigma}$). Hence this approach should be an especially useful approximation when the local energy scales (in this case $\bar{U}$) exceed the magnitude of the coupling V to the host. To proceed, the fermionic cluster operators $c_{\mathbf{K}\sigma}$ ($c^{\dagger}_{\mathbf{K}\sigma}$) are expanded in terms of Hubbard operators $X_{mn} = |m\rangle\langle n|$,

$$c_{\mathbf{K}\sigma} = \sum_{m,n} C^{mn}_{\mathbf{K}\sigma} X_{mn}, \quad c^{\dagger}_{\mathbf{K}\sigma} = \sum_{m,n} C^{mn*}_{\mathbf{K}\sigma} X_{nm}, \tag{158}$$

where $\{|m\rangle\}$ are the eigenstates of the local Hamiltonian, Eq. (157),

$$H_{c,\mathrm{loc}} = \sum_{m} E_m X_{mm} \tag{159}$$

with eigenenergies E_m and $C^{mn}_{\mathbf{K}\sigma} = \langle m|c_{\mathbf{K}\sigma}|n\rangle$. Since the X_{mn} do not obey standard fermionic commutation relations, the conventional Feynman diagram technique cannot be used for a perturbational expansion and the concept of resolvents must be introduced instead (Kuramoto, 1983). The matrix elements of these resolvents in the space of the local eigenstates have the form

$$R^{-1}_{mn}(z) = (z - E_m)\delta_{mn} - \Sigma^{R}_{mn}(z), \tag{160}$$

where the resolvent self-energy $\Sigma^R(z)$ collects renormalization effects of the individual molecular states $\{|m\rangle\}$ due to the hybridization to the host.

Keeping only the lowest-order contributions to the resolvent self-energy Σ^R [for a detailed discussion see, Bickers (1987); Maier *et al.* (2000b)] defines the noncrossing approximation and leads to the analytical expression

$$\Sigma^{R}_{mn}(z) = -\frac{1}{\pi}\sum_{\mathbf{K},\sigma}\sum_{l,l'}\left[\int_{-\infty}^{+\infty} d\varepsilon f(\varepsilon)\,\mathrm{Im}\,\Gamma(\mathbf{K},\varepsilon) C^{ml}_{\mathbf{K}\sigma} \times R_{ll'}(z+\varepsilon) C^{nl'*}_{\mathbf{K}\sigma} + \int_{-\infty}^{+\infty} d\varepsilon f(-\varepsilon)\,\mathrm{Im}\,\Gamma(\mathbf{K},\varepsilon) C^{lm*}_{\mathbf{K}\sigma} \times R_{ll'}(z-\varepsilon) C^{l'n}_{\mathbf{K}\sigma}\right], \tag{161}$$

where $\Gamma(\mathbf{K},\varepsilon)$ is defined by Eq. (99). Note that the host degrees of freedom enter only through $\Gamma(\mathbf{K},\varepsilon)$, i.e., there is no need to explicitly calculate the auxiliary host parameters $V_{\mathbf{K}}(\tilde{\mathbf{k}})$ and $\lambda_{\mathbf{k}}$ of the cluster Hamiltonian, Eq. (98). Written in terms of Hubbard operators, the cluster Green's function $G_c(\mathbf{K},z) = \langle\langle c_{\mathbf{K}\sigma}; c^{\dagger}_{\mathbf{K}\sigma}\rangle\rangle_z$ becomes

$$G_c(\mathbf{K},z) = \sum_{m,n,m',n'} C^{mm'}_{\mathbf{K}\sigma} C^{nn'*}_{\mathbf{K}\sigma} \langle\langle X_{mm'}; X_{n'n}\rangle\rangle_z.$$

Within the noncrossing approximation

$$\langle\langle X_{mm'}; X_{n'n}\rangle\rangle_z = \frac{1}{Z_c}\oint_{\mathcal{C}} dz' \frac{e^{-\beta z'}}{2\pi i} R_{nm}(z') R_{m'n'}(z'+z),$$

where Z_c denotes the cluster partition function, $\beta = 1/T$ the inverse temperature and the contour $\mathcal{C}$ encircles all singularities of the integrand counterclockwise.

Although the application of this approximation was illustrated for the DCA cluster model, it can in principle also be applied to solve the cellular DMFT cluster problem, Eq. (94). The fact that in the cellular DMFT the hybridization function Γ is a matrix in the N_c cluster sites, however, complicates this task considerably.

One can show analytically that the noncrossing approximation can produce a low-energy scale depending nonanalytically on the bare model parameters (Müller-Hartmann, 1984) and that certain general features like universality in this energy scale are present, too (Fischer, 1997). Although the noncrossing approximation breaks down at low temperatures (Grewe, 1983; Kuramoto,

1983; Müller-Hartmann, 1984), there exists a finite window down to temperatures of the order of an effective Fermi-liquid scale where it produces reliable results (Bickers, 1987; Cox and Grewe, 1987; Pruschke *et al.*, 1993b; Fischer, 1997).

A rather different question is whether these results are only qualitatively or even quantitatively correct. Here, the answer depends on the system under consideration. Going beyond a single Anderson impurity at $U=\infty$ introduces the need to include diagrams beyond the lowest-order noncrossing approximation (Bickers *et al.*, 1987; Pruschke and Grewe, 1989; Heindl *et al.*, 2000). Neglecting these so-called vertex corrections means that the magnitude of a possible Fermi-liquid scale will be grossly underestimated. However, in the case of strong nonlocal fluctuations, as one would expect in 2D problems, such a scale will in general be extremely small or even zero anyway. Here, the influence of vertex corrections can be expected to be less severe and the noncrossing approximation even quantitatively reliable.

Even with these restrictions, solution of the noncrossing approximation still becomes formidable as the cluster size N_c increases. The number of eigenstates and hence number of coupled equations (160) and (161) that have to be solved self-consistently grows exponentially. Thus, although the study of larger clusters is in principle possible, the noncrossing approximation technique is very limited in cluster size and so far has only been applied to $N_c=4$ size clusters.

C. Nonperturbative techniques

Nonperturbative techniques solve the effective cluster problem (numerically) exactly. This advantage comes at the expense of allowing only small cluster sizes to be treated. The size restriction on the cluster quantum Monte Carlo technique described in the following section is basically the same as in the case of quantum Monte Carlo for finite-size systems. For the exact diagonalization and numerical renormalization-group approaches discussed in the next sections, however, a Hamiltonian for both the cluster and the host degrees of freedom needs to be explicitly simulated, further limiting the usefulness of these methods.

1. Quantum Monte Carlo

a. Introduction

The quantum Monte Carlo (QMC) method is a powerful and general technique for solving quantum cluster problems. It has several advantages, including the ability to treat relatively large clusters (compared to other exact methods), the simplicity of the required code, and the fact that only the excluded cluster Green's function $\mathcal{G}$ and the coarse-grained interaction $\bar{U}$ are required as inputs. Quantum Monte Carlo is also numerically exact, with small and controllable sources of systematic and statistical errors. Its disadvantages include the fact that there is a minus sign problem that is unpredictable, difficulties in calculating real-frequency results, and the numerical expense of the approach.

The quantum Monte Carlo algorithm for clusters is based on an algorithm of Hirsch and Fye that was developed to simulate the Anderson impurity problem (Hirsch and Fye, 1986). It was later generalized to solve the DMFT and DCA effective impurity problems by Jarrell (1992) and Jarrell, Maier, Huscroft, and Moukouri (2001), respectively. Although the algorithm is formulated using a path integral in imaginary time, the maximum-entropy method may be used to analytically continue the quantum Monte Carlo data to obtain real-frequency spectra (Jarrell and Gubernatis, 1996).

The quantum Monte Carlo algorithm uses the action of the effective cluster model, Eq. (92), as a starting point and therefore can be equally applied within the cellular DMFT and the DCA. It requires as inputs the initial bare Green's function $\mathcal{G}$ and the form of the coarse-grained interaction[6] $\bar{U}$. This is an advantage, since due to the required self-consistency of embedded cluster techniques, we generally do not know the auxiliary parameters of the cluster Hamiltonian.

Several steps are required to evaluate the path integrals of this action using the quantum Monte Carlo method. We first introduce Hubbard-Stratonovich fields, which are required to decouple the interaction, transforming a problem of interacting electrons to one of noninteracting particles coupled to time-dependent Hubbard-Stratonovich fields. The fermionic and bosonic fields are then integrated out, and the integrals over the decoupling fields are performed with a Monte Carlo algorithm. Measurements of any diagrammatic quantity are accomplished by decomposing the associated operators using Wick's theorem (both connected and disconnected contractions must be included) and then averaging the result over the Monte-Carlo-generated field configurations.

b. Quantum Monte Carlo for the simple Hubbard model

As a specific example, we consider the simple Hubbard model with a local interaction of strength U. Since this interaction is local, it is unaffected by coarse graining, so $\bar{U}=U$. To approximate the time integrals in the action, we introduce a discrete time grid with L slices and a time step $\Delta\tau=\beta/L$. The interacting part of the action is then decoupled by mapping it to an auxiliary Ising field via a discrete Hirsch-Hubbard-Stratonovich transformation (Hirsch, 1983),

$$e^{-\Delta\tau U\Sigma_{\mathbf{i}}(n_{\mathbf{i}\uparrow}-1/2)(n_{\mathbf{i}\downarrow}-1/2)}=\frac{1}{2}e^{-\Delta\tau U/4}\prod_{\mathbf{i}}\sum_{s_{\mathbf{i}}=\pm 1}e^{\alpha s_{\mathbf{i}}(n_{\mathbf{i}\uparrow}-n_{\mathbf{i}\downarrow})}, \tag{162}$$

where $\cosh(\alpha)=e^{\Delta\tau U/2}$ and the index $\mathbf{i}$ denotes the cluster sites. With this change, the cluster action takes the form

[6]It is also possible to treat the interaction in a self-consistent manner, as was described by Hettler *et al.* (2000).

$$S_c[\gamma,\gamma^*] = \sum_{\mathbf{i},l;\mathbf{i}',l',\sigma} \gamma^*_{\mathbf{i},l,\sigma}\mathcal{G}^{-1}(\mathbf{i},l;\mathbf{i}',l')\gamma_{\mathbf{i}',l',\sigma} - \sum_{\mathbf{i}=1}^{N_c}\sum_{l=1}^{N_l}\sum_{\sigma}\alpha\gamma^*_{\mathbf{i},l,\sigma}\sigma s_{\mathbf{i},l}\gamma_{\mathbf{i},l-1,\sigma}, \tag{163}$$

where l denotes the time slice τ_l and $\mathcal{G}(\mathbf{i},l;\mathbf{i}',l') \equiv \mathcal{G}_{\mathbf{i}\mathbf{i}'}(\tau_l-\tau_{l'})$ the excluded-cluster Green's function defined in Eq. (91). Now we integrate out the remaining cluster Grassmann variables. The partition function then becomes

$$Z \propto \int \mathcal{D}[\gamma]\mathcal{D}[\gamma^*]e^{-S_c[\gamma,\gamma^*]} = \mathrm{Tr}_{\{s_{\mathbf{i},l}\}}\prod_{\sigma}\det(G_{c_\sigma;s_{\mathbf{i},l}})^{-1}, \tag{164}$$

where factors that are fixed during the quantum Monte Carlo process have been ignored. $(G_{c_\sigma;s_{il}})^{-1}$ is the inverse-cluster Green's-function matrix with elements

$$(G_{c_\sigma;s_{\mathbf{i}l}})^{-1}_{\mathbf{i},\mathbf{j},l,l'} = \mathcal{G}^{-1}_{\mathbf{i},\mathbf{j},l,l'} - \delta_{\mathbf{i},\mathbf{j}}\delta_{l',l-1}\alpha\sigma s_{\mathbf{i},l}. \tag{165}$$

A Monte Carlo algorithm is used to perform the remaining integral over the Hirsch-Hubbard-Stratonovich fields. The Markov process in this algorithm proceeds by suggesting local changes of the Hirsch-Hubbard-Stratonovich fields at one point in space-time. These changes are accepted or rejected according to the change in their Boltzmann weight, the argument of the trace in Eq. (164). If the change is accepted, the Green's function must be updated accordingly. Several approximations, i.e., changes to these equations that are beyond linear order in $\Delta\tau$, are necessary to obtain an efficient algorithm. First, we reexponentiate the first term on the right-hand side of Eq. (165), obtaining in a simple matrix notation in space-time

$$G^{-1}_{c_\sigma} = \mathcal{G}^{-1} - T(e^{V_\sigma}-1), \tag{166}$$

where T is $\delta_{\mathbf{i},\mathbf{j}}\delta_{l-1,l'}$ and $V_\sigma(\mathbf{i},l) \equiv \alpha s_{\mathbf{i},l}\sigma$. Note that the term in the parentheses is beyond zeroth order in $\Delta\tau$. Therefore, to first order in $\Delta\tau$, we may write

$$G^{-1}_{c_\sigma} = \mathcal{G}^{-1} + (\mathcal{G}^{-1}-1)(e^{V_\sigma}-1), \tag{167}$$

since $\mathcal{G}^{-1}-1 = -T+\mathcal{O}(\Delta\tau)$. Therefore the inverse Green's functions for two different field configurations, $\{s_{\mathbf{i}l}\}$ and $\{s'_{\mathbf{i}l}\}$, are related by

$$G'^{-1}_{c_\sigma}e^{-V'_\sigma} = G^{-1}_{c_\sigma}e^{-V_\sigma} - e^{-V_\sigma} + e^{-V'_\sigma}. \tag{168}$$

Or, after multiplying by $e^{V'_\sigma}$, and collecting terms,

$$G'^{-1}_{c_\sigma} - G^{-1}_{c_\sigma} = (G^{-1}_{c_\sigma}-1)e^{-V_\sigma}(e^{V'_\sigma}-e^{V_\sigma}). \tag{169}$$

Multiplying from the left by G_c and from the right by G'_c, we find

$$G'_{c_\sigma} = G_{c_\sigma} + (G_{c_\sigma}-1)(e^{V'_\sigma-V_\sigma}-1)G'_{c_\sigma} \tag{170}$$

or

$$G_{c_\sigma}G'^{-1}_{c_\sigma} = 1 + (1-G_{c_\sigma})(e^{V'_\sigma-V_\sigma}-1). \tag{171}$$

The quantum Monte Carlo algorithm proposes changes in the Hubbard-Stratonovich field configuration $\{s_{\mathbf{i},l}\} \to \{s'_{\mathbf{i},l}\}$ and accepts these changes with the transition probability $P_{s\to s'}$. Thus, to implement the algorithm, we need $P_{s\to s'}$ and a relation between the cluster Green's functions G_c and G'_c for the two different auxiliary field configurations. To simplify the notation, we introduce a combined space-time index $i=(\mathbf{i},l)$ and consider only local changes in the fields $s_m \to s'_m = -s_m$. As can be inferred from Eq. (164), the probability of a configuration $\{s_i\}$ is $P_s \propto \det(G^{-1}_{c_{\uparrow}\{s_i\}})\det(G^{-1}_{c_{\downarrow}\{s_i\}})$.[7] On the other hand, detailed balance requires $P_{s'}P_{s'\to s} = P_sP_{s\to s'}$ for all s'. We may satisfy this requirement either by defining the transition probability $P_{s\to s'} = R/(1+R)$, where

$$R \equiv \frac{P_{s'}}{P_s} = \frac{\det(G_{c\uparrow})\det(G_{c\downarrow})}{\det(G'_{c\uparrow})\det(G'_{c\downarrow})} \tag{172}$$

is the relative weight of two configurations, or by setting $P_{s\to s'} = \mathrm{minimum}(R,1)$. The first choice is called the "heat-bath" algorithm, and the second the "Metropolis" algorithm which is often superior. If the difference between two configurations is due to a flip of a single Hubbard-Stratonovich field at the mth location in the cluster space-time (Hirsch and Fye, 1986), we obtain from Eq. (171)

$$R = \prod_{\sigma}[1+(1-G_{c\sigma,mm})(e^{-\alpha\sigma(s_m-s'_m)}-1)]^{-1}. \tag{173}$$

For either the Metropolis or the heat-bath algorithm, if the change is accepted, we must update the Green's function accordingly. The relationship between G_c and G'_c is given by Eq. (170),

$$G'_{c\sigma,ij} = G_{c\sigma,ij} + \frac{(G_{c\sigma,im}-\delta_{im})(e^{-\alpha\sigma(s_m-s'_m)}-1)}{1+(1-G_{c\sigma,mm})(e^{-\alpha\sigma(s_m-s'_m)}-1)}G_{c\sigma,mj}. \tag{174}$$

The quantum Monte Carlo procedure is initialized by setting $G_{c\sigma,ij}=\mathcal{G}_{ij}$ and choosing the corresponding field configuration with all $s_i=0$. Then we use Eq. (175) to create a Green's function corresponding to a meaningful field configuration [i.e., $s_i=\pm1$, for each $i=(\mathbf{i},l)$ or the $\{s_i\}$ from a previous run or iteration] and proceed by stepping through the space-time of the cluster, proposing local changes $s_i \to -s_i$. We accept the change if $P_{s'\to s}$ is greater than a random number between 0 and 1 and update the Green's function according to Eq. (175). After roughly one hundred warmup sweeps through the

[7] If P_s is not positive definite, then $|P_s|$ is used as the sampling weight, and its sign is appended to the measurement. I.e., for a measurement m and sign S, $\langle m\rangle_P = \langle mS\rangle_{|P|}/\langle S\rangle_{|P|}$.

space-time lattice of the cluster, the system generally comes into equilibrium and we begin to make measurements.

c. Measurements

Several points must be considered when making measurements in the quantum Monte Carlo procedure. First, for a given configuration of the Hirsch-Hubbard-Stratonovich fields, the problem is noninteracting. Thus the estimators of any correlation function may be constructed by taking all allowed Wick's contractions (both connected and disconnected). Any quantity that may be represented in terms of the Green's functions (and perhaps the Hirsch-Hubbard-Stratonovich fields themselves) may be measured. Second, great care must be taken when constructing the estimators of the measurements. Different estimators may yield different results due to the systematic and statistical error in the quantum Monte Carlo procedure. It is important to choose the optimal form of the estimator of each measurement, and then use all the prior knowledge (exact limits, symmetries, etc.) that we have to reduce the error.

For example, one difficulty encountered with the quantum Monte Carlo algorithm is that a reliable transform from imaginary-time quantities to Matsubara frequencies is required. A careful treatment of the frequency summation or the imaginary-time integration is crucial in order to ensure the accuracy and the stability of the algorithm and to maintain the correct high-frequency behavior of the Green's function (Jarrell *et al.*, 1993; Deisz *et al.*, 1997; Blümer, 2002). We need to evaluate the following integral:

$$G_c(\mathbf{K},i\omega_n) = \int_0^\beta d\tau e^{i\omega_n\tau} G_c(\mathbf{K},\tau). \tag{175}$$

But from the quantum Monte Carlo algorithm we know the function $G_c(\mathbf{K},\tau)$ only at a discrete subset of the interval $[0,\beta]$. As may be readily seen by discretizing the above equation, the estimate of $G_c(\mathbf{K},i\omega_n)$ becomes inaccurate at high frequencies. This is formalized by Nyquist's theorem, which tells us that above the frequency $\omega_c=\pi/\Delta\tau$ unphysical results are produced by conventional quadrature techniques. For example, a rectangular approximation to the integral in Eq. (175) yields a $G_c(\mathbf{K},i\omega_n)$ that is periodic in ω_n. This presents a difficulty, since causality requires that

$$\lim_{\omega_n\to\infty} G_c(\mathbf{K},i\omega_n) = \frac{1}{i\omega_n} + \mathcal{O}(1/\omega_n^2). \tag{176}$$

This problem may be avoided by using the high-frequency information from other sources. For example, some of the perturbation-theory results discussed in Sec. III.B have the correct asymptotic behaviors. Alternatively, we can use the Green's function from the previous iteration, which has the correct high-frequency behavior. We then compute the Matsubara-frequency Green's function from the imaginary-time quantum Monte Carlo Green's function as (Jarrell *et al.*, 1993)

$$G_c(\mathbf{K},i\omega_n) = G_{c,pt}(\mathbf{K},i\omega_n) + \int_0^\beta d\tau e^{i\omega_n\tau}[G_c(\mathbf{K},\tau) - G_{c,pt}(\mathbf{K},\tau)], \tag{177}$$

where $G_{c,pt}$ is any Green's function with the correct high-frequency behavior. The integral is computed by first interpolating the difference $G_c(\mathbf{K},\tau)-G_{c,\mathrm{pt}}(\mathbf{K},\tau)$ using an Akima spline, and then integrating the spline (a technique often called oversampling). The smooth Akima spline suppresses spurious high-frequency behavior so that $G_c(\mathbf{K},i\omega_n)=G_{c,\mathrm{pt}}(\mathbf{K},i\omega_n)$ when $\omega_n \gg \omega_c$. The resulting self-energy, extracted from $\Sigma_c(\mathbf{K},i\omega_n) = 1/\mathcal{G}(\mathbf{K},i\omega_n) - 1/G_c(\mathbf{K},i\omega_n)$ is still not accurate at high frequencies since it reflects either the perturbation theory or the previous iteration. However, the exact high-frequency form is known. Thus we can fit the high-frequency self-energy, at frequencies at or below the Nyquist cutoff $\pi/(\Delta\tau)$, to the form

$$\Sigma_c(\mathbf{K},i\omega_n) \approx a(\mathbf{K})/(i\omega_n) + b(\mathbf{K})/\omega_n^2. \tag{178}$$

In some cases a and b are known exactly. We may then append this form to the self-energy at frequencies higher than $\pi/(\Delta\tau)$.

2. Exact diagonalization

The Lanczos exact diagonalization method (Haydock *et al.*, 1975) provides a numerical way to diagonalize the Hamiltonian of a finite-size system. Since the cluster model in the cluster perturbation theory formalism is identical to the model of a finite-size system with open boundary conditions, the regular Lanczos exact diagonalization method can be applied in this case without modification (Sénéchal *et al.*, 2000). For the cluster model of embedded-cluster theories, however, it needs to be generalized to account for self-consistent coupling to the host. Exact diagonalization has been used to solve the impurity problem of the DMFT (Caffarel and Krauth, 1994; Si *et al.*, 1994). It is natural to extend its use to that of a cluster solver in quantum cluster theories. This was demonstrated by Bolech *et al.* (2003) in an application of the cellular DMFT to the 1D Hubbard model. The general method of exact diagonalization (Haydock *et al.*, 1975) need not be reviewed here. We only outline the specific implementation necessary for a cluster theory.

Exact diagonalization is a wave-function-based method, i.e., it is applied to diagonalize the effective cluster Hamiltonian, for example, the Hamiltonian in Eq. (94). To this end, the hybridization function $\mathbf{\Gamma}(z)$ [see Eq. (93)] is fitted to the form (96) to obtain estimates for the auxiliary parameters of the host, $\lambda_{ij}(\tilde{\mathbf{k}})$ and $V_{ij}(\tilde{\mathbf{k}})$. In order to apply exact diagonalization to the cluster Hamiltonian, one must discretize the auxiliary host degrees of freedom, i.e., the sum over $\tilde{\mathbf{k}}$, to a finite set of N_h orbitals. Applying exact diagonalization to the resulting Hamiltonian, one can then compute a cluster self-energy $\mathbf{\Sigma}^c$ (Caffarel and Krauth, 1994), and from the

cluster self-energy a new estimate of the coarse-grained Green's function $\bar{\mathbf{G}}$ to close the self-consistency loop.

The Hilbert space of the resulting Hamiltonian increases exponentially with the cluster size N_c and the number of wave vectors N_h representing the host. For exact diagonalization to be feasible, the total number of "sites" $N=N_c+N_h$ must be of the order of $N\sim 20$. Furthermore, for the distinction of the lattice into cluster and host to make sense, N_h must be greater than or equal to N_c. This size limitation may be prohibitive for anything but 1D systems. Moreover, by applying exact diagonalization to solve the cluster model one abandons the thermodynamic limit, one of the advantages of cluster mean-field theories. Still, exact diagonalization is an exact method and can deal with more complicated interactions than the simple on-site Hubbard repulsion, as shown by Bolech *et al.* (2003), who considered nearest-neighbor interactions.

3. Wilson's numerical renormalization group

Over the past ten years, Wilson's numerical renormalization group (Wilson, 1975; Krishnamurthy *et al.*, 1980a, 1980b) has become a major computational tool for the study of quantum impurity problems. Its advantages are that it (i) is nonperturbative, (ii) can handle exponentially small energy scales with unprecedented accuracy, and (iii) does not suffer from any principle limitations regarding the parameter space of the model. In addition, through the inspection of the flow of the spectrum of the Hamiltonian under the renormalization-group transformation, the method provides direct, very detailed information about the structure of the low-energy spectrum.

Originally, its application was limited to static quantities (Wilson, 1975; Krishnamurthy *et al.*, 1980a, 1980b), but the calculation of dynamical properties is also possible (for a comprehensive overview of the early work see Hewson, 1993), hence its application to the DMFT impurity problem (Sakai and Kuramoto, 1994; Shimizu and Sakai, 1995). The direct calculation of the one-particle self-energy from the numerical renormalization group (Bulla *et al.*, 1998) triggered a variety of applications within the DMFT framework (Bulla, 1999; Pruschke *et al.*, 2000; Bulla *et al.*, 2001; Zitzler *et al.*, 2002, 2004; Pruschke and Zitzler, 2003) at both $T=0$ and finite temperatures.

Given this tremendous success, the obvious question is whether an extension of the numerical renormalization group might be useful for quantum cluster problems. Let us therefore briefly repeat the basic steps in this approach. The procedure starts by picking a number $\Lambda>1$ and an interval on the energy axis that contains the support of the density of states of the bath degrees of freedom. As depicted in Fig. 10, this interval is then partitioned into exponentially decreasing intervals $[\Lambda^{-(n+1)},\Lambda^{-n}]$ for $\epsilon>0$ with $n=0,1,\ldots$, and likewise for $\epsilon<0$. Within each interval, a Fourier decomposition of the bath operators is performed; the fundamental approximation of the numerical renormalization group consists of neglecting all Fourier components except for the homogeneous one. As a final step, the resulting Hamiltonian is tridiagonalized, resulting in

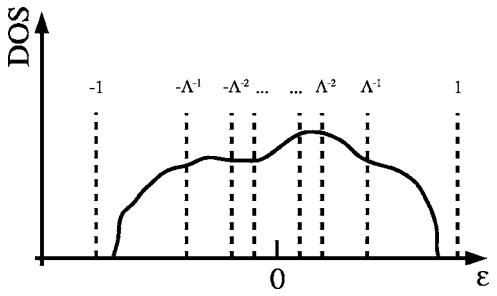

FIG. 10. Schematic setup of the numerical renormalization group. The energy axis is partitioned into exponentially decreasing intervals.

$$H_{\mathrm{QI}} \approx H_{\mathrm{Imp}} + \sum_{\sigma}\sum_{n=1}^{\infty} (\varepsilon_n a_{n\sigma}^{\dagger} a_{n\sigma} + t_{n-1} a_{n-1\sigma}^{\dagger} a_{n\sigma} + \mathrm{H.c.}), \tag{179}$$

where H_{Imp} denotes the Hamiltonian of the "impurity" and the operators $a_{n\sigma}^{(\dagger)}$ represent the bath degrees of freedom. Note that the Hamiltonian (179) represents a semi-infinite chain with the impurity at its left end. Wilson (1975) showed that the quantities $t_n \propto \Lambda^{-n/2}$. If $\bar{t}_n=\sqrt{\Lambda^n}t_n$ and $\bar{\varepsilon}_n=\sqrt{\Lambda^n}\varepsilon_n$, one can cast the Hamiltonian in a recurrency form,

$$\bar{H}_{N+1} = \sqrt{\Lambda}\bar{H}_N + \sum_{\sigma} \bar{\varepsilon}_{N+1} a_{N+1\sigma}^{\dagger} a_{N+1\sigma} + \sum_{\sigma} (\bar{t}_N a_{N\sigma}^{\dagger} a_{N+1\sigma} + \mathrm{H.c.}). \tag{180}$$

Given the eigenvalues and eigenvectors of $\bar{H}_N$, $\bar{H}_{N+1}$ can be constructed straightforwardly. Since at each of these steps the dimension of the Hilbert space increases by a factor of 4, the practical use would be limited by the same constraints as conventional exact diagonalization, only more severely, because the construction of $\bar{H}_{N+1}$ requires a knowledge of the whole set of eigenvectors and eigenvalues of $\bar{H}_N$. However, the multiplication of $\bar{H}_N$ by $\sqrt{\Lambda}>1$ expands the bandwidth of the spectrum and, because $\bar{t}_N=O(1)$, the low-energy properties of $\bar{H}_{N+1}$ are determined by a restricted set of low-lying states of $\bar{H}_N$ only. This observation is put into a practical computational scheme by the following algorithm: (i) At step $N\geqslant 0$ ($N=0$ corresponds to H_{Imp}), diagonalize $\bar{H}_N$ and calculate all interesting local properties for that particular chain length. (ii) Use a suitable number N_{NRG} of the lowest eigenstates of $\bar{H}_N$ to construct the next Hamiltonian $\bar{H}_{N+1}$ according to (180). (iii) Continue with (i) until the desired accuracy for the ground state is reached. Note that step (ii) ensures that, no matter how long the chain becomes, the dimension of the Hamilton

matrix to diagonalize can be fixed to a manageable number.

As has been discussed extensively in the literature (Wilson, 1975; Krishnamurthy *et al.*, 1980a, 1980b; Hewson, 1993), a knowledge of the local properties at chain length N provides the means to calculate physically interesting quantities (thermodynamics and dynamics) at energy scales or temperatures scales $\propto\sqrt{\Lambda^{-N}}$. This exponential decrease in successive energy scales explains why the numerical renormalization group is suitable for studies of problems with extremely small dynamical energy scales. Of course, as usual there is a price to pay, namely, a loss of accuracy in high-energy features (Hewson, 1993).

Up to now the discussion has been restricted to spin degeneracy. However, it is obvious that additional degrees of freedom do not influence the general lines of argument. In fact, for a problem with $L \geqslant 1$ internal degrees of freedom, in addition to the spin (like cluster sites or several orbitals per site), the result (179) acquires the form

$$H_{\mathrm{QI}} \approx H_{\mathrm{Imp}} + \sum_{l=1}^{L} \sum_{\sigma} \sum_{n=1}^{\infty} (\varepsilon_n^l a_{nl\sigma}^\dagger a_{nl\sigma} + t_{n-1}^l a_{n-1l\sigma}^\dagger a_{nl\sigma} + \mathrm{H.c.}), \tag{181}$$

where H_{Imp} is again of arbitrary structure. Likewise, the recurrency relation (180) can be set up and the algorithm extended. However, a simple example demonstrates that for $L>1$ the technique can easily become useless. For a typical application to the single-impurity Anderson model one chooses a $\Lambda=2$ and $N_{\mathrm{NRG}}=1000$. This is sufficient to obtain very accurate results for all relevant physical quantities. Let us now consider the next step, an orbitally degenerate problem with $L=2$. Without coupling between the orbitals, this corresponds to two independent single-impurity Anderson models that we try to solve in a single calculation. Obviously, to obtain the same accuracy as in the true single-impurity case, one needs at least $N_{\mathrm{NRG}}=1000^2$ or $\Lambda=2^2$ [for a more detailed discussion of the issue of the accuracy of the numerical renormalization group see Paula *et al.* (1999), and references therein].

While $N_{\mathrm{NRG}}=1000^2$ is beyond all numerical possibilities, because one needs the complete spectrum, a too large Λ introduces a huge loss in accuracy, both at high and low energies (Oliveira and Oliveira, 1994). As long as $L=2$ the loss can be partially compensated for by respecting the additional symmetries in the system (Sakai *et al.*, 1989) or other numerical tricks (Oliveira and Oliveira, 1994). However, to use this approach as a generic tool for solving the effective quantum cluster problem arising in embedded-cluster techniques, one must have much larger values of L accessible. While the numerical renormalization group is still applicable for a study of qualitative effects of nonlocal correlations with $N_c=2$ (see results in Sec. IV.D.1), the preceding discussion makes it clear that already for $N_c=4$ one is far beyond any practical limit for this method.

IV. APPLICATIONS TO STRONGLY CORRELATED MODELS

In this section we review the application of various quantum cluster approaches to a selection of standard models of strongly correlated electron systems. We put special emphasis on the capabilities and advantages of these techniques over both finite-size simulations and DMFT. In Sec. IV.A we show that quantum cluster approaches are complementary to finite-size simulations, i.e., that taken together the information obtained from both techniques can yield conclusive results. The effects of nonlocal correlations on single- and two-particle spectra as well as phase diagrams are emphasized throughout the discussions of the Falicov-Kimball model in Sec. IV.B, the 1D Hubbard model in Sec. IV.C, and the 2D Hubbard model in Sec. IV.D. Due to space restrictions we have to omit recent applications of the cluster perturbation theory and DCA to electron-phonon systems and refer the reader to the articles by Hohenadler *et al.* (2003) and Hague (2003), respectively.

A. Complementarity of finite-size and quantum cluster simulations

Finite-size simulations and quantum cluster approaches yield exact solutions in the infinite-cluster-size limit. At finite cluster size N_c, quantum cluster approaches differ from finite-size simulations by the coupling to a self-consistent dynamic host. At cluster size $N_c=1$, this difference is most pronounced: While finite-size simulations reduce to the atomic limit, quantum cluster approaches reduce to the DMFT, i.e., a highly nontrivial approximation to the infinite lattice. Thus it is instructive to compare quantum cluster results with those obtained from finite-size simulations systematically as a function of cluster size. This has been done in the half-filled 2D Hubbard model using the DCA/QMC algorithm, i.e., DCA combined with quantum Monte Carlo as a cluster solver, by Huscroft *et al.* (2001) and Moukouri and Jarrell (2001) and with DCA/FLEX by Aryanpour, Hettler, and Jarrell (2003).

In the 2D Hubbard model at half-filling, the antiferromagnetic correlation length ζ increases with decreasing temperature and diverges at $T=0$. In finite-size simulations, i.e., in a finite-size lattice with periodic boundary conditions, the system freezes when the correlation length exceeds the system size and a gap to excitations opens. As the system size is increased this tendency is reduced. Correlation-induced gaps are thus generally overestimated in finite-size simulations for smaller clusters since the system is artificially closer to criticality. In contrast, in quantum cluster approaches the system is in the thermodynamic limit with correlations restricted to the cluster size. Hence the system never freezes. As the cluster size is increased, longer-ranged correlations are progressively included. The effects of correlations therefore increase with cluster size.

This behavior is illustrated in Fig. 11, where we reproduce the results obtained from DCA/QMC and finite-

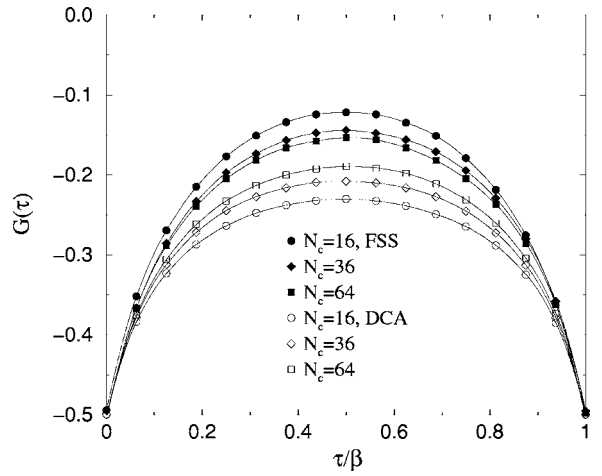

FIG. 11. The imaginary-time Green's function $G(\mathbf{k},\tau)$ at $\mathbf{k}=(\pi,0)$ in the half-filled 2D Hubbard model, calculated with finite-size quantum Monte Carlo (filled symbols) and DCA (open symbols) when $U=4.4t$ and $\beta=4/t$. From Moukouri and Jarrell, 2001. See also Aryanpour, Hettler, and Jarrell, 2003.

size QMC simulations for the imaginary-time Green's function $G(\mathbf{k},\tau)$ at the Fermi wave vector $\mathbf{k}=(\pi,0)$ for different cluster sizes N_c. One can see that $|G(\mathbf{k},\tau)|$ decays faster from its value at $\tau=\beta/2$ when correlation effects are stronger, so the gap is more pronounced. With increasing cluster size, the DCA and finite-size results for $G(\mathbf{k},\tau)$ converge from opposite directions. Consistent with the expectation that correlation effects are overestimated in finite-size simulations but underestimated in the DCA, the decay is stronger for smaller system sizes in finite-size simulations, while the DCA results show the opposite behavior. Since the two techniques become identical in the infinite-cluster-size limit, the exact $G(\mathbf{k},\tau)$ curve is bracketed by the finite-size and DCA curves. For methods like the FLEX (see Sec. III.B.1) for which calculations with much larger clusters are feasible, scaling of the results to the infinite system is possible (see Fig. 12). The extrapolations of finite-size

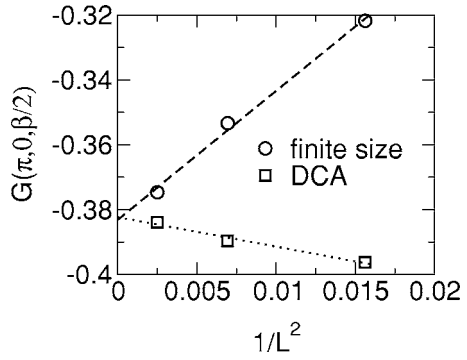

FIG. 12. The imaginary-time Green's function $G(\mathbf{k},\tau)$ at $\mathbf{k}=(\pi,0)$, $\tau=\beta/2$ in the half-filled 2D Hubbard model, calculated with finite-size FLEX method (circles) and DCA/FLEX method (squares) when $U=1.57t$ for various cluster sizes $N_c=L\times L$. Both methods scale as $1/L^2$ and coverge to a single value as $L\to\infty$. From Aryanpour, Hettler, and Jarrell, 2003.

FLEX and DCA/FLEX to the infinite system ($1/L^2\to 0$) coincide within numerical uncertainties, thus allowing the determination of the infinite-lattice FLEX result with unprecedented accuracy.

This complementarity is also seen in results for the spectral gap in the 2D half-filled Hubbard model (see Huscroft *et al.*, 2001 and Aryanpour, Hettler, and Jarrell, 2003). In the DCA the gaps converge from small to large as the cluster size increases, while the converse occurs in finite-size simulations. Although we have only shown results of the DCA, we expect the cellular DMFT to show similar size dependence, since DCA and cellular DMFT share the same nature (see discussion in Sec. II.D). Results obtained with the cluster perturbation theory algorithm, however, can be viewed to some extent as a periodic continuation of finite-size simulations. Thus it is an open question whether the cluster perturbation method shows similar complementarity.

B. 2D Falicov-Kimball model

The usefulness of the discussed cluster theories was first demonstrated in an application of the DCA to the 2D Falicov-Kimball model by Hettler *et al.* (1998, 2000). While the Falicov-Kimball model is a particularly gentle test bed for novel approaches, it allows us to study the effects of nonlocal fluctuations.

The Falicov-Kimball model can be considered as a simplified Hubbard model in which one spin species has zero hopping amplitude. The Hamiltonian reads

$$H=-t\sum_{\langle i,j\rangle} d_i^\dagger d_j + U\sum_i \left(n_i^d-\frac{1}{2}\right)\left(n_i^f-\frac{1}{2}\right), \tag{182}$$

with $n_i^d=d_i^\dagger d_i$ and $n_i^f=f_i^\dagger f_i$. For a 2D square lattice the bandwidth of the noninteracting system is $W=8t$. At half-filling and $D\geqslant 2$ the system has a second-order phase transition from a homogeneous high-temperature phase to a charge-density wave (CDW) with ordering vector $\mathbf{Q}=(\pi,\pi)$ for any nonzero U (Brandt and Schmidt, 1986, 1987). The universality class is that of the 2D Ising model, the strong-coupling limit $U/t\gg 1$ of the Falicov-Kimball model. Hettler *et al.* (2000) evaluated the Falicov-Kimball model within the DCA by a combination of Monte Carlo methods and exact enumeration for small clusters. Since the DMFT is a single-site theory ($N_c=1$), it yields an unphysical temperature-independent density of states (DOS) of the mobile d electrons (Brandt and Mielsch, 1989) due to the constraint of half-filling (one electron per site of either the d or f variety). In a cluster theory with $N_c>1$ this artifact is absent, since a redistribution of Boltzmann weight with temperature is possible among the various configurations of d or f electrons on the cluster sites, while maintaining the condition of half-filling on average. This temperature dependence is demonstrated in Fig. 13, where a pseudogap develops in the local DOS with decreasing temperature. This pseudogap can be interpreted as a precursor of the eventual transition to a CDW phase, which features a full gap at the Fermi level. In addition

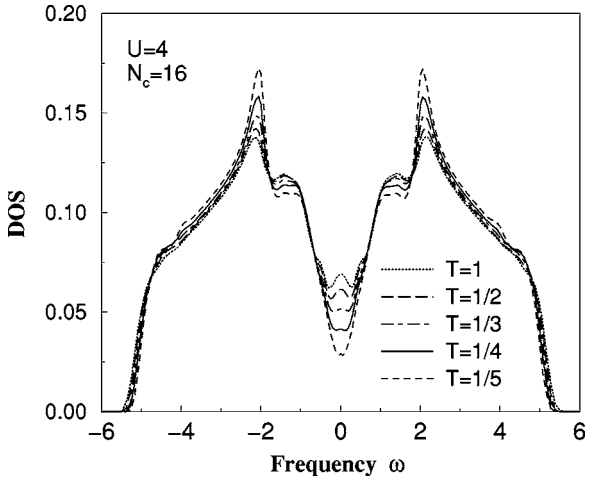

FIG. 13. Density of states, of the 2D Falicov-Kimball model for a 4×4 cluster at various temperatures calculated with the DCA. The DOS develops a pseudogap as the temperature approaches $T_c\approx0.189t$ ($U=4t$) due to the nonlocal CDW fluctuations present in the DCA ($N_c>1$). In the DMFT ($N_c=1$), there is no T dependence of the DOS above T_c. From Hettler *et al.*, 2000.

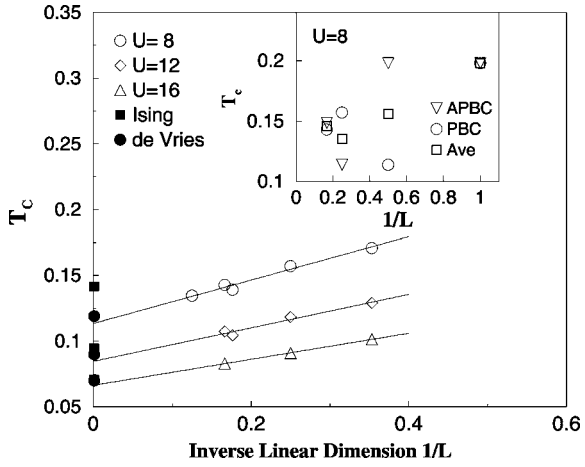

FIG. 14. T_c in the 2D Falicov-Kimball model as a function of the inverse linear cluster size for $U/t=8,12,16$ calculated with the DCA. The Ising limit, and finite-size estimates of T_c are shown for comparison. The inset shows that the influence of the cluster boundary conditions on T_c disappears rapidly with increasing cluster size. From Hettler *et al.*, 2000.

to the gap, there is fine structure in the DOS, related to an exchange energy J_{eff}. This is better observed in the momentum-resolved spectral function (see Hettler *et al.*, 2000; Laad and van den Bossche, 2000).

As stated above, the Falicov-Kimball model has an instability to a phase with CDW order. As discussed in Secs. I.B and II.D, embedded-cluster theories exhibit phase transitions at some temperature that, due to their residual mean-field character, lies above the exact T_c of the infinite system. As the cluster size increases, one expects the effect of the mean field to decrease, leading to a decreasing T_c with increasing cluster size. The N_c dependence of the transition temperature T_c is shown in Fig. 14, together with a comparison with the T_c obtained from finite-size methods (de Vries *et al.*, 1993a, 1993b, 1994) and T_c of the 2D Ising model with exchange coupling $J=t^2/(2U)$. The extrapolated cluster results agree with the finite-size estimates and, for large values of U, also with the results obtained from the 2D Ising model. For smaller U however, charge fluctuations begin to play a larger role, suppressing the T_c compared to that of the Ising model which lacks charge fluctuations.

The effect of different boundary conditions in the DCA cluster is illustrated in the inset.[8] In small clusters the effect is strong, but already in a 6×6 cluster the bulk of the cluster dominates and the boundaries play a minor role.

When $N_c=1$ only charge fluctuations with an energy scale U are present. In a cluster theory the nonlocal "spin" fluctuations with an effective energy scale J_{eff} ($\propto1/2U$ for large U) must also be observable in thermodynamic quantities like the entropy and the specific heat. These quantities were computed by Hettler *et al.* (2000) via a maximum-entropy method (Huscroft *et al.*, 2000). For better comparison, the calculations were performed in the uniform phase, even at temperatures below the CDW ordering T_c by not allowing for the symmetry breaking. The results for a 2×2 cluster are shown in Fig. 15, where the ratio of the specific heat C to the temperature T is plotted for the DCA and the DMFT.

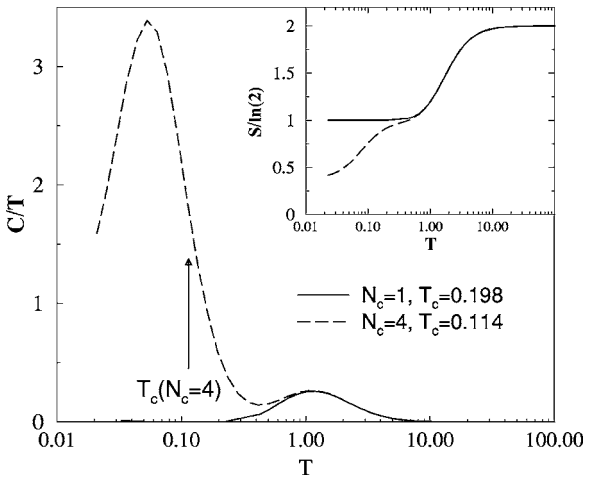

FIG. 15. Specific heat vs temperature for single-site and 2×2 clusters calculated with the DCA and exact enumeration when $U=8t$. For $N_c=1$, there is a single peak with integrated weight ln(2) associated with the suppression of local charge fluctuations. For $N_c=4$, there is an additional peak at lower temperatures associated with critical fluctuations near the charge-ordering transition temperature. T_c for $N_c=4$ is indicated by an arrow. In the inset the entropy $S(T)=\int_0^T dT'[C(T')/T']$ is shown in units of ln(2). From Hettler *et al.*, 2000.

[8]According to the derivation of the DCA formalism (see Secs. II.A and II.B, and Fig. 3) the DCA cluster has periodic boundary conditions. By shifting the set of cluster **K** points, one can simulate however, different boundary conditions.

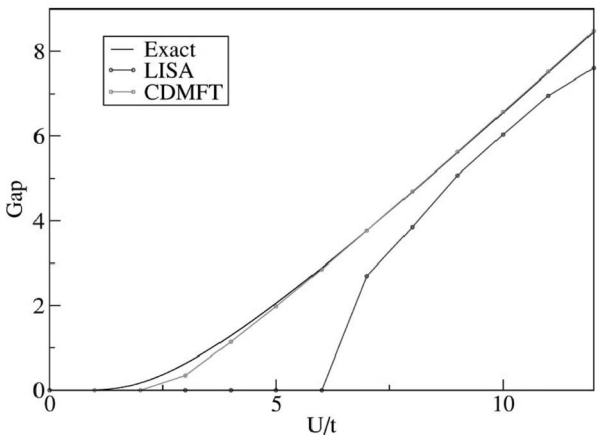

FIG. 16. Spectral gap in the half-filled 1D Hubbard model as a function of U/t calculated with DMFT local-impurity self-consistent approximation (LISA) and cellular DMFT for a two-site cluster, $N_c=2$, compared to the exact result. From Bolech *et al.*, 2003.

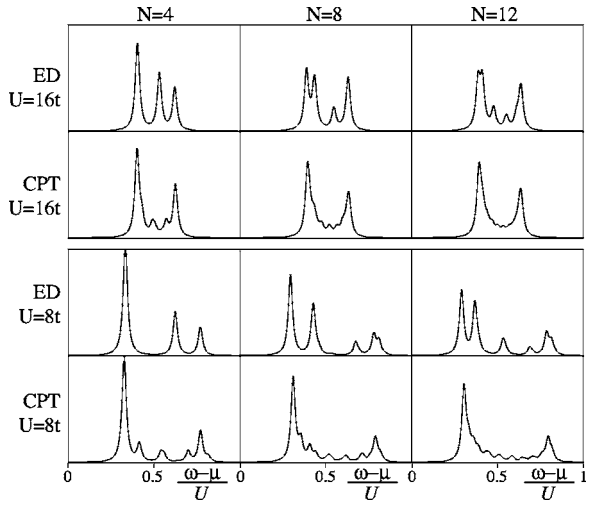

FIG. 17. The spectral function $A(k,\omega)$ at $k=\pi/2$ in the half-filled 1D Hubbard model when $U=16t$ (top) and $U=8t$ (bottom), calculated with ordinary exact diagonalization and with cluster perturbation theory for cluster sizes $N=4,8,12$. From Sénéchal *et al.*, 2000.

The appearance of a second peak at lower temperature is a clear indication of additional nonlocal fluctuations present on the cluster. The effect on the entropy is also strong, as shown in the inset.

C. 1D Hubbard model

In this section we discuss the application of quantum cluster approaches to the 1D Hubbard model (in the usual notation),

$$\mathcal{H} = -t\sum_{i,\sigma}(c^{\dagger}_{i+1\sigma}c_{i\sigma} + \text{H.c.}) + U\sum_{i} n_{i\uparrow}n_{i\downarrow}, \tag{183}$$

which provides a nontrivial test ground for these techniques. In one dimension quantum fluctuations are stronger than in higher dimensions. Hence quantum cluster approaches that cut off correlations beyond the length scale set by the cluster size are expected to be less efficient than in higher dimensions. If quantum cluster approaches accurately describe the physics in one dimension, they are highly likely to capture the physics in two and three dimensions. In addition, since the exact ground state of the 1D Hubbard model is known from the Bethe-ansatz solution (Lieb and Wu, 1968), a quantitative comparison of certain static quantities is possible. Fairly reliable results for dynamical quantities can be obtained from the density-matrix renormalization method.

Bolech *et al.* (2003) applied the cellular DMFT exact diagonalization method to the 1D Hubbard model and systematically compared the results with those obtained from the DMFT and DMRG approaches. As an example of this study we show in Fig. 16 a comparison of the exact result with that obtained from DMFT (referred to as LISA for "local impurity self-consistent approximation") and cellular DMFT for the single-particle spectral gap $\Delta(U)$ as a function of the on-site Coulomb repulsion U in the half-filled case. The total number of sites in the effective cluster model including cluster and bath sites was fixed to six in the exact diagonalization approach (see Sec. III.C.2).

In contrast to the exact result which shows a finite Mott gap for all values of U, the $N_c=1$ (LISA) spectral gap is reduced to much smaller values and even vanishes at $U/t\approx 6$. The $N_c=2$ cellular DMFT result shows the Mott transition at a much smaller value, $U/t\approx 2$, above which it follows the exact result quite accurately. The existence of this spurious Mott transition in one dimension originates in the spatial cutoff of correlations. This result shows, however, that the inclusion of nearest-neighbor correlations already can lead to a significant improvement over the single-impurity results. Larger cluster sizes should produce even better results, and indeed a comparison of the nearest-neighbor Green's function with DMRG results shows systematic improvements with increasing cluster size (Bolech *et al.*, 2003).

A related fundamental feature in 1D correlated systems is the breakdown of the Fermi-liquid picture because of spin-charge separation as described in the concept of Luttinger liquids (see, for example, Voit, 1994). In a Fermi liquid, the spectral weight $A(\mathbf{k},\omega)$ is centered around a single quasiparticle peak at $\omega=\epsilon_{\mathbf{k}}$, while in a Luttinger liquid, $A(\mathbf{k},\omega)$ is distributed between two singularities associated, respectively, with spin and charge excitations (spinons and holons). Sénéchal *et al.* (2000) have calculated $A(\mathbf{k},\omega)$ in the 1D Hubbard model using the cluster perturbation theory formalism. Figure 17 shows a comparison of this quantity at the Fermi wave vector $k=\pi/2$ as calculated by ordinary exact diagonalization and its infinite lattice extension within the cluster perturbation theory method for various cluster sizes N when $U=8t$ (bottom) and $U=16t$ (top).

While no sign of spin-charge separation is seen in the pure exact diagonalization results, the cluster perturba-

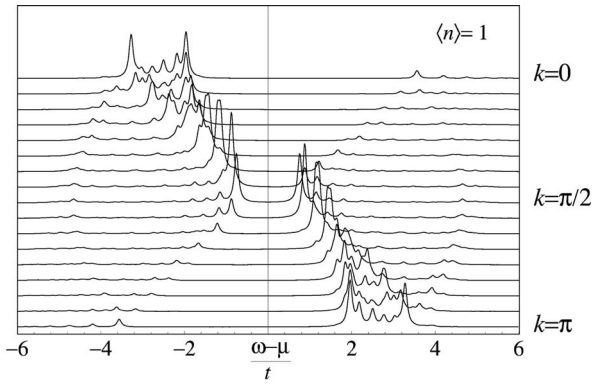

FIG. 18. The spectral function $A(k,\omega)$ in the half-filled 1D Hubbard model when $U=4t$, calculated with CPT for $N_c=12$. From Sénéchal *et al.*, 2000.

tion theory method reveals the two branches of the spectral weight indicative of spin-charge separation. The two-peak structure resolves more clearly as the cluster size increases. Since propagation between clusters requires the spinon and holon to recombine, spin-charge separation can only exist on length and time scales limited by the cluster size. Consequently it takes fairly large clusters to clearly resolve this feature.

The analysis of the k-dependent spectral function in Fig. 18 shows that the spinon and holon branches have different dispersions and can be clearly identified together with the gap at the chemical potential at $k=\pi/2$. An extension of these $T=0$ results to $T>0$ by Aichhorn *et al.* (2003) within a novel low-temperature Lanzcos algorithm revealed that the spin-charge separation persists at finite, low temperatures.

As shown by these studies, quantum cluster approaches can be very useful in exploring the complex behavior of the 1D Hubbard model. Even studies with small cluster sizes are consistent with well-known results such as the existence of spin-charge separation. This success in the 1D case shows great promise for applications of cluster methods in two or three dimensions, where they are expected to be even more efficient, since correlations are less pronounced.

D. 2D Hubbard model

Interest in the 2D Hubbard model (in the usual notation),

$$\mathcal{H}=\sum_{ij,\sigma} t_{ij}c_{i\sigma}^{\dagger}c_{j\sigma}+U\sum_{i} n_{i\uparrow}n_{i\downarrow}, \tag{184}$$

has revived recently, in particular since it is believed to capture the physics of the superconducting planes in high-temperature superconductors (Zhang and Rice, 1988, 1990; Anderson, 1997b). This section reviews various applications of quantum cluster approaches to the 2D Hubbard model at half-filling and at finite doping, including results for a possible Mott-Hubbard transition, antiferromagnetism and its precursors, pseudogap phenomena, and superconductivity.

1. Metal-insulator transition

The question of a possible metal-insulator transition in the 2D Hubbard model at half-filling ($\epsilon_o=t_{ii}=-U/2$) is under active research. This problem was studied in the unfrustrated model, i.e., with only nearest-neighbor hopping $t_{ij}=\epsilon_o\delta_{ij}-t\delta_{\langle ij\rangle}$ within the DCA/QMC approach by Moukouri and Jarrell (2001) and with the two-site composite-operator method (see Sec. II.I) by Stanescu and Phillips (2001). The frustrated case (additional next-nearest-neighbor hopping $t'\delta_{\langle\langle ij\rangle\rangle}$) was investigated by Parcollet *et al.* (2004).

Numerical calculations have shown that the ground state of the unfrustrated model is an antiferromagnetic insulator with the Néel temperature $T_{\mathrm{N}}=0$ constrained by the Mermin-Wagner theorem. Hence a spectral gap exists at $T=0$. However, the central question of the origin of the gap and its relation to antiferromagnetic ordering is less understood. Is the gap a direct consequence of the antiferromagnetic ordering at $T=0$ or does it arise from strong correlations at higher temperatures?

To appreciate the significance of this issue it is important to understand the fundamental difference between antiferromagnetic insulators, i.e., insulators due to magnetic ordering, and Mott insulators, i.e., insulators due to electronic correlations. Antiferromagnetic insulators result from the doubling of the unit cell in the ordered state and are therefore adiabatically connected to band insulators, which have an even number of electrons per unit cell. In contrast, paramagnetic Mott insulators have an odd number of electrons per unit cell and are therefore fundamentally different from band insulators.

At strong coupling ($U\gg W$) the situation is well understood: A charge gap of order U develops in the spectrum below temperatures $T\approx U$ due entirely to strong electronic correlations. The spins are coupled by the exchange interaction $J=4t^2/U$ and govern the low-energy physics. As a result spin and charge are separated. Systems in this regime are hence Mott insulators and the antiferromagnetic ordering at $T=0$ is merely the result of the Mott transition at higher temperatures.

Different scenarios, however, exist for the weak-coupling regime ($U\ll W$): In the weak-coupling point of view, a spin-density wave forms at $T=0$ due to the nesting of the Fermi surface and leads to the doubling of the unit cell. Hence the gap in the spectrum is a direct consequence of the antiferromagnetism at $T=0$. This perturbative point of view is referred to as the Slater mechanism. It is in contrast to the second opinion due to Anderson (1997a, 1997b), who argued that the 2D half-filled Hubbard model is always in the strong-coupling regime, so that a Mott gap is present for all $U>0$ as in one dimension (see Sec. IV.C). As the temperature decreases, local moments develop because of the opening of the Mott gap, which then order at $T=0$. Thus the antiferromagnet at $T=0$ is a consequence of the Mott transition.

The metal-insulator transition in the half-filled Hubbard model has been extensively studied within the

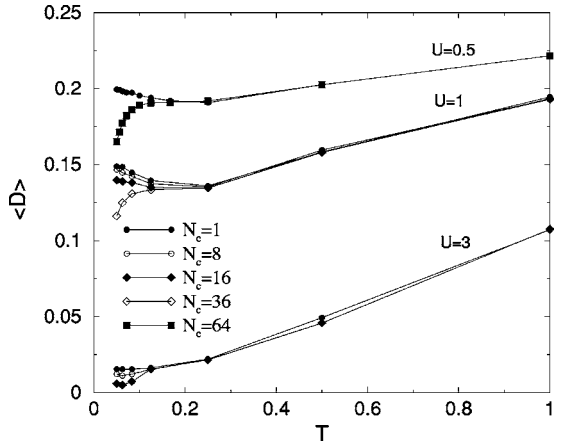

FIG. 19. Double occupancy as a function of temperature for different values of U in the half-filled 2D Hubbard model calculated with the DCA/QMC method for various cluster sizes N_c. Energies are in units of $4t$. Here, $t=0.25$, so the lines for $U=0.5,1,2$ correspond to $U/t=2,4,12$. From Moukouri and Jarrell, 2001.

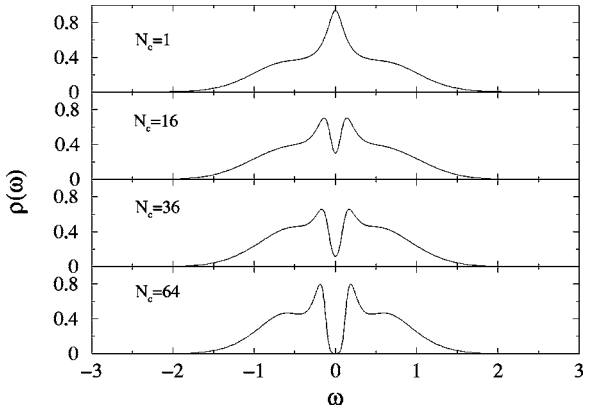

FIG. 20. Density of states when $U/t=4$ at $T=0.125t$ in the half-filled 2D Hubbard model calculated with the DCA/QMC for various cluster sizes N_c. From Moukouri and Jarrell, 2001.

DMFT (for a review see Georges *et al.*, 1996). In the DMFT one can easily disentangle the effects leading to antiferromagnetic and Mott gaps. The DMFT equations for the paramagnetic state of the bipartite Bethe lattice are identical with the equations of the fully frustrated infinite-dimensional model (Georges *et al.*, 1996). This justifies the study of the paramagnetic solution within the antiferromagnetic phase of the unfrustrated model, which shows a first-order Mott metal-insulator transition ending at a finite-temperature critical point (Georges *et al.*, 1996). Although this justification does not hold for $N_c>1$, one can still study the paramagnetic solution by enforcing the spin symmetry and hence avoiding the opening of a full spectral gap due entirely to magnetic ordering. Following this approach, Moukouri and Jarrell (2001) studied the metal-insulator transition in the unfrustrated 2D half-filled Hubbard model using the DCA/QMC approach systematically as a function of cluster size N_c. The metal-insulator transition can be identified by analyzing the behavior of the double occupancy $\langle D\rangle = \langle n_\uparrow n_\downarrow\rangle$. This quantity is shown in Fig. 19 for different values of the Coulomb repulsion U and cluster size N_c.

When $N_c=1$ the double occupancy displays evidence for a metal-insulator transition when U is of the order of the bandwidth $W=8t=2$: $\langle D\rangle$ is monotonically increasing with temperature when $U=3$, but displays a minimum for $U=0.5$ and 1 indicating the emergence of quasiparticle states at the chemical potential at low temperatures. When $N_c>1$ the situation is radically different: In the strong-coupling regime ($U=3$), local fluctuations dominate and $\langle D\rangle$ is essentially independent of N_c except at very low temperatures. In contrast, in the weak-coupling regime, the minimum found for $N_c=1$ flattens progressively as N_c increases from 8 to 16. When $N_c\geqslant 36$ a downturn in $\langle D\rangle$ appears at low temperatures. By opening a gap and hence localizing the moments, the system can gain free energy by taking advantage of the short-ranged magnetic correlations.

The results for the DOS shown in Fig. 20 support the evidence from the double occupancy. The quasiparticle Kondo-like resonance at the chemical potential for $N_c=1$ is destroyed by nonlocal correlations when $N_c>1$. As N_c increases, a gap opens at the chemical potential and the Hubbard sidebands become more pronounced, consistent with the suppression of $\langle D\rangle$. Given the fact that DCA always underestimates correlation-induced spectral gaps (see Sec. IV.A), these simulations indicate the absence of a weak-coupling regime in the unfrustrated 2D Hubbard model at half-filling, consistent with Anderson's point of view. Another interesting question is whether this result changes at zero temperature, $T=0$, and the metal-insulator transition predicted by DMFT returns. As evidence that even at $T=0$ one must expect a gap in the spectra for any $U>0$, we show here first the DCA results at $T=0$ obtained with Wilson's numerical renormalization group for a cluster size of $N_c=2$. The appropriate tiling of the Brillouin zone is shown in Fig. 21, and the resulting coarse-grained spectral functions $\bar{A}(\mathbf{K},w)=-(1/\pi)\mathrm{Im}\bar{G}(\mathbf{K},w)$ for the two cluster $\mathbf{K}$ points are shown in Fig. 22. Even for small values of U a well-defined gap exists in the spectrum at the Fermi energy. Note that all calculations were done in the paramagnetic phase, i.e., the concept of a Slater insulator does not apply here. The gap quickly increases with increasing U and at the same time the system gains more spectral weight in the incoherent parts of the spectrum, begining to resemble what one expects from Mott localized states.

The DCA results (Moukouri and Jarrell, 2001) were confirmed in a similar cluster study by Stanescu and Phillips (2001) using the two-site composite-operator method discussed in Sec. II.I. Figure 23 shows the results of this study for the temperature dependence of the value of the DOS at the chemical potential $\rho(0)$ in the 1D and 2D models for small $U=2t$. As a consequence of the shape of the noninteracting DOS, the 2D result for $\rho(0)$ is enhanced over the 1D result. However, in both

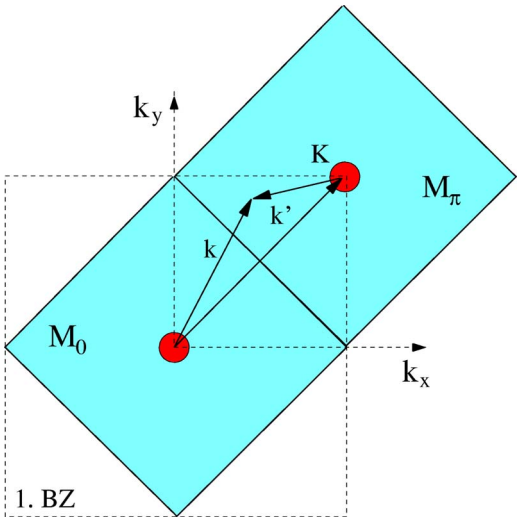

FIG. 21. (Color in online edition) Tiling of the first Brillouin zone for $N_c=2$.

one and two dimensions, $\rho(0)$ falls to zero as the temperature decreases, indicating the absence of a metallic state at half-filling even for small U.

To elucidate the role of antiferromagnetic correlations in the opening of the Mott gap, the frustrated Hubbard model may be studied. In the t-t' Hubbard model, a next-nearest-neighbor hopping t' between sublattices strongly frustrates antiferromagnetic correlations. This model was studied by Parcollet *et al.* (2004) for $t'=t$ on a 2×2 cluster using the cellular DMFT/QMC approach. We reproduce their results for the U dependence of the double occupancy $d_{\mathrm{occ}}=1/4\Sigma_{i=1}^{4}\langle n_{i\uparrow}n_{i\downarrow}\rangle$ for different temperatures in Fig. 24. Similar to the behavior found in DMFT, d_{occ} displays a downturn at a critical value U_c, indicating a transition from a metallic to an insulating state. An inspection of the spectral weight $A(\mathbf{k},0)$ at the chemical potential reveals that the gap opens first in the region around $\mathbf{k}=(\pi,0)$ (Parcollet *et al.*, 2004). These results were substantiated by a cluster perturbation theory study of the frustrated 2D Hubbard model (Sénéchal and Tremblay, 2004) for $t'=-0.4t$. Although not the focus of this study, the results show further evidence of a Mott transition at a finite value of U in the filling dependence of the chemical potential.

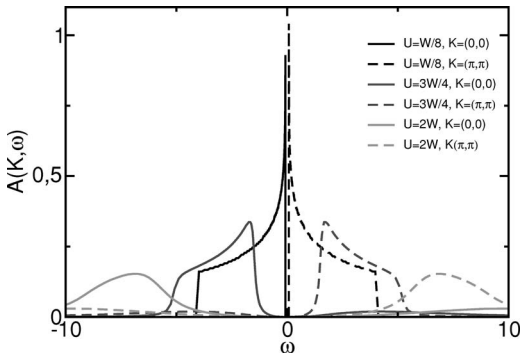

FIG. 22. DCA coarse-grained spectral functions for different values of U obtained from $N_c=2$ DCA/numerical renormalization group calculations at $T=0$. For all $U>0$ a gap exists at the Fermi energy.

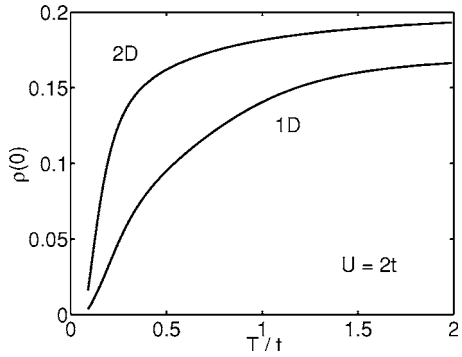

FIG. 23. Density of states as a function of temperature at the chemical potential in the 1D and 2D half-filled Hubbard model when $U=2t$ calculated with a two-site composite-operator approximation. From Stanescu and Phillips, 2001.

The existence of the Mott transition in the frustrated Hubbard model and its absence in the unfrustrated model seem to indicate that antiferromagnetic correlations play a key role in the opening of a Mott gap at weak coupling. Since the opening of the gap occurs in the paramagnetic solution, it cannot be attributed to the existence of antiferromagnetic ordering. Thus the conclusion reached from these cluster studies is that a symbiosis of local-moment formation and short-ranged antiferromagnetic correlations cause the gap to open at finite temperatures (Moukouri and Jarrell, 2001).

2. Antiferromagnetism and precursors

If the simulations are performed without enforcing the spin symmetry or frustrating the lattice, the system is able to transform to a state with antiferromagnetic order. Since the system is two dimensional, we know from

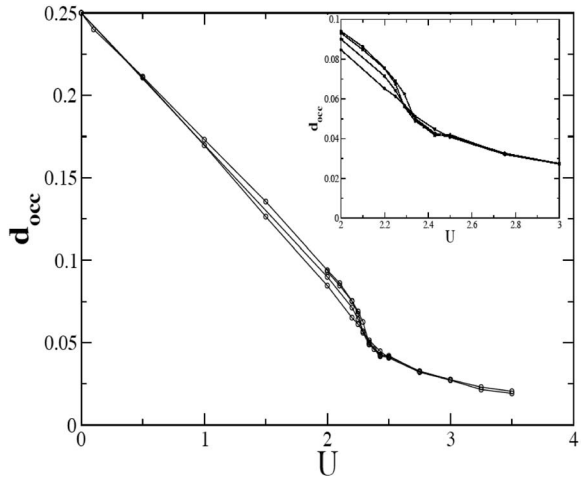

FIG. 24. Double occupancy as a function of U in the frustrated 2D Hubbard model with $t'=t$ for different temperatures (from top to bottom) $T/t=1/5,4/30,1/10,1/11$, calculated with the cellular DMFT/QMC method. From Parcollet *et al.*, 2004.

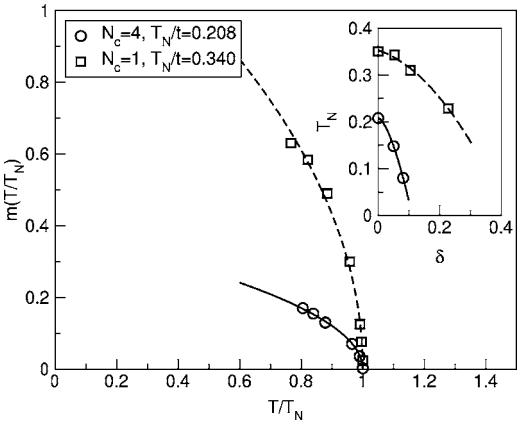

FIG. 25. Sublattice magnetization as a function of temperature in the half-filled 2D Hubbard model calculated with the DCA/NCA method for cluster sizes $N_c=1,4$ when $U=4t$. Inset: Neél temperature vs doping. From Maier, 2001.

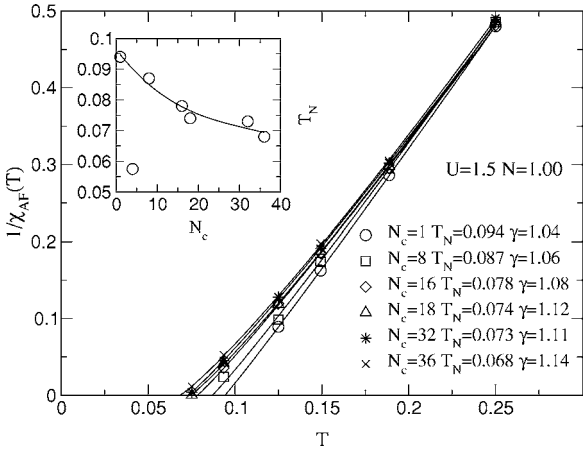

FIG. 26. Inverse antiferromagnetic susceptibility vs temperature in the half-filled 2D Hubbard model calculated with the DCA/QMC method for various cluster sizes N_c when $U=6t$. The lines are fits to the function $(T-T_N)^{\gamma}$. Inset: Corresponding Neél temperatures as a function of the cluster size. Energies are in units of $4t$. From Jarrell, Maier, Huscroft, and Moukouri, 2001.

the Mermin-Wagner theorem that the true Néel temperature T_N is necessarily zero. As discussed in Secs. II.D.2 and I.B, however, finite transition temperatures are predicted even in two dimensions due to the residual mean-field character of quantum cluster approaches, but expected to fall to zero with increasing cluster size.

As discussed in Secs. II.G and II.F, phase transitions can be identified from the disordered (here paramagnetic) state by calculating the corresponding susceptibility, or from the ordered state by computing the order parameter. The calculation of order parameters is shown in Fig. 25, where we plot the DCA/NCA result for the sublattice magnetization $m=1/N\Sigma_{i,\sigma}e^{i\mathbf{Q}\cdot\mathbf{x}_i}\sigma n_{i\sigma}$ [see Eq. (124)] as a function of the reduced temperature $t=T/T_N$ in the 2D half-filled Hubbard model for the cluster sizes $N_c=1$ and $N_c=4$ when $U=4t$. The $N_c=4$ Néel temperature $T_N=0.208t$ is reduced from the $N_c=1$ result $T_N=0.304t$ and the order parameter is strongly suppressed. As expected, nonlocal spin fluctuations suppress antiferromagnetism.

Figure 26 shows the DCA/QMC result for the temperature dependence of the inverse antiferromagnetic susceptibility $1/\chi_{AF}$ at $U=6t$ for various cluster sizes N_c in the paramagnetic state. At high temperatures the susceptibility is independent of N_c due to the lack of nonlocal fluctuations. In contrast to finite-size simulations, the low-temperature susceptibility diverges at $T=T_N$, indicating instability to the antiferromagnetic state. When $N_c=1$ the susceptibility diverges with a critical exponent $\gamma\approx 1$ as expected for a mean-field theory. Consistent with the DCA/NCA results the susceptibility diverges at lower temperatures when $N_c>1$ with larger exponents indicative of fluctuation effects. However, as discussed in Sec. I.B, these critical exponents reflect the behavior at intermediate temperatures. Very close to the transition, there must a region of mean-field behavior. However, this region is very difficult to resolve with DCA/QMC techniques, due to numerical noise, which is especially large near the transition.

As shown in the inset, the transition temperatures fall very slowly with the cluster size N_c. As detailed in Sec. II.D.4, fluctuation effects in clusters with linear size $L_c=2$ are overproportionally enhanced since its coordination number is reduced compared to the original system. Hence the $N_c=4$ result does not fall on the curve, similar to the behavior seen in DCA studies of the Falicov-Kimball model (Hettler *et al.*, 2000).

The question arises of whether the same nonlocal fluctuations which are responsible for suppressing the antiferromagnetism result in precursors of the antiferromagnetic phase transition. The onset of antiferromagnetic correlations on short time and length scales may be signaled by a pseudogap in the DOS as a precursor to the antiferromagnetic gap. This was predicted by Kampf and Schrieffer (1990) using a phenomenological ansatz for the weak-coupling Hubbard model based on the presence of strong antiferromagnetic spin fluctuations. On a microscopic level, this question has been addressed by finite-size quantum Monte Carlo in the 2D Hubbard model by Vekic and White (1993) and Creffield *et al.* (1995) and by approximate many-body techniques by Deisz *et al.* (1996) and Moukouri *et al.* (1999). But the results have been inconclusive due to the limitations of these techniques.

Within quantum cluster approaches the pseudogap phenomenon was first studied by Maier *et al.* (2000b) using the DCA/NCA formalism. In contrast to $N_c=1$ where a Kondo-like quasiparticle peak emerges at the chemical potential as the temperature is decreased [identical to the $D=\infty$ DMFT result (Georges *et al.*, 1996)], a pseudogap was found when nonlocal correlations were included in $N_c=4$ simulations. For larger cluster sizes, the emergence of the pseudogap in the DOS was explored by DCA/QMC techniques in Huscroft *et al.* (2001) and DCA/FLEX in Aryanpour, Hettler, and

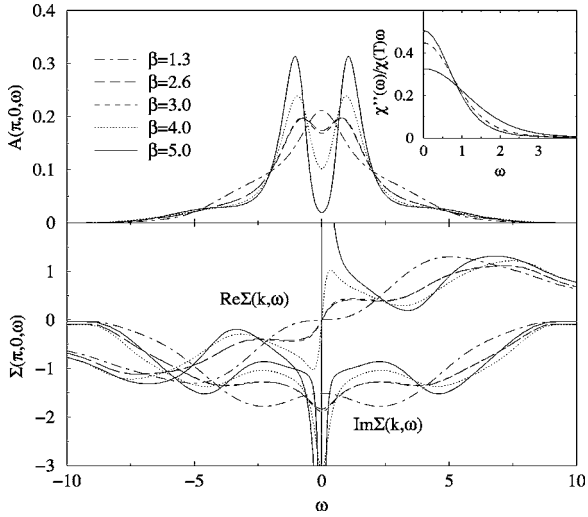

FIG. 27. Spectral function $A(\mathbf{k},\omega)$ and the real $\mathrm{Re}\,\Sigma(\mathbf{k},\omega)$ and imaginary $\mathrm{Im}\,\Sigma(\mathbf{k},\omega)$ parts of the self-energy for various temperatures at $\mathbf{k}=(\pi,0)$ in the 2D half-filled Hubbard model for $U=5.2t$ calculated with the DCA/QMC method for a 64-site cluster ($N_c=64$). From Huscroft *et al.*, 2001.

Jarrell (2003). Figure 27 displays the DCA/QMC results for the spectral function $A(\mathbf{k},\omega)$ and the self-energy $\Sigma(\mathbf{k},\omega)$ at the Fermi wave vector $\mathbf{k}=(\pi,0)$ in the paramagnetic state for a 64-site cluster ($N_c=64$) at various temperatures. With decreasing temperature a pseudogap develops in $A(\mathbf{k},\omega)$ at the Fermi wave vector $\mathbf{k}=(\pi,0)$. Simultaneously the slope of $\mathrm{Re}\,\Sigma(\mathbf{k},0)$ becomes positive at $\mathbf{k}=(\pi,0)$ signaling the appearance of two new solutions in the quasiparticle equation $\omega-\epsilon_{\mathbf{k}}+\mu-\mathrm{Re}\,\Sigma(\mathbf{k},\omega)=0$. In addition to the strongly damped solution at $\omega=0$, which is also present in the noninteracting system, these two new quasiparticle solutions appear on both sides of $\omega=0$. A consequence of the antiferromagnetic order on short time and length scales, they can be viewed as precursors of the doubling of the unit cell in the antiferromagnetic state. The pseudogap is generated by the local minimum in $\mathrm{Im}\,\Sigma(\mathbf{k},\omega)$, which signals the breakdown of Fermi-liquid behavior.

By studying the system on a triangular lattice, Imai and Kawakami (2002) investigated the effects of frustration on the pseudogap in the half-filled 2D Hubbard model using the DCA/NCA and DCA/FLEX approaches. Figure 28 schematically illustrates the triangular lattice and the choice of cluster wave vectors in the corresponding Brillouin zone for $N_c=4$. For $t'=0$ this setup corresponds to the unfrustrated system and the effects of frustration can be systematically studied as t' is increased to its maximal value $t'=t$. Figure 29 reproduces the results for the DOS and coarse-grained spectra $\bar{A}(\mathbf{K},\omega)$ for different values of the frustration t'. As the geometrical frustration increases from $t'=0$ to $t'=t$, antiferromagnetic spin fluctuations are suppressed. Consequently the pseudogap in the unfrustrated system diminishes and a quasiparticle peak develops at the chemical potential. The change in the DOS mainly originates

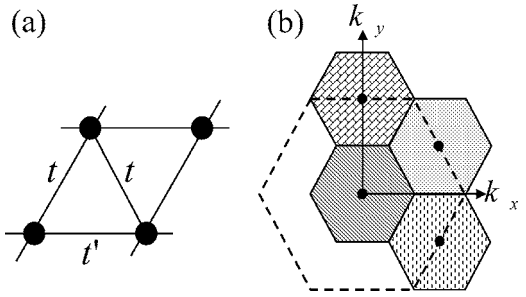

FIG. 28. Illustration of the triangular lattice with (a) hopping amplitudes t and t' and (b) DCA coarse-graining cells in the first Brillouin zone (dashed line) of the triangular lattice when $N_c=4$. Cluster $\mathbf{K}$ points are indicated by the dots. From Imai and Kawakami, 2002.

in the region in momentum space around $\mathbf{K}=(\pi,\pi/\sqrt{3})$ where the Fermi surface is located. These results are thus consistent with an antiferromagnetic spin-fluctuation-driven pseudogap.

3. Pseudogap at finite doping

The properties of the Hubbard model away from half-filling are of great interest especially in the context of high-temperature superconductors. Contrary to Fermi-liquid theory, low-energy spin excitations in high-temperature superconductors are suppressed at low temperatures, as evidenced by Knight-shift experiments. Concomitantly, the Fermi surface is gapped along certain directions in the Brillouin zone as indicated in angle-resolved photoemission spectroscopy (ARPES)

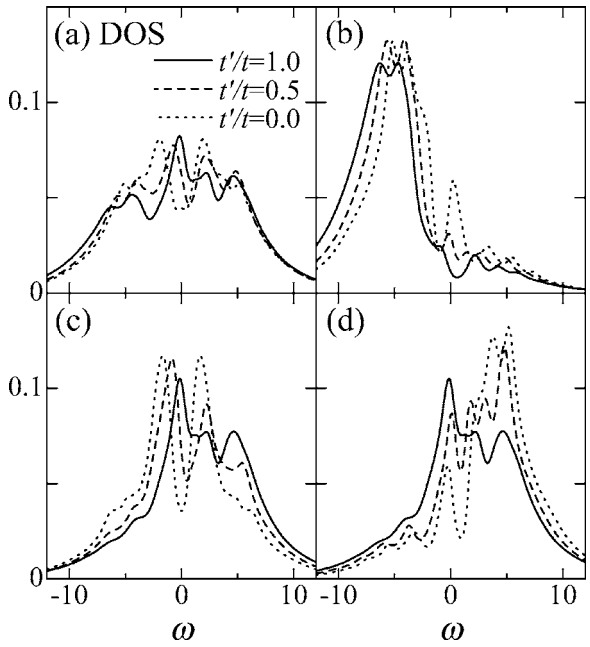

FIG. 29. The 2D half-filled frustrated Hubbard model: (a) density of states; coarse-grained single-particle spectral functions $\bar{A}(\mathbf{K},\omega)$ for (b) $\mathbf{K}=(0,0)$, (c) $\mathbf{K}=(\pi,\pi/\sqrt{3})$, and (d) $\mathbf{K}=(0,2\pi/\sqrt{3})$ for various values of the frustration t' when $U=6t$ and $T=0.6t$. From Imai and Kawakami, 2002.

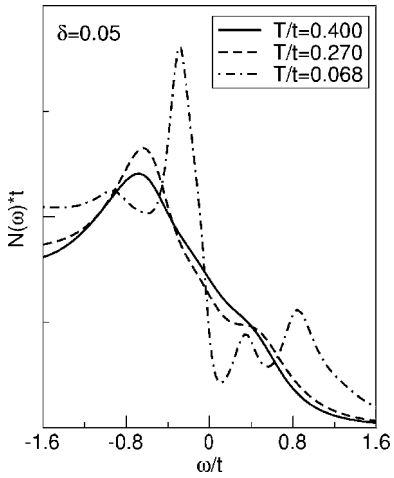

FIG. 30. Density of states for various temperatures in the 2D Hubbard model at 5% doping when $U=12t$ near the chemical potential ($\omega=0$) calculated with the DCA/NCA for a four-site cluster, $N_c=4$. From Maier, 2001.

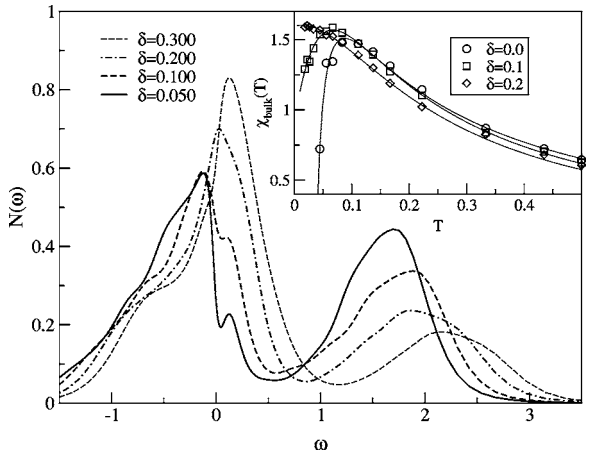

FIG. 31. Density of states for various dopings δ in the 2D Hubbard model at $T=0.092t$ and $U=8t$ calculated with DCA/quantum Monte Carlo for a four-site cluster, $N_c=4$. Inset: Uniform spin susceptibility as a function of temperature. Energies are in units of $4t$. From Jarrell, Maier, Hettler, *et al.*, 2001.

experiments. This pseudogap phenomenon[9] has proven a great challenge for theories of strongly correlated systems.

The DMFT has provided great insight into the evolution of spectra in doped Mott insulators. Exact results based on the self-consistent mapping onto an Anderson impurity model show that the system is a Fermi liquid in the metallic state in the absence of symmetry breaking below a coherence temperature reminiscent of the Kondo temperature (Georges and Kotliar, 1992). Hence the spin susceptibility becomes finite at low temperatures in contrast to the experimental results in underdoped cuprates. Furthermore, Müller-Hartmann (1989a) showed that because the self-energy is momentum independent, volume and shape of the Fermi surface are identical to the noninteracting Fermi surface. Thus DMFT does not include the effects that lead to the emergence of a pseudogap in the spin and quasiparticle spectrum and cluster extensions are necessary.

Within quantum cluster approaches the pseudogap phenomenon in the doped 2D Hubbard model was studied with the DCA/NCA approach by Maier *et al.* (2000b) and Maier (2001), with the DCA/QMC approach by Jarrell, Maier, Hettler, and Tahvildarzadeh (2001) and by Maier, Jarrell, *et al.* (2002), with the two-site composite-operator method by Stanescu and Phillips (2003, 2004) and with the cluster perturbation theory by Sénéchal and Tremblay (2004).

Figure 30 shows the DCA/NCA result for the low-energy DOS in the 2D Hubbard model at 5% doping ($\delta=0.05$) around the chemical potential ($\omega=0$) calculated on a four-site cluster ($N_c=4$). At high temperature $T>0.3t$ no pseudogap is seen in the DOS. As the temperature is lowered the DOS distorts at the chemical potential and a pseudogap emerges at $\omega=0$ when $T\lesssim 0.3t$.

These noncrossing approximation results were confirmed in DCA/QMC simulations by Jarrell, Maier, Hettler, and Tahvildazadeh (2001), which we reproduce in Fig. 31. At low temperatures a pseudogap is observed in the DOS at dopings $\delta\lesssim 0.2$. This depression of quasiparticle states at the chemical potential is accompanied by a downturn of the uniform magnetic susceptibility shown in the inset. For low to intermediate doping it develops a maximum defining a crossover temperature T^*. Below T^*, quasiparticle and low-energy spin excitations are suppressed by nonlocal correlations similar to what is observed in the experiment. At the same time, the charge susceptibility (not shown) displays qualitatively different behavior, forming a strong low-energy peak at low temperatures (see Maier, Jarrell, Macridin, and Zhang, 2004, 2002, and Fig. 37), which signals the emergence of coherent charge excitations below T^*. The $N_c=4$ DCA results are thus consistent with a spin-charge separated picture as in Anderson's resonating valence bond (RVB) theory. This is not surprising since, as we discussed in Sec. IV.D.2, fluctuations are enhanced in the $N_c=4$ cluster due to the "too small" coordination number. It is known that small coordination numbers favor the spin-charge-separated RVB state (Anderson, 1987) over the Néel state. Indeed the RVB state was shown to be the ground state of a 2×2 Heisenberg model with periodic boundary conditions and a large gap to the first excited state (Dagotto and Moreo, 1988).

The corresponding four-site DCA/QMC result for the momentum-resolved spectral function $A(\mathbf{k},\omega)$ in the pseudogap regime is displayed in Fig. 32 for energies near the chemical potential between points of high symmetry, $\Gamma=(0,0)$, $X=(\pi,0)$, and $M=(\pi,\pi)$ in the first Brillouin zone. The overall dispersion of the band crossing the chemical potential $\omega=0$ follows that of the noninteracting system, $\epsilon_{\mathbf{k}}$. While coherent quasiparticles exist

[9]For a review on the pseudogap phenomenon see Timusk and Statt (1999).

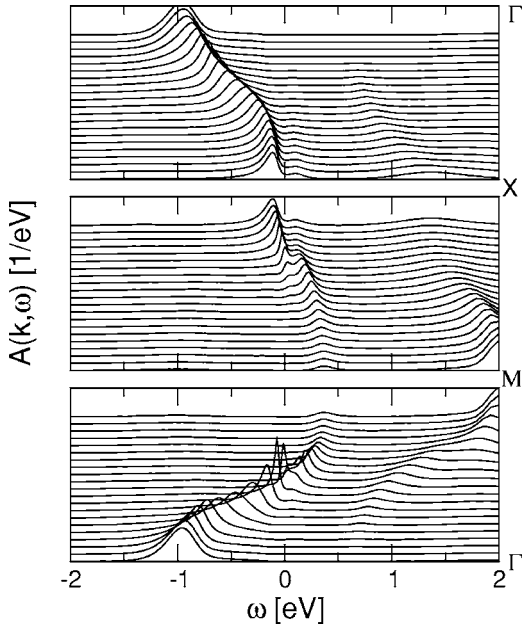

FIG. 32. The spectral function $A(\mathbf{k},\omega)$ near the chemical potential in the 5% doped 2D Hubbard model at $T=0.88t$ and $U=8t$ along high-symmetry directions in the first Brillouin zone between $\Gamma=(0,0)$, $X=(\pi,0)$, and $M=(\pi,\pi)$ calculated with the DCA/QMC method for a four-site cluster $N_c=4$. The DCA self-energy was interpolated using a smooth spline (see Sec. II.D.4).

along $\Gamma\rightarrow M$, the pseudogap is seen near $X=(\pi,0)$ at the chemical potential $\omega=0$. The anisotropy of the pseudogap is thus consistent with that observed in ARPES measurements on underdoped hole-doped cuprates.

Qualitatively similar results for the emergence of the quasiparticle spectrum in the doped 2D Hubbard model were obtained by Stanescu and Phillips (2003) using the two-site composite-operator approach discussed in Sec. II.I (see also Stanescu and Phillips, 2004). Figure 33 illustrates their results for the doping dependence of the chemical potential μ, the imaginary part of the self-energy $\mathrm{Im}\,\Sigma$, and the U dependence of the low-energy DOS. At half-filling the chemical potential has a discontinuity, indicating the absence of mid gap states. In agreement with DCA/QMC results (Jarrell, Maier, Hettler and Tahvildarzadeh, 2001; Jarrell, Maier, Huscroft, and Moukouri, 2001) and DCA/NCA (Maier, 2001) results, $|\mathrm{Im}\,\Sigma|$ is large in the underdoped pseudogap regime ($n=0.97$) and acquires Fermi-liquid behavior at larger doping $n\leqslant 0.80$, indicated by the parabolic minimum at the chemical potential. As illustrated in the inset, the depth of the pseudogap decreases as U increases, suggesting a pseudogap scale compatible with t^2/U.

Sénéchal and Tremblay (2004) recently investigated the difference in pseudogap behavior between electron- and hole-doped high-temperature superconductors using cluster perturbation theory for the 2D $t-t'-t''$ Hubbard model. As illustrated in the Fermi-surface plots in Fig. 34, their results at $U=8t$ demonstrate that the

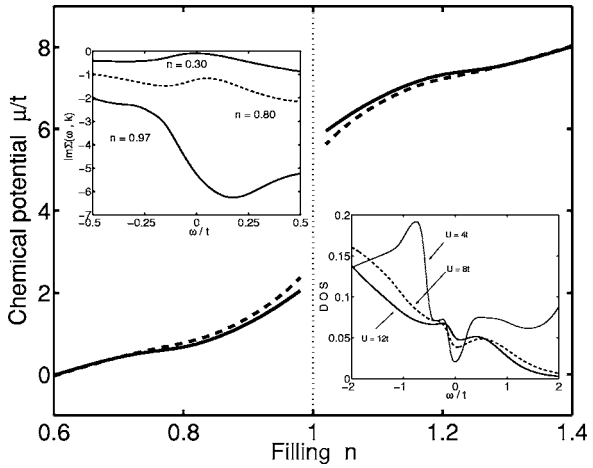

FIG. 33. The doping dependence of the chemical potential in the 2D Hubbard model calculated with the two-site composite-operator method; dashed line, $T=0.15t$; solid line, $T=0.07t$. Right inset: DOS for various values of U at 5% doping ($n=0.95$). Left inset: Imaginary part of the self-energy evaluated at a Fermi momentum (0.3,2.10) for $n=0.97$, (0.3,1.84) for $n=0.80$, and (0.3,1.06) for $n=0.3$. From Stanescu and Phillips, 2003.

pseudogap in hole-doped systems (right side) occurs near $X=(\pi,0)$ at optimal doping consistent with the results discussed above. In electron-doped systems (left side), however, the pseudogap appears at the crossing points of the Fermi surface with the antiferromagnetic Brillouin-zone boundary at moderate interaction $U=4t$. When U is large, however (not shown), the Fermi surface only survives in the neighborhood of $(\pi,0)$ and $(0,\pi)$. As shown in the lower panels of Fig. 34 the

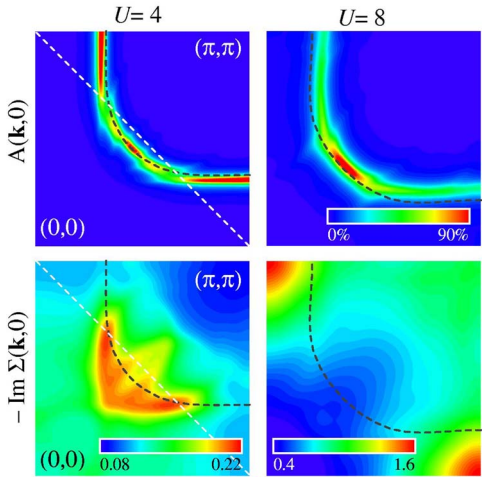

FIG. 34. (Color in online edition) Intensity plot of the spectral function $A(\mathbf{k},0)$ (top) and imaginary part of the self-energy $\mathrm{Im}\,\Sigma(\mathbf{k},0)$ (bottom) of the 2D Hubbard model calculated with cluster perturbation theory on a 3×4-site cluster. The left side shows the results in the first quadrant of the Brillouin zone for the 17% electron-doped system at $U=4t$ and the right side for the 17% hole-doped system at $U=8t$. The dashed line represents the Fermi surface of the noninteracting system. From Sénéchal and Tremblay, 2004.

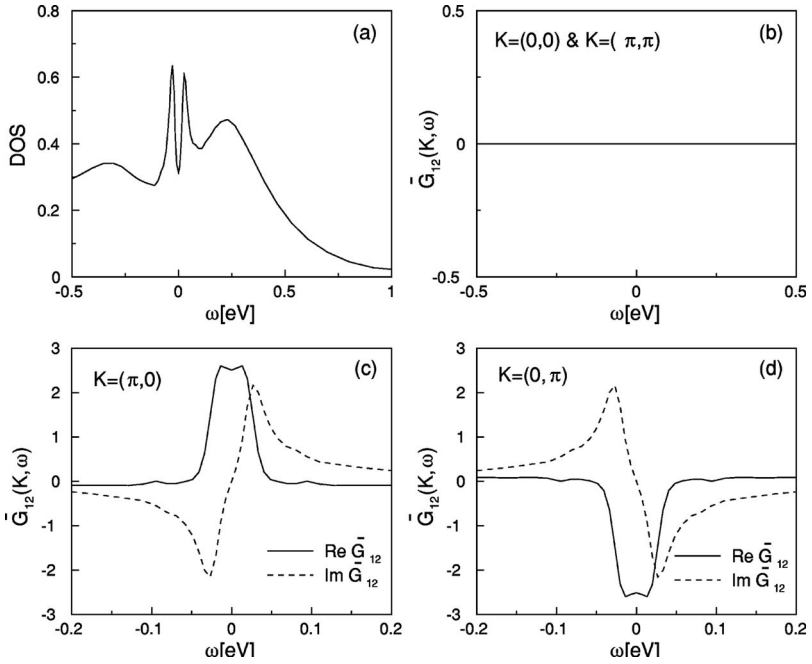

FIG. 35. Comparison of different DCA cells: (a) density of states near the chemical potential; (b), (c), and (d) coarse-grained anomalous Green's function $\bar{G}_{12}(\mathbf{K},\omega)\equiv\bar{F}(\mathbf{K},\omega)$ in the superconducting state of the 2D Hubbard model at 19% doping, $T=0.047t$, $U=12t$ for different cluster $\mathbf{K}$ points calculated with DCA/NCA for a four-site cluster, $N_c=4$. From Maier *et al.*, 2000a.

pseudogap in both cases is generated by a large scattering rate $|\mathrm{Im}\,\Sigma(\mathbf{k},0)|$ at the chemical potential. A unified picture of the spectral properties of the electron- and hole-doped cuprates thus emerges from these results if the interaction strength U is allowed to be doping dependent. To reproduce the experimental observations in optimally doped cuprates, large values of U seem necessary in hole-doped ($U\approx 8t$) systems, while smaller values of U describe the electron-doped systems ($U\lesssim 6t$) (Sénéchal and Tremblay, 2004).

4. Superconductivity

It is well known from weak-coupling finite-size FLEX results (Bickers *et al.*, 1989) and phenomenological theories (Monthoux *et al.*, 1991; Scalapino, 1999) that antiferromagnetic spin fluctuations mediate pairing with d-wave symmetry and cause a pseudogap in underdoped systems. Recent numerical renormalization-group studies (Halboth and Metzner, 2000; Zanchi and Schulz, 2000) in fact show strong evidence that the ground state of the weak-coupling 2D Hubbard model is superconducting with a d-wave order parameter at finite doping when $t'=0$, and when t' is finite even at half-filling. Finite-size QMC simulations for the doped 2D Hubbard model in the intermediate coupling regime $U\sim W$ support the idea of a spin-fluctuation driven interaction mediating d-wave superconductivity (for a review, see Scalapino, 1999). The fermion sign problem, however, limits these calculations to temperatures too high to study a possible transition. These calculations are also restricted to relatively small system sizes, making statements for the thermodynamic limit problematic, and inhibiting studies of the low-energy physics. These shortcomings do not apply to embedded-cluster theories which are built for the thermodynamic limit. Cluster sizes larger than 1 are necessary, however, to describe a possible transition to a state with a nonlocal (d-wave) order parameter as discussed in Sec. II.F.

In optimally doped cuprates, the spin fluctuations are known to be short ranged, extending over a few lattice spacings. Hence quantum cluster approaches should provide an adequate methodology to study superconductivity in these systems. Pairing in the 2D Hubbard model was studied using the DCA/NCA by Maier *et al.* (2000a), and with the DCA/QMC approach by Jarrell, Maier, Hettler, and Tahvildarzadeh (2001), Jarrell, Maier, Huscroft, and Moukouri (2001), and Maier, Jarrell, Macridin, and Slezak (2004). The possible coexist-

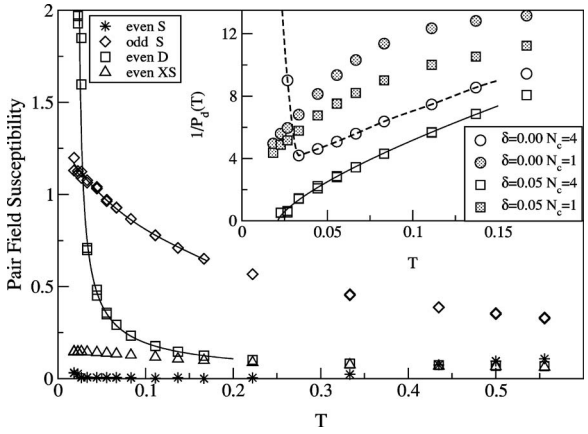

FIG. 36. Pair-field susceptibilities vs temperature in the even-frequency s-wave, extended s-wave (xs), d-wave, and odd-frequency s-wave channels in the 2D Hubbard model at 5% doping, $U=8t$ calculated with the DCA/QMC method for a four-site cluster, $N_c=4$. Inset: Inverse d-wave pair-field susceptibility vs temperature for different dopings and cluster sizes. The solid line is a fit to $b(T-T_c)^\gamma$ with $T_c=0.084t$ and $\gamma=0.72$. Temperatures are in units of $4t$. From Jarrell, Maier, Hettler, and Tahvildarzadeh, 2001.

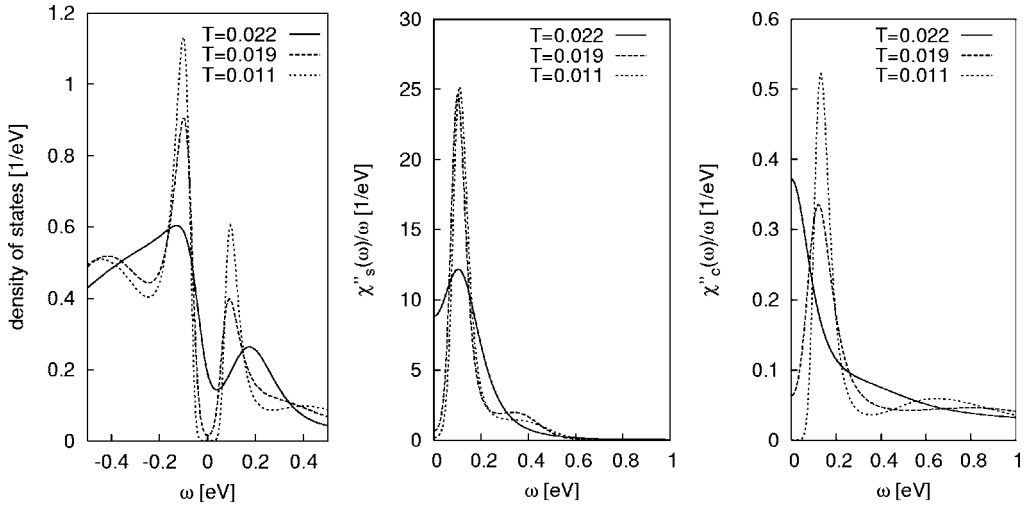

FIG. 37. DOS (left), local dynamic spin susceptibility (center), and local dynamic charge susceptibility (right) in the 2D Hubbard model at 5% doping at different temperatures above and below the critical temperature $T_c=0.0218=0.087t$ calculated with the DCA/QMC method for a four-site cluster, $N_c=4$. Temperatures are in units of $4t$. From Maier, Jarrell, Macridin, and Zhang, 2004.

ence of superconductivity with antiferromagnetic order was investigated by Lichtenstein and Katsnelson (2000).

The results of four-site ($N_c=4$) DCA simulations for the doped 2D Hubbard model show an instability to a superconducting phase with a $d_{x^2-y^2}$-wave order parameter at low enough temperatures. As a typical example of this transition, Fig. 35 shows the DCA/NCA result for the DOS and the coarse-grained anomalous Green's function $\bar{G}_{12}(\mathbf{K},\omega)\equiv\bar{F}(\mathbf{K},\omega)$ defined in Eq. (110) at different cluster $\mathbf{K}$ points near the chemical potential in the superconducting state. $\bar{G}_{12}(\mathbf{K},\omega)$ vanishes at $\mathbf{K}=(0,0)$ and (π,π) but is finite at $(\pi,0)$ and $(0,\pi)$ with opposite signs. Since the $\mathbf{K}$ dependence of the coarse-grained order parameter $\bar{\Delta}_{\mathbf{K}}$ is given by the $\mathbf{K}$ dependence of the coarse-grained anomalous Green's function [see Eq. (114)], this result is consistent with a $d_{x^2-y^2}$ symmetry of the order parameter. The finite pair amplitude is also reflected in the DOS depicted in the upper left part, where the lower subband of the full spectrum is shown. It displays the opening of a pseudogap at zero frequency.

Jarrell, Maier, Hettler and Tahvidarzadeh (2001) and Jarrell, Maier, Huscroft, and Moukouri (2001) used DCA/QMC to search for many different types of superconductivity, including s, extended s, p, and d wave, of both even and odd frequency. Of these, only the odd-frequency s-wave and even-frequency d-wave pair-field susceptibilities were strongly enhanced, and only the d-wave susceptibility diverged. This is illustrated in Fig. 36 where the pair-field susceptibilities are plotted versus temperature at 5% doping. As illustrated in the inset, for $N_c=1$ there is no tendency towards pairing. As detailed in Sec. II.F, the DMFT is not able to describe pairing with symmetries lower than the lattice symmetry (i.e., p, d wave, etc.). For $N_c=4$ and $\delta=0$ the inverse susceptibility rises abruptly as the temperature is lowered and the Mott gap opens in the DOS. The Mott gap becomes more pronounced as N_c increases (see Sec. IV.D.1), so that for larger clusters the gap prevents superconductivity even for $U<W$. If charge excitations are gapped, then pairing is suppressed. At half-filling, for $U=8t$ the gap is of order U, and thus much larger than the magnetic exchange energy $J\sim 4t^2/U=0.5t$. Hence the opening of the Mott gap suppresses any magnetically mediated pairing. Away from half-filling the width of the pseudogap in the charge excitation spectrum is much smaller, of the order of J (see Sec. IV.D.3), so that magnetically mediated pairing is possible.

More insight in the nature of pairing was gained from further DCA/QMC studies of the 2D Hubbard model (Maier, Jarrell, Macridin, and Slezak, 2004). Figure 37 shows the DCA/QMC result for the evolution of the DOS, the local dynamic spin and local dynamic charge susceptibility[10] as the temperature decreases below the critical temperature T_c. As discussed in Sec. IV.D.3, the normal-state low-temperature DOS and spin susceptibility display a pseudogap, i.e., a depression of low-energy quasiparticle and spin excitations. Both quantities evolve smoothly across the superconducting transition with the pseudogap changing to a superconducting gap[11] below T_c. However, since the charge susceptibility is peaked at zero frequency even slightly above T_c, it changes abruptly upon pairing to show the same behavior as the spin susceptibility, including the superconducting gap at low frequencies. Remarkably, well below T_c all quantities display narrow peaks at $\omega\approx 0.1$ eV, delim-

[10]Note that in the DCA, local quantities are identical in the lattice and on the cluster and thus are easily calculated.

[11]Note that due to the finite resolution in momentum space, the DCA underestimates low-energy spectral weight in superconductors where the gap has nodes on the Fermi surface. As a result, a fully developed gap is found at low temperatures instead of a DOS that vanishes linearly in frequency, as expected for a d-wave superconductor.

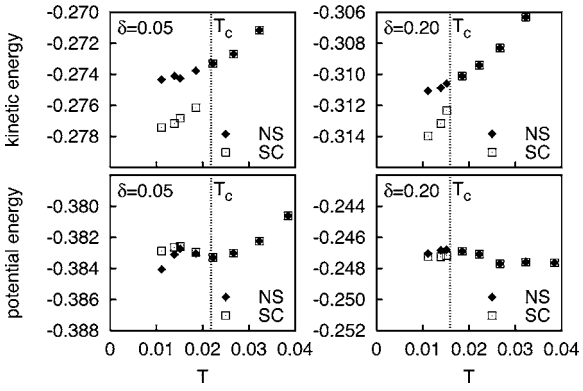

FIG. 38. Kinetic (top) and potential (bottom) energies vs temperature in the normal (NS) and superconducting (SC) states in the 2D Hubbard model at 5% (left) and 20% (right) doping for $U=8t$ calculated with the DCA/QMC method on a four-site cluster ($N_c=4$). T_c is indicated by the vertical dotted lines. Temperatures are in units of $4t$. From Maier, Jarrell, Macridin, and Slezak, 2004.

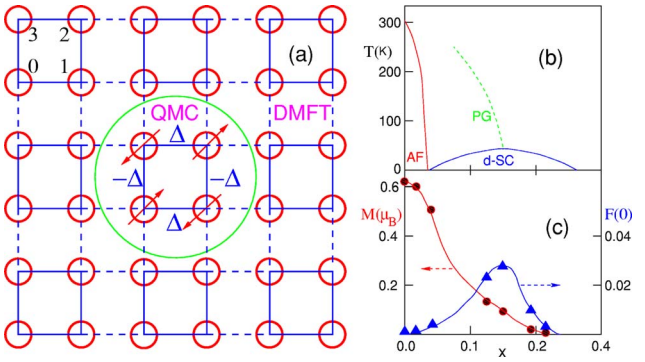

FIG. 39. (Color in online edition) Four-site cluster calculation for the 2D Hubbard model: (a) Schematic representation of an antiferromagnetic d-wave 2×2 periodically repeated cluster. (b) Generic phase diagram of high-temperature superconductor. (c) Magnetic (M) and d-wave superconducting (F) order parameters versus hole doping in the 2D Hubbard model at $\beta t=15$, $t'=-0.15t$, $U=4.8t$ calculated with a four-site cluster approach similar to the DCA/QMC method. From Lichtenstein and Katsnelson, 2000.

iting the superconducting gap. This clearly indicates the formation of quasiparticles below T_c. It is important to note, however, that the absence of quasiparticles in the normal state undermines the very foundation of the BCS theory of conventional superconductors where pairing is a result of a Fermi surface instability that relies on the existence of quasiparticles in a Fermi liquid (Schrieffer, 1993).

DCA/QMC results for the condensation energy further establish the unconventional character of superconductivity in the 2D Hubbard model (Maier, Jarrell, Macridin, and Slezak, 2004). Figure 38 presents the kinetic (top) and potential (bottom) energies, Tr($\mathbf{tG}$) and Tr($\mathbf{\Sigma G}$), respectively, of the superconducting (SC) and normal-state (NS) solution as a function of temperature at low doping $\delta=0.05$ (left) and optimal doping $\delta=0.20$ (right). For both doping levels, the kinetic energy in the superconducting state is reduced compared to the normal state, while the potential energies are almost identical. This result is in agreement with recent optical experiments which show that the superconducting transition in the cuprates is due to a lowering of the electronic kinetic energy (Molegraaf *et al.*, 2002). It further supports the evidence that pairing in the Hubbard model is fundamentally different from BCS pairing which occurs through a reduction of the electronic potential energy accompanied by a slight increase in the kinetic energy.

The possibility of coexisting d-wave superconducting and antiferromagnetic order in the 2D Hubbard model was investigated by Lichtenstein and Katsnelson (2000) using a four-site cluster approach similar to the DCA/QMC method [see Fig. 39(a)]. In this approach, an 8×8 matrix representation of the Green function is required to account for both the antiferromagnetic order parameter $\langle c_{i\uparrow}^{\dagger}c_{j\downarrow}\rangle$ and the superconducting order parameter $\langle c_{i\downarrow}c_{j\uparrow}\rangle$. Figure 39(c) reproduces the results for the two order parameters as a function of doping at fixed temperature in the weak-coupling regime ($U=4.8t$). The authors find that the antiferromagnetic order parameter coexists with the d-wave superconducting order parameter over a wide range of doping. Consistent with the DCA/QMC results, the antiferromagnetic order parameter is maximal at zero doping where the superconducting order parameter vanishes due to the opening of the gap.

5. Phase diagram

The results reviewed in the preceding sections illustrate that quantum cluster approaches applied to the 2D Hubbard model are able to capture the complex behavior observed in high-temperature superconductors. The qualitative agreement with experiments is summarized in the $N_c=4$ DCA/QMC temperature-doping (T-δ) phase diagram of the 2D Hubbard model in the intermediate-coupling regime $U=W$ shown in Fig. 40. The antiferromagnetic and d-wave superconducting phase boundaries were determined by the instabilities of the paramagnetic phase as indicated by the divergence of the corresponding susceptibilities. Therefore these results do not allow any conclusions about a possible coexistence of the antiferromagnetic and d-wave superconducting phases for $\delta<0.5$. The results obtained by Lichtenstein and Katsnelson (2000), however, suggest this coexistence at least for weak coupling [see Fig. 39(c)].

The pseudogap crossover temperature T^* determined by the peak in the uniform spin susceptibility (see Fig. 31) serves as a boundary separating the observed Fermi-liquid and non-Fermi-liquid behavior. For $T<T^*$ the self-energy shows non-Fermi-liquid character for the parts on the Fermi surface near $\mathbf{k}=(\pi,0)$ (see Fig. 33). Quasiparticle and low-energy spin excitations are suppressed as indicated by the pseudogap in the DOS and the spin susceptibility (see Fig. 37). At $\delta\gtrsim0.2$ Fermi-

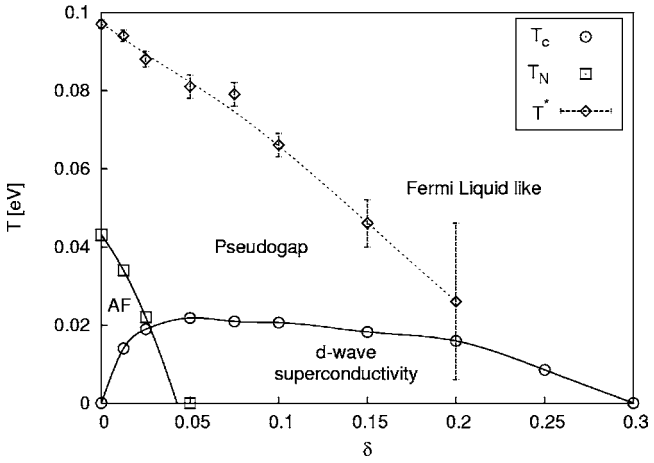

FIG. 40. Temperature-doping phase diagram of the 2D Hubbard model when $U=8t$ calculated with DCA/QMC for a four-site cluster, $N_c=4$. The error bars on T^* result from the difficulty in locating the maximum in the uniform spin susceptibility. Regions of antiferromagnetism, d-wave superconducting, and pseudogap behavior can be seen.

liquid behavior is recovered (see Fig. 33). At low temperatures, the system is antiferromagnetic near half-filling. The d-wave superconducting phase at finite doping has its maximum transition temperature at $\delta \approx 0.05$.

As indicated in Sec. IV.D.3, the $N_c=4$ DCA cluster favors the spin-charge separated RVB state. The $N_c=4$ results may thus be interpreted within the RVB picture (Anderson, 1987): The pairing of spins in singlets below the crossover temperature T^* results in the suppression of low-energy spin excitations and consequently in a pseudogap in the density of states. Charge excitations are quasifree as indicated by the zero-frequency peak in the charge susceptibility (see Fig. 37). Well below the transition spin and charge degrees of freedom recombine, forming electrons which pair. Frustrated kinetic energy is recovered as indicated by the reduction of the kinetic energy as the system goes superconducting (see Fig. 38).

Although the properties of high-temperature superconductors are well described by the $N_c=4$ results, it is important to ask the question whether the phase diagram and in particular the observed RVB nature of the results are stable when the cluster size is increased. While the pseudogap temperature T^* may be expected to persist with increasing N_c, the Neél temperature is expected to fall to zero, as discussed in Sec. I.B (see also Fig. 26). Superconductivity, however, may persist as Kosterlitz-Thouless topological order (Kosterlitz, 1973; Kosterlitz and Thouless, 1973). Larger cluster simulations (Maier, Jarrell, Schulthess, and White, 2005), however, indicate that superconductivity persists at finite temperatures in larger clusters, albeit with reduced transition temperature.

6. Studies of related models

a. Stripes in the t-J model

Several numerical studies indicate that there is a tendency for doped holes to form stripes separated by antiferromagnetic domains in strongly correlated systems (for a review see Dagotto, 1994). Cluster perturbation theory is the quantum cluster method of choice to study the large unit cells in the inhomogeneous stripe phase, which complicate if not preclude the application of the numerically more expensive embedded-cluster techniques (cellular DMFT, DCA). A thorough study of stripes in the large U limit of the Hubbard model, the t-J model, was conducted by Zacher *et al.* (2002a, 2002b) within the cluster perturbation theory. To implement cluster perturbation theory for this problem, the authors divided the lattice into alternating clusters of metallic stripes and antiferromagnetic domains. The intercluster hopping linking these clusters was treated perturbatively within the theory. The enforced stripe pattern in this implementation prohibits exploration of the stability of stripes, but allows the investigation of the effects of the stripe pattern on the single-particle excitations. In systems with less than 12% doping the technique was shown to reproduce salient ARPES features in selected high-temperature superconductors if a site-centered 3 +1 stripe pattern, i.e., half-filled antiferromagnetic three-leg ladders separated by doped one-leg chains, was chosen (Zacher *et al.*, 2002b). At higher dopings the comparison with ARPES indicates that the weight of bond-centered stripes with a 2+2 pattern increases in which excess holes proliferate out of the stripes into the antiferromagnetic domain (Zacher *et al.*, 2002a).

b. Spectral properties of the three-band Hubbard model

In the context of high-temperature superconductors, the single-band Hubbard model can be viewed as a low-energy approximation of the more complex and more realistic three-band Hubbard model (Emery, 1987; Emery and Reiter, 1988). The three-band Hubbard model takes into account the p_x and p_y oxygen orbitals in addition to the Cu d degrees of freedom in the superconducting CuO_2 planes. The cluster perturbation theory study of its spectral properties by Dahnken *et al.* (2002) shows very good agreement with ARPES data on high-temperature superconductors at half-filling as well as in the doped system including a holelike Fermi surface at high doping which splits into an electronlike and a holelike branch when a bilayer hopping $t_\perp$ is included.

c. Cluster simulations of the periodic Anderson model

The periodic Anderson model is widely considered to be a paradigm for a variety of rare-earth and actinide compounds, including the heavy-fermion systems. It is composed of a strongly hybridizing band of d electrons weakly coupled to localized f electrons described by the Hamiltonian

$$H = -t\sum_{ij,\sigma}(d^{\dagger}_{i\sigma}d_{j\sigma} + \text{H.c.}) + \epsilon_d\sum_{i,\sigma} n^d_{i\sigma} + \epsilon_f\sum_{i,\sigma} n^f_{i\sigma} + U\sum_i n^f_{i\uparrow}n^f_{i\downarrow} + V\sum_{i,\sigma}(d^{\dagger}_{i\sigma}f_{i,\sigma} + \text{H.c.}). \quad (185)$$

DMFT simulations of the periodic Anderson model reveal an antiferromagnetic insulating phase at half-filling of both the f and the d bands. The gap is set by the Kondo coherence scale T_0 which is strongly enhanced compared to the single-impurity model scale. When the d band is doped away from half-filling while the f band remains roughly half-filled, the system becomes more metallic, and the Kondo scale is strongly suppressed compared to that of the SIAM. In both the insulator and metal, the temperature dependence of the impurity susceptibility and many other low temperature quantities deviate strongly from that of the single-impurity Anderson model (Tahvildar-Zadeh *et al.*, 1997).

Nonlocal corrections were studied by Shimizu (2002) who used the DCA together with the noncrossing approximation as a cluster solver to study the single-particle spectra. He finds large deviations from the DMFT result due to the effects of Ruderman-Kittel-Kasuya-Yosida (RKKY) exchange. At half-filling, where the RKKY exchange is strong and antiferromagnetic, he finds a large gap of the order of the RKKY exchange energy. When the filling of the conduction band is small and the RKKY exchange is weaker and ferromagnetic, the coherence peak is restored.

V. CONCLUSIONS AND PERSPECTIVES

In this review we have tried to convey the message that quantum cluster approaches provide powerful theoretical tools for the study of the rich phenomenology in systems dominated by strong electronic interactions. Quantum cluster approaches are nonperturbative in nature, their quality can be systematically improved by increasing the cluster size, and they provide complementary information to finite-size simulations. By mapping the lattice problem to a finite-size cluster they describe short-ranged correlations within the cluster accurately while approximating longer-ranged physics on the mean-field level. Of the various attempts to add nonlocal corrections to local approximations such as DMFT, we have focused in this review on three established quantum cluster approaches which we believe play the major role in the description of many-particle systems.

The cluster perturbation theory provides a very economical way to calculate the single-particle dynamics by continuing the results of an isolated finite-size cluster to the thermodynamic limit. For a cluster consisting of a single site only, this method is identical to the Hubbard-I approximation, while it recovers the exact result in the infinite-cluster limit. When combined with the self-energy-functional approach, the cluster perturbation theory can also be used to study instabilities to broken-symmetry phases.

Both embedded-cluster techniques, the dynamical cluster approximation and the cellular dynamical mean-field theory, are superior to the CPT in that they map the lattice to an embedded cluster instead of the cluster perturbation theory's isolated cluster. This leads to a self-consistent theory with a single-particle coupling between the cluster and the host. As a result, both DCA and cellular DMFT naturally allow for the study of phase transitions and they provide thermodynamically consistent results on the one- and two-particle level.

The cellular DMFT can be viewed as a direct generalization of DMFT to a cluster in real space. The mapping between lattice and cluster problems is identical to that of the long established molecular CPA for disordered systems. It leads to a cluster with open boundary conditions which violates translational symmetries. In contrast, the DCA cluster is defined in cluster reciprocal space. Hence the DCA cluster has periodic boundary conditions and therefore preserves the translational symmetries of the lattice. This difference in boundary conditions translates directly to different asymptotic behaviors for large linear cluster sizes L_c, and the decision of which method to use for a given problem strongly depends on the quantities of interest: Local quantities, such as the local density of states when defined on central cluster sites converge faster in the cellular DMFT since they do not directly couple to the mean field. Due to the large mean-field coupling of the surface sites, however, the cellular DMFT converges slowly, with corrections of order $\mathcal{O}(1/L_c)$, for quantities extended over the cluster. The DCA converges more quickly, as $\mathcal{O}(1/L_c^2)$, due to the periodic boundary conditions on the cluster.

Quantum cluster approaches reduce the complexity of the infinite lattice problem by mapping it to a cluster with fewer spatial degrees of freedom. The numerous methods employed to solve the DMFT equations are in principle available for the study of the effective cluster model. However, as the complexity of this task rapidly increases with cluster size, potential cluster solvers are faced with severe size limitations. As the most promising techniques we reviewed perturbative approaches including the fluctuation-exchange approximation and the noncrossing approximation as well as nonperturbative techniques including quantum Monte Carlo and the numerical renormalization group.

We discussed the application of quantum cluster approaches to a wide range of problems in condensed-matter physics. The information gained from these studies has led to significant progress in the field of strongly correlated electron systems. Even studies using small cluster sizes opened up new insight in problems such as one-dimensional systems, the Mott-Hubbard transition in two dimensions, and high-temperature superconductivity.

Larger-cluster-size studies are inevitable, however, to verify or possibly disprove the information obtained from small clusters. This task is severely hampered by the rapidly increasing complexity with cluster size. Future progress therefore is closely linked to improvements in the efficiency and flexibility of the techniques

used to solve the effective cluster problem. Within quantum cluster approaches we explored a coarse-graining approximation in k space. To further reduce the complexity, the same idea could be extended to the frequency domain. By coarse-graining the frequency dependence of irreducible quantities, correlations on long time scales are neglected, while the short-time-scale behavior is described accurately. An important aspect in this context is again the causality question. First test results are encouraging; they show that coarse graining in Matsubara space leads to acausalities, while coarse-graining the real frequency axis does not face this problem (Aryanpour, Hettler, and Jarrell, 2003).

Another route to defeating the cluster size problem is to develop hybrid algorithms that treat different length scales in the problem with different accuracy. As a promising step in this direction, Hague *et al.* (2004) have developed a hybrid technique which maps the infinite lattice onto two embedded clusters of different size, thus dividing the problem into three length scales. Short-ranged correlations described by the small cluster are treated accurately within quantum Monte Carlo, correlations of intermediate length scale are treated perturbatively in the large cluster using the fluctuation-exchange approximation, and the long-ranged physics beyond the size of the larger cluster is again approximated on the mean-field level.

To improve comparisons with experiments and to achieve predictive capability, the inclusion of the specifics of the actual materials is required. Along the lines of the local-density approximation+DMFT approach, one can use electronic structure calculations to parametrize the models studied by quantum cluster approaches. The first steps in this direction have been taken by Poteryaev *et al.* (2004). A more integrated approach to the *ab initio* description of strongly correlated systems by combining the ideas of density-functional theory and quantum cluster approaches remains an important and challenging task.

ACKNOWLEDGMENTS

It is a pleasure to acknowledge useful discussions with K. Aryanpour, G. Baskaran, N. Blümer, R. Bulla, A. Gonis, B. Gyorffy, H. Keiter, J. Keller, G. Kotliar, H. R. Krishnamurthy, A. Lichtenstein, M. Mukherjee, E. Müller-Hartmann, A. N. Tavildar-Zadeh, P. van Dongen, and M. Vojta. This work was supported in part by NSF Grant Nos. DMR-0312680, DMR-0113574, and DMR-0073308 and by the DFG through SFB 484. We acknowledge supercomputer support by the Leibniz Computer Center, the Max-Planck Computer Center Garching under Grant No. h0301, the Ohio Supercomputer Center, the Pittsburgh Supercomputer Center (NSF), and the Center for Computational Sciences at the Oak Ridge National Laboratory. Part of this research was performed by T.M. as Eugene P. Wigner Fellow and staff member at the Oak Ridge National Laboratory, managed by UT-Battelle, LLC, for the U.S. Department of Energy under Contract No. DE-AC05-00OR22725.

REFERENCES

Abrikosov, A., L. Gorkov, and I. Dzyaloshinski, 1963, *Methods of Quantum Field Theory in Statistical Physics* (Dover, New York).
Aichhorn, M., M. Daghofer, H. Evertz, and W. v.d. Linden, 2003, Phys. Rev. B **67**, 161103.
Akima, H., 1970, J. Assoc. Comput. Mach. **17**, 589.
Anderson, P., 1961, Phys. Rev. **124**, 41.
Anderson, P., 1997a, Adv. Phys. **46**, 3.
Anderson, P. W., 1987, Science **235**, 1196.
Anderson, P. W., 1997b, *The Theory of Superconductivity in the High-T_c Cuprates* (Princeton University Press, Princeton, NJ).
Aryanpour, K., M. H. Hettler, and M. Jarrell, 2002, Phys. Rev. B **65**, 153102.
Aryanpour, K., M. H. Hettler, and M. Jarrell, 2003, Phys. Rev. B **67**, 085101.
Aryanpour, K., T. A. Maier, and M. Jarrell, 2005, Phys. Rev. B **71**, 037101.
Baym, G., 1962, Phys. Rev. **127**, 1391.
Baym, G., and L. Kadanoff, 1961, Phys. Rev. **124**, 287.
Beeby, J. L., and S. F. Edwards, 1962, Proc. R. Soc. London, Ser. A **274**, 395.
Bethe, H. A., 1935, Proc. R. Soc. London, Ser. A **150**, 552.
Betts, D., S. Masui, N. Vats, and G. Stewart, 1996, Can. J. Phys. **74**, 54.
Betts, D., S. Masui, N. Vats, and G. Stewart, 1999, Can. J. Phys. **77**, 353.
Betts, D., J. Schulenburg, G. Stewart, J. Richter, and J. Flynn, 1998, J. Phys. A **31**, 7685.
Betts, D., and G. Stewart, 1997, Can. J. Phys. **75**, 47.
Bickers, N., 1987, Rev. Mod. Phys. **59**, 845.
Bickers, N., D. Cox, and J. Wilkins, 1987, Phys. Rev. B **36**, 2036.
Bickers, N., D. Scalapino, and S. White, 1989, Phys. Rev. Lett. **62**, 961.
Bickers, N., and S. R. White, 1990, Phys. Rev. B **43**, 8044.
Biroli, G., and G. Kotliar, 2002, Phys. Rev. B **65**, 155112.
Biroli, G., O. Parcollet, and G. Kotliar, 2004, Phys. Rev. B **69**, 205108.
Blümer, N., 2002, Ph.D. thesis (Institute of Physics, University of Augsburg).
Bolech, C., S. Kancharla, and G. Kotliar, 2003, Phys. Rev. B **67**, 075110.
Brandt, U., and U. Mielsch, 1989, Z. Phys. B: Condens. Matter **75**, 365.
Brandt, U., and R. Schmidt, 1986, Z. Phys. B: Condens. Matter **63**, 45.
Brandt, U., and R. Schmidt, 1987, Z. Phys. B: Condens. Matter **67**, 43.
Bulla, R., 1999, Phys. Rev. Lett. **83**, 136.
Bulla, R., T. Costi, and D. Vollhardt, 2001, Phys. Rev. B **64**, 045103.
Bulla, R., A. Hewson, and T. Pruschke, 1998, J. Phys.: Condens. Matter **10**, 8365.
Caffarel, M., and W. Krauth, 1994, Phys. Rev. Lett. **72**, 1545.
Cox, D., and N. Grewe, 1987, Z. Phys. B: Condens. Matter **71**, 321.
Creffield, C., E. Klepfish, E. Pike, and S. Sarkar, 1995, Phys. Rev. Lett. **75**, 517.
Dagotto, E., 1994, Rev. Mod. Phys. **66**, 763.
Dagotto, E., and A. Moreo, 1988, Phys. Rev. B **38**, 5087.

Dahnken, C., M. Aichhorn, W. Hanke, E. Arrigoni, and M. Potthoff, 2004, Phys. Rev. B **70**, 245110.
Dahnken, C., E. Arrigoni, and W. Hanke, 2002, J. Low Temp. Phys. **126**, 949.
Deisz, J., D. Hess, and J. Serene, 1996, Phys. Rev. Lett. **76**, 1312.
Deisz, J., D. Hess, and J. Serene, 1997, Phys. Rev. B **55**, 2089.
Deisz, J., D. Hess, and J. Serene, 2003, *Recent Progress in Many Body Theories*, Vol. 4 (Plenum, New York).
de Vries, P., K. Michelsen, and H. De Raedt, 1993a, Z. Phys. B: Condens. Matter **92**, 353.
de Vries, P., K. Michelsen, and H. De Raedt, 1993b, Phys. Rev. Lett. **70**, 2463.
de Vries, P., K. Michelsen, and H. De Raedt, 1994, Z. Phys. B: Condens. Matter **95**, 475.
Ducastelle, F., 1974, J. Phys. C **7**, 1795.
Elliot, D., and K. Rao, 1982, *Fast Transorms: Algorithms, Analyses, and Applications* (Academic, New York).
Emery, V., 1987, Phys. Rev. Lett. **58**, 2794.
Emery, V., and G. Reiter, 1988, Phys. Rev. B **38**, 4547.
Fetter, A., and J. Walecka, 1971, in *Quantum Theory of Many-Particle Systems*, International Series in Pure and Applied Physics, edited by Leonard E. Schiff (McGraw-Hill, New York).
Fischer, K., 1997, Phys. Rev. B **55**, 13575.
Fisher, M., and M. Barber, 1972, Phys. Rev. Lett. **28**, 1516.
Freericks, J. K., and V. Zlatić, 2003, Rev. Mod. Phys. **75**, 1333.
Georges, A., and G. Kotliar, 1992, Phys. Rev. B **45**, 6479.
Georges, A., G. Kotliar, W. Krauth, and M. Rozenberg, 1996, Rev. Mod. Phys. **68**, 13.
Goldenfeld, N., 1992, *Lectures on Phase Transitions and the Renormalization Group*, Frontiers in Physics (Addison-Wesley, Reading, MA), Vol. 85.
Gonis, A., 1992, in *Green Functions for Ordered and Disordered Systems*, Studies in Mathematical Physics, edited by Evan Groesen and E. M. de Jager (North-Holland, Amsterdam), Vol. 4.
Grewe, N., 1983, Z. Phys. B: Condens. Matter **53**, 271.
Grewe, N., 1987, Z. Phys. B: Condens. Matter **67**, 323.
Grewe, N., H. Keiter, and T. Pruschke, 1988, Z. Phys. B: Condens. Matter **71**, 75.
Gros, C., and R. Valenti, 1993, Phys. Rev. B **48**, 418.
Gros, C., and R. Valenti, 1994, Ann. Phys. (Leipzig) **3**, 460.
Haan, O., J. Klaeke, and K. Müller, 1992, Phys. Rev. B **46**, 5723.
Hague, J., 2003, J. Phys.: Condens. Matter **15**, 2535.
Hague, J., M. Jarrell, and T. Schulthess, 2004, Phys. Rev. B **69**, 165113.
Halboth, C., and W. Metzner, 2000, Phys. Rev. B **61**, 7364.
Haydock, R., V. Heine, and M. J. Kelly, 1975, J. Phys. C **8**, 2591.
Heindl, W., T. Pruschke, and J. Keller, 2000, J. Phys.: Condens. Matter **12**, 2245.
Hettler, M. H., M. Mukherjee, M. Jarrell, and H. R. Krishnamurthy, 2000, Phys. Rev. B **61**, 12739.
Hettler, M. H., A. N. Tahvildar-Zadeh, M. Jarrell, T. Pruschke, and H. R. Krishnamurthy, 1998, Phys. Rev. B **58**, R7475.
Hewson, A., 1993, *The Kondo Problem to Heavy Fermions*, Cambridge Studies in Magnetism (Cambridge University Press, Cambridge, England), Vol. 2.
Hirsch, J., 1983, Phys. Rev. B **28**, 4059.
Hirsch, J., and R. Fye, 1986, Phys. Rev. Lett. **56**, 2521.
Hohenadler, M., M. Aichhorn, and W. v.d. Linden, 2003, Phys. Rev. B **68**, 184304.
Hubbard, J., 1963, Proc. R. Soc. London, Ser. A **276**, 238.
Huscroft, C., R. Gass, and M. Jarrell, 2000, Phys. Rev. B **61**, 9300.
Huscroft, C., M. Jarrell, T. Maier, S. Moukouri, and A. Tahvildarzadeh, 2001, Phys. Rev. Lett. **86**, 139.
Imai, Y., and N. Kawakami, 2002, Phys. Rev. B **65**, 233103.
Itzykson, C., and J.-M. Drouffe, 1989, *Statistical Field Theory* (Cambridge University Press, Cambridge, England).
Jarrell, M., 1992, Phys. Rev. Lett. **69**, 168.
Jarrell, M., H. Akhlaghpour, and T. Pruschke, 1993, in *Quantum Monte Carlo Methods in Condensed Matter Physics*, edited by M. Suzuki (World Scientific, Singapore), pp. 221–234.
Jarrell, M., and J. Gubernatis, 1996, Phys. Rep. **269**, 133.
Jarrell, M., and D. Johnson, 2004, unpublished.
Jarrell, M., and H. R. Krishnamurthy, 2001, Phys. Rev. B **63**, 125102.
Jarrell, M., T. Maier, M. H. Hettler, and A. N. Tahvildarzadeh, 2001, Europhys. Lett. **56**, 563.
Jarrell, M., T. Maier, C. Huscroft, and S. Moukouri, 2001, Phys. Rev. B **64**, 195130.
Jarrell, M., and T. Pruschke, 1993, Z. Phys. B: Condens. Matter **90**, 187.
Jones, B., and C. Varma, 1987, Phys. Rev. Lett. **58**, 843.
Jones, B., C. Varma, and J. Wilkins, 1988, Phys. Rev. Lett. **61**, 125.
Kakehashi, Y., 2002, Phys. Rev. B **66**, 104428.
Kampf, A., 1991, Phys. Rev. B **44**, 2637.
Kampf, A., and J. Schrieffer, 1990, Phys. Rev. B **42**, 7967.
Keiter, H., and C. Czycholl, 1983, J. Magn. Magn. Mater. **31-34**, 477.
Keiter, H., and J. Kimball, 1970, Phys. Rev. Lett. **25**, 672.
Keiter, H., and J. Kimball, 1971, Int. J. Magn. **1**, 233.
Kikuchi, R., 1951, Phys. Rev. **81**, 988.
Kim, C., Y. Kuramoto, and T. Kasoya, 1990, J. Phys. Soc. Jpn. **59**, 2414.
Kosterlitz, J., 1973, J. Phys. C **7**, 1046.
Kosterlitz, J., and D. Thouless, 1973, J. Phys. C **6**, 1181.
Kotliar, G., S. Savrasov, G. Pallson, and G. Biroli, 2001, Phys. Rev. Lett. **87**, 186401.
Krishnamurthy, H., J. Wilkins, and K. Wilson, 1980a, Phys. Rev. B **21**, 1003.
Krishnamurthy, H., J. Wilkins, and K. Wilson, 1980b, Phys. Rev. B **21**, 1044.
Kuramoto, Y., 1983, Z. Phys. B: Condens. Matter **53**, 37.
Kuramoto, Y., 1985, *Theory of Heavy Fermions and Valence Fluctuations*, edited by T. Kasuya and T. Saso, Springer Series in Solid State (Springer Verlag, Heidelberg), Vol. 62, p. 152
Laad, M. S., and M. van den Bossche, 2000, J. Phys.: Condens. Matter **12**, 2209.
Landau, D., 1976, Phys. Rev. B **13**, 2997.
Lichtenstein, A. I., and M. I. Katsnelson, 2000, Phys. Rev. B **62**, R9283.
Lieb, E., and F. Wu, 1968, Phys. Rev. Lett. **20**, 1445.
Lombardo, P., M. Avignon, J. Schmalian, and K. Bennemann, 1996, Phys. Rev. B **54**, 5317.
Lyness, J., T. Sorevik, and P. Keast, 1991, Math. Comput. **56**, 243.
Maier, T., 2001, *Nonlocal Dynamical Correlations in Strongly Interacting Fermion Systems* (Logos Verlag Berlin, Berlin).
Maier, T., O. Gonzalez, M. Jarrell, and T. Schulthess, 2002, in *Two Quantum Cluster Approximations*, edited by D. P.

Landau, K. K. Mon, and H. B. Schüttler, Springer Proceedings in Physics (Springer, New York), Vol. 15.
Maier, T., and M. Jarrell, 2002, Phys. Rev. B **65**, 041104.
Maier, T., M. Jarrell, A. Macridin, and C. Slezak, 2004, Phys. Rev. Lett. **92**, 027005.
Maier, T., M. Jarrell, A. Macridin, and F.-C. Zhang, 2002, e-print cond-mat/0208419.
Maier, T., M. Jarrell, T. Pruschke, and J. Keller, 2000a, Phys. Rev. Lett. **85**, 1524.
Maier, T., M. Jarrell, T. Pruschke, and J. Keller, 2000b, Eur. Phys. J. B **13**, 613.
Maier, T., M. Jarrell, T. Schulthess, P. Kent, and J. White, 2005, e-print cond-mat/0504529.
Maier, T., M. Zölfl, T. Pruschke, and J. Keller, 1999a, Eur. Phys. J. B **7**, 377.
Maier, T., M. Zölfl, T. Pruschke, and J. Keller, 1999b, Physica B **259**, 747.
Matsumoto, H., and F. Mancini, 1997, Phys. Rev. B **55**, 2095.
Metzner, W., and D. Vollhardt, 1989, Phys. Rev. Lett. **62**, 324.
Minh-Tien, T., 1998, Phys. Rev. B **58**, R15965.
Minh-Tien, T., 1999a, Europhys. Lett. **47**, 582.
Minh-Tien, T., 1999b, Phys. Rev. B **60**, 16371.
Minh-Tien, T., 2001, Phys. Rev. B **63**, 165117.
Molegraaf, H. J. A., C. Presura, D. van der Marel, P. H. Kes, and M. Li, 2002, Science **295**, 2239.
Monthoux, P., A. Balatsky, and D. Pines, 1991, Phys. Rev. Lett. **67**, 3448.
Moukouri, S., S. Allen, F. Lemay, B. Kyong, D. Poulin, Y. Vilk, and A.-M. Tremblay, 1999, Phys. Rev. B **61**, 7887.
Moukouri, S., and M. Jarrell, 2001, Phys. Rev. Lett. **87**, 167010.
Müller-Hartmann, E., 1984, Z. Phys. B: Condens. Matter **57**, 293.
Müller-Hartmann, E., 1989a, Z. Phys. B: Condens. Matter **76**, 211.
Müller-Hartmann, E., 1989b, Z. Phys. B: Condens. Matter **74**, 507.
Nordheim, J., 1931a, Ann. Phys. (Leipzig) **9**, 607.
Nordheim, J., 1931b, Ann. Phys. (Leipzig) **9**, 641.
Okamoto, S., A. Millis, H. Monien, and A. Fuhrmann, 2003, Phys. Rev. B **68**, 195121.
Oliveira, W., and L. Oliveira, 1994, Phys. Rev. B **49**, 11986.
Pairault, S., D. Sénéchal, and A.-M. Tremblay, 1998, Phys. Rev. Lett. **80**, 5389.
Pairault, S., D. Sénéchal, and A.-M. Tremblay, 2000, Eur. Phys. J. B **16**, 85.
Parcollet, O., G. Biroli, and G. Kotliar, 2004, Phys. Rev. Lett. **92**, 226402.
Parmenter, R. H., 1955, Phys. Rev. **97**, 587.
Paula, C., M. Silva, and L. Oliveira, 1999, Phys. Rev. B **59**, 85.
Poteryaev, A., A. Lichtenstein, and G. Kotliar, 2004, Phys. Rev. Lett. **93**, 086401.
Potthoff, M., 2003a, Eur. Phys. J. B **36**, 335.
Potthoff, M., 2003b, Eur. Phys. J. B **32**, 429.
Potthoff, M., M. Aichhorn, and C. Dahnken, 2003, Phys. Rev. Lett. **91**, 206402.
Pozgajčić, K., 2004, e-print cond-mat/0407172.
Pruschke, T., R. Bulla, and M. Jarrell, 2000, Phys. Rev. B **61**, 12 799.
Pruschke, T., D. Cox, and M. Jarrell, 1993a, Europhys. Lett. **21**, 593.
Pruschke, T., D. Cox, and M. Jarrell, 1993b, Phys. Rev. B **47**, 3553.
Pruschke, T., and N. Grewe, 1989, Z. Phys. B: Condens. Matter **74**, 439.
Pruschke, T., M. Jarrell, and J. Freericks, 1995, Adv. Phys. **44**, 187.
Pruschke, T., and R. Zitzler, 2003, J. Phys. Chem. **15**, 7867.
Roth, L. M., 1969, Phys. Rev. **184**, 451.
Sakai, O., and Y. Kuramoto, 1994, Solid State Commun. **89**, 307.
Sakai, O., and Y. Shimizu, 1992, J. Phys. Soc. Jpn. **61**, 2333.
Sakai, O., Y. Shimizu, and T. Kasuya, 1989, J. Phys. Soc. Jpn. **59**, 3666.
Sakai, O., Y. Shimizu, and T. Kasuya, 1990, Solid State Commun. **75**, 81.
Scalapino, D., 1999, J. Low Temp. Phys. **117** (3-4), 179.
Schiller. A., and K. Ingersent, 1995, Phys. Rev. Lett. **75**, 113.
Schmalian, J., P. Lombardo, M. Avignon, and K. Bennemann, 1996, Physica B **222-224**, 602.
Schoen, J. M., 1969, Phys. Rev. **184**, 858.
Schrieffer, J., 1993, *Theory of Superconductivity* (Addison-Wesley, Reading, MA).
Schwartz, L., F. Brouers, A. V. Vedyayev, and H. Ehrenreich, 1971, Phys. Rev. B **4**, 3383.
Sénéchal, D., D. Perez, and M. Pioro-Ladriére, 2000, Phys. Rev. Lett. **84**, 522.
Sénéchal, D., D. Perez, and D. Plouffe, 2002, Phys. Rev. B **66**, 075129.
Sénéchal, D., and A.-M. Tremblay, 2004, Phys. Rev. Lett. **92**, 126401.
Shiba, H., 1971, Prog. Theor. Phys. **46**, 77.
Shimizu, Y., 2002, J. Phys. Soc. Jpn. **71**, 1166.
Shimizu, Y., and O. Sakai, 1995, *Computational Physics as a New Frontier in Condensed Matter Research* (The Physical Society of Japan), p. 42.
Si, Q., M. J. Rozenberg, G. Kotliar, and A. E. Ruckenstein, 1994, Phys. Rev. Lett. **72**, 2761.
Soven, P., 1967, Phys. Rev. **156**, 809.
Stanescu, T. D., and P. Phillips, 2001, Phys. Rev. B **64**, 235117.
Stanescu, T. D., and P. Phillips, 2003, Phys. Rev. Lett. **91**, 017002.
Stanescu, T. D., and P. Phillips, 2004, Phys. Rev. B **69**, 245104.
Stewart, G., D. Betts, and J. Flynn, 1997, J. Phys. Soc. Jpn. **66**, 3231.
Sumi, H., 1974, J. Phys. Soc. Jpn. **36**, 770.
Suzuki, M., 1986, J. Phys. Soc. Jpn. **55**, 4205.
Tahvildar-Zadeh, A., M. Jarrell, and J. Freericks, 1997, Phys. Rev. B **55**, R3332.
Tanh-Hai, D., and T. Minh-Tien, 2001, J. Phys.: Condens. Matter **13**, 5625.
Taylor, D., 1967, Phys. Rev. **156**, 1017.
Timusk, T., and B. Statt, 1999, Rep. Prog. Phys. **62**, 61.
Tsukada, M., 1969, J. Phys. Soc. Jpn. **26**, 684.
van Dongen, P., 1994, Phys. Rev. B **50**, 14016.
Vekic, M., and S. White, 1993, Phys. Rev. B **47**, 1160.
Vidberg, H. J., and J. W. Serene, 1977, J. Low Temp. Phys. **19**, 179.
Voit, J., 1994, Rep. Prog. Phys. **57**, 977.
Weiss, P., 1907, J. Phys. Radium **6**, 661.
Wilson, K., 1975, Rev. Mod. Phys. **47**, 773.
Zacher, M. G., R. Eder, E. Arrigoni, and W. Hanke, 2002a, Phys. Rev. B **65**, 045109.
Zacher, M. G., R. Eder, E. Arrigoni, and W. Hanke, 2002b, Phys. Rev. Lett. **85**, 2585.
Zanchi, D., and H. Schulz, 2000, Phys. Rev. B **61**, 13609.

Zhang, F., and T. Rice, 1988, Phys. Rev. B **37**, 3759.
Zhang, F., and T. Rice, 1990, Phys. Rev. B **41**, 7243.
Zitzler, R., T. Pruschke, and R. Bulla, 2002, Eur. Phys. J. B **27**, 473.
Zitzler, R., N. Tong, T. Pruschke, and R. Bulla, 2004, Phys. Rev. Lett. **93**, 016406.
Zölfl, M., T. Maier, T. Pruschke, and J. Keller, 2000, Eur. Phys. J. B **13**, 47.